A thermogravimetric investigation into the synthesis of cobalt fluoride

by

Bernard Mabena Vilakazi

Submitted in partial fulfilment of the requirements for the degree

Master of Science

In the Faculty of Natural & Agricultural Sciences
University of Pretoria
Pretoria
October 2018

Supervisor: Dr Liezel van der Merwe

Co-supervisor: Dr Kobus Wagener

Declaration:

I, Bernard Mabena Vilakazi declare that the thesis/dissertation, which I hereby submit for the degree Masters of Science at the University of Pretoria, is my own work and has not previously been submitted by me for a degree at this or any other institution.

SIGNATURE:

DATE:

Acknowledgements

I would like to express my deepest gratitude towards the following people and organizations.

- My supervisor, Dr Liezel van der Merwe for her guidance, support and insightful discussions during the course of my studies. Thank you very much for the encouragement and patience, I would not have achieved this without your help.
- My co-supervisor Dr Kobus Wagener for having afforded me the opportunity, and the support.
- Dr Andrew Pienaar for having started this fruitful journey with me.
- Necsa for the financial support and for having afforded me the opportunity to use their facilities.
- Dr David Kock and Mr John Le Roux for the inputs and comments pertaining to my studies.
- Mr Tshepo Ntsoane for having performed the XRD analysis and assisting with the interpretation of the results.
- Ms Ntombizdwa Mabena for the ATR-FTIR and Raman spectroscopy analysis.
- Thanks to all my colleagues within Delta-F.
- My wife and kids for the support, understanding and patience during my studies.
- Special thanks to my parents and siblings for the unwavering support.

Abstract

Fluorochemicals are valuable organic compounds manufactured by PELCHEM, the chemical manufacturing company of NECSA (The South African Nuclear Energy Corporation of South Africa). Fluorochemicals are manufactured through the fluorination of hydrocarbons to yield fluorocarbons. Fluorination is achieved using hydrogen fluoride and fluorine as the fluorination agent.

The process in which fluorine is used as fluorinating agent is not viable owing to the high energy of reaction released with possible fragmentation of the hydrocarbon taking place. Cobalt trifluoride is known to be a mild fluorinating agent and yields less heat of reaction. Though the method has been used throughout the world, it has not been exploited within Necsa. It is therefore the aim of Necsa to establish another fluorination technology in which cobalt fluoride is utilized as a fluorinating agent. If successfully established, this technology will yield huge benefits for Necsa.

Cobalt fluoride is quite expensive to obtain from the commercial market. It is therefore the aim of this study to investigate dry methods in which cobalt (III) fluoride is synthesised from the less expensive oxide form. This project will be undertaken in two phases, (i) the synthesis of cobalt fluoride and (ii) the usage of this compound in the fluorination of organic compounds. The current study focuses on the first phase, the investigation of synthesis of cobalt (III) fluoride from the mixed oxidation state oxide form, Co_3O_4.

Cobalt (III) fluoride may be manufactured through direct fluorination using fluorine gas, but this process would result in high operational costs as fluorine is more expensive than hydrogen fluoride. As a result, our synthesis route involved sequential fluorination of cobalt oxide with hydrogen fluoride and then fluorine gas. Fluorine gas was used only for the fluorination of the cobalt (II) fluoride, resulting in lower amounts of fluorine used, thereby leading to significant savings in costs.

Firstly, simulation of the reaction of Co_3O_4 with HF and F_2 was carried out through thermodynamic equilibrium composition calculations using the HSC Chemistry software

program. The thermodynamic data was then used as guideline to which the actual experimental reactions should be performed. Prior to the fluorination reactions, a study on the thermal analysis and spectroscopic characterisation of commercial Co_3O_4, CoO and CoF_2 compounds used as starting materials, as well as CoF_3 which was the desired product was performed. Spectroscopic characterisation techniques used included XRD, ATR-FTIR and Raman. The results of this study indicates that fluorination reactions should be carried out under dry conditions and at temperatures below 600 ^oC to limit decomposition and sublimation of CoF_3.

Four reactions were carried out to investigate the synthesis of CoF_3: (i) Co_3O_4 with HF, (ii) Co_3O_4 with F_2, (iii) CoF_2 with F_2, and (iv) a sequential reaction of Co_3O_4 with HF and then F_2. These reactions were conducted on a thermogravimetric analyser. The degree of fluorination of the respective reactions was followed via the mass uptakes recorded at various isotherms. The ideal temperature condition for the synthesis of CoF_2 through reaction of Co_3O_4 with HF was found to be 500 ^oC, whilst the ideal temperature for the synthesis of CoF_3 through reaction of Co_3O_4 with F_2 and CoF_2 with F_2 was found to be 300 ^oC and 400 ^oC respectively. These results were used to successfully synthesise CoF_3 through a sequential reaction of Co_3O_4 with HF and F_2 gas. XRD and ATR-FTIR analyses were instrumental in the characterization of the reaction products obtained. The next phase of the project will be the design and construction of a suitable laboratory scale reactor to produce sufficient cobalt trifluoride for the fluorination efforts.

List of abbreviations and symbols

ca	Approximately
ATR-FTIR	Attenuated Total reflectance-Fourier Transform Infrared Spectroscopy
Co	Cobalt
CoO	Cobalt monoxide, cobaltous oxide
Co_3O_4	Cobalt (II,III) oxide, cobalt mixed oxide, cobaltic oxide
CoF_2	Cobalt (II) fluoride
CoF_3	Cobalt (III) fluoride
^oC	Degree Celsius
F_2	Fluorine gas
G^o	Gibbs free energy, standard
HF	Hydrogen fluoride gas
%	Percentage
T	Temperature
TGA	Thermogravimetric Analyzer, Thermogravimetric analysis
XRD	X-ray powder diffraction

Contents

List of Figures

List of Tables

1 Introduction

1.1 Background

The South African Nuclear Energy Corporation, Necsa, has as its primary mandate to pursue nuclear technology excellence for sustainable social and economic development. Part of its mandate is fulfilled through the manufacture of fluorochemical products that have found widespread use across multiple market sectors like the petrochemical, pharmaceutical and a host of other sectors. These fluorochemical products are produced by Pelchem, SOC Ltd, a subsidiary of Necsa with a unique fluorination technology capability. Various technologies are listed in the literature for the production of a variety of these fluorochemicals. One prominent method that is utilized within Necsa is the fluorination of organic compounds with hydrogen fluoride (HF) and fluorine (F_2) gases used as fluorinating agents.

Fluorine has for some time been used as a fluorinating agent of organic compounds, but the process was found to yield high energy of reaction with possible fragmentation of hydrocarbons taking place (Chambers, 2004). As a result, a mild fluorinating agent was sought and cobalt fluoride identified as suitable compound for this purpose (Goldwhite, 1986, Sandford, 2003). Though this method is known and has been used throughout the world, it has not been exploited within Necsa and South Africa as a whole. It is the therefore the intention of Necsa to establish a technology platform in which cobalt (III) fluoride is used as a fluorinating agent. This study therefore seeks to investigate the synthesis of cobalt (III) fluoride that will in turn be used as a fluorinating agent for the manufacture of fluorocarbons. Hydrocarbons are organic compounds with the formula C_xH_y, whereas fluorocarbons possess only carbon and fluorine atoms in their formula, C_xF_y, with all hydrogen atoms replaced by fluorine atoms.

If successfully established, the cobalt fluoride technology will result in huge benefits and economic returns as it involves usage of less expensive starting reagents. This technology

will also provide Necsa with the capacity to choose and use the most viable fluorination method for a particular product based on the requirements on the local or international market. One prominent industrial method in which cobalt fluoride is used as the fluorinating agent for the production of fluorochemicals is known as the Fowler process.

1.2 The Fowler process

The Fowler process is a technology that was developed during the Manhattan project (Goldwhite, 1986), specifically for the manufacture of fluorocarbons. It was during the Manhattan project whereby a need for materials that were capable to handle the highly reactive and corrosive uranium hexafluoride arose. Fluorocarbons were identified and found to be inert and capable of handling uranium hexafluoride (UF_6) (Grosse and Cady, 1947). It was therefore necessary to develop a method for the manufacture of fluorocarbons. The Fowler process was then established for this purpose. The process occurs in two stages: firstly cobalt (II) fluoride is reacted with F_2 to form cobalt (III) fluoride, and the cobalt (III) fluoride is subsequently used in the second stage as a fluorine source for the actual conversion of hydrocarbons to fluorocarbons. During the fluorination process, CoF_3 is converted back to CoF_2 that can then be reused. Fluorine is a unique element and its presence in fluorocarbon compounds imparts unique physical and chemical properties, owing to the strong C-F bond these fluorocarbons possess (Sandford, 2003). These properties makes fluorocarbon compounds very useful in industries like the pharmaceutical (Lemal, 2004).

1.3 Fluorocarbon applications

Some of the known fluorocarbon industrial applications are as refrigerants, solvents, fluoropolymers and anaesthetics. Chlorofluorocarbons (CFC) has for some time been used as refrigerants, but these compounds were found to be environmentally unfriendly as they contribute to ozone depletion owing to the chlorine they possess. For this reason chlorofluorocarbons were replaced by fluorocarbons (Kurosawa et al., 1997). The absence

of chlorine in fluorocarbons makes these compounds perfect as refrigerants as they are easily degraded in the atmosphere and do not contribute to ozone depletion (Lemal, 2004).

Other advantages of fluorocarbons are their high durability as well as high resistance to hydrolysis, microbial degradation, high temperature, X-ray radiation and nuclear radiation (Lewandowski et al., 2006). An example of a commonly known fluoropolymer is polytetrafluoroethene (PTFE). Due to its high resistance to wettability, PTFE has been used as a coating material, and metal surfaces coated with PTFE neither wets with water or oils.

1.4 Problem statement

Fluorine has been used as a fluorinating agent for the conversion of hydrocarbons to fluorocarbons. However, the process in which fluorine is used as the fluorinating agent yield a high energy of reaction, with possible fragmentation of the hydrocarbon taking place (Chambers, 2004). Additionally, fluorine is expensive and a fluorination process in which fluorine is used as sole fluorinating agent would result in high operational costs. It is for this reason that other fluorination routes with less heat of reaction and less costs were sought. Cobalt (III) fluoride was identified as a suitable fluorinating agent for this purpose (Goldwhite, 1986, Sandford, 2003). Though cobalt (III) fluoride is available in the commercial market, the material is highly expensive and difficult to handle, owing to its susceptibility to atmospheric moisture. It is therefore the objective of this study to investigate economical methods for the synthesis of CoF_3 using the less expensive and easy to handle cobalt oxides.

1.5 Aim and objectives of the study

Of the few cobalt oxides listed in literature, CoO, CoO_2, Co_2O_3, Co_3O_4 and CoO(OH), only Co_3O_4 and CoO are stable and useful in industry (Tang et al., 2008). Of these two oxides, Co_3O_4 also known as the mixed oxide, was found to be relatively cheaper and was chosen as the primary oxide used for our fluorination studies. It is therefore the aim of this study

to synthesize CoF_3 through sequential reaction of Co_3O_4 with hydrogen fluoride and fluorine gas. The fluorination reactions have to be performed on a thermogravimetric analyser (TGA) capable of handling HF and F_2 gas. The TGA instrument brings a unique capability as it makes it possible to follow the degree of fluorination from the respective mass uptakes obtained at the various temperature conditions at which reactions are performed.

1.6 Research approach

Prior to fluorination reactions, the thermochemical properties of cobalt oxides (CoO, Co_3O_4) were determined through heat treatment in nitrogen and air on a thermogravimetric analyser, (TGA). With the thermochemical properties established, fluorination reactions were then performed via two steps. Firstly, cobalt oxide, Co_3O_4, was reacted with hydrogen fluoride to form cobalt (II) fluoride, CoF_2, which upon further treatment with fluorine converts to the highest oxidation state metal fluoride, CoF_3 as in equation (1-1) and (1-2):

$$Co_3O_4(s) + 4HF(g) \rightarrow CoF_2(s) + 2CoOF(s,g) + 2H_2O(g) \quad (1\text{-}1)$$

$$CoF_2(s) + 0.5F_2(g) \rightarrow CoF_3(s) \quad (1\text{-}2)$$

For comparison and academic purposes, fluorinations were also performed on cobalt (II) oxide, CoO, as presented in equation (1-3) and (1-4):

$$CoO(s) + 2HF(g) \rightarrow CoF_2(s) + H_2O(g) \quad (1\text{-}3)$$

$$2CoF_2(s) + F_2(g) \rightarrow 2CoF_3(s) \quad (1\text{-}4)$$

All fluorination experiments were performed on a thermogravimetric analyser that has been modified to handle corrosive gases like HF and F_2. The TGA is housed within a glovebox to maintain inert operational conditions, as the product formed (CoF_3) is susceptible to atmospheric moisture (Friedt and Adloff, 1969, Groult et al., 2017).

Though CoF_3 can be formed through direct fluorination of Co_3O_4 with F_2, the process would result in high operational costs as fluorine is more expensive in comparison to

hydrogen fluoride (Banks et al., 1994). As a result, fluorinations were performed first with hydrogen fluoride, then with fluorine to yield cobalt (III) fluoride. This process resulted in decreased amounts of fluorine used, leading to significant savings in costs in comparison to the process in which fluorine is used as the sole fluorinating agent.

Due to its instability to atmospheric moisture, only a few analytical instruments are suitable for characterization of the CoF_3 product. In our work, X-ray powder diffraction (XRD), Attenuated Total Reflectance-Fourier Transform Infra-red (ATR-FTIR) spectroscopy and Raman spectroscopy were used for characterization purposes. These instruments possess special sample holders that allows loading of samples without having been exposed to atmospheric moisture. The loading was performed in a dry atmosphere within the glove box. Most analytical instruments involves exposure of a sample to the atmosphere, and are therefore rendered unsuitable for characterization of the CoF_3 product synthesised in our study.

1.7 Structure of the thesis

The thesis is organised into six chapters as follows:

Chapter 1: Introduction - provides a brief introduction and background of the study, the problem statement, objectives and study approach.

Chapter 2: Literature review - gives an overview of the physicochemical properties and the origin of cobalt oxide.

Chapter 3: Thermodynamic equilibrium calculations - where HSC chemistry software is used to simulate and predict product formation of our reaction studies.

Chapter 4: Characterization of cobalt compounds - provides a detailed thermochemical characterization of the oxides as starting material utilized in our fluorination reactions.

Chapter 5: Reactions of Co_3O_4 with HF and F_2 - presents and discusses the results obtained from the fluorination of the mixed oxide (Co_3O_4) with hydrogen fluoride and fluorine, reactions of cobalt difluoride with fluorine and the sequential fluorination of Co_3O_4 with hydrogen fluoride and then fluorine in a single experimental run.

Chapter 6: Reactions of CoO with HF and F_2 - presents and discusses the results obtained for the fluorination of CoO with HF as well as with F_2.

Chapter 7: Conclusion and recommendations - covers the conclusions and recommendations of the work.

2 Literature study

2.1 Introduction

Hydrocarbons are organic compounds made up of carbon and hydrogen atoms C_xH_y, whilst fluorocarbons are composed of carbon and fluorine atoms, C_xF_y, with some or all of the hydrogen atoms replaced with fluorine atoms. It is the combination of the stronger bond between carbon and fluorine, and the relative smaller size of the fluorine atom that makes the replacement of hydrogen atoms with fluorine atoms relatively easy (Sen et al., 1987). Fluorine is the element with the highest electronegativity, and the bond between fluorine and carbon is known to be one of the strongest bonds in organic chemistry (O'Hagan, 2008). Fluorocarbons possess unique physical and chemical properties which makes these compounds attractive within the refrigerant and pharmaceutical industries (Sandford, 2003).

Fluorocarbons are colorless compounds with a high density, and low surface energy which makes these compounds immiscible in most organic solvents like ethanol and acetone. One prominent known fluorocarbon is tetrafluoroethylene (TFE), a monomer of polytetrafluorotheylene (PTFE) better known as Teflon™.

Fluorine gas (F_2) has been used for the conversion of hydrocarbons to fluorocarbons for some time. However, F_2 is known to be extremely reactive and highly expensive, and a process in which fluorine is used as the sole fluorinating agent, though feasible, could result in high operational costs incurred. Fluorine is ten times more expensive than hydrogen fluoride gas (Banks et al., 1994). For this reason, this study focuses on alternative fluorinating agents that would yield the same objective, though with less energy of reaction consumed.

Transition metal fluorides like CoF_3, AgF_2 and MnF_3 are known to be powerful fluorinating agents for the conversion of hydrocarbons to fluorocarbons and were identified as ideal

compounds for this purpose. Compared to fluorination with F_2, CoF_3 results in less energy evolved (Haszeldine and Smith, 1950). However, obtaining CoF_3 from the commercial market was costly and the material was a challenge to handle owing to its susceptibility to atmospheric moisture. The viable option would therefore be to synthesise CoF_3 from the mixed oxide, Co_3O_4. HF and F_2 gases are known to be useful fluorinating agents for the preparation of higher metal fluorides from metal oxides (Tumarov, 1993). Hence, methods for the synthesis of CoF_3 were investigated through treatment of the oxide with HF and F_2 gases. The CoF_3 synthesised will in turn be used as a fluorinating agent for the conversion of fluorocarbons from hydrocarbons. This process would yield significant savings in costs as HF was less expensive in comparison to F_2. The price of HF is reported to be US$1-3/kg while that of F_2 is US$15-20/kg (Crouse, 2015). The process in which F_2 is used as fluorine source is energy consuming with fragmentation of the hydrocarbon a possibility (Chambers, 2004). On the other hand, fluorination with cobalt trifluoride was found to be less exothermic and seen as an ideal fluorinating agent for fluorocarbon synthesis (Lewandowski et al., 2006).

2.2 Occurrence and physical properties of cobalt metal

Cobalt (Co) is a hard, bluish-white shiny metal with a density of 8.9 g/cm^3 , and a melting and boiling point of 1493 ^{o}C and 3100 ^{o}C respectively (Report on Critical Raw materials, 2014). Co is a transition metal found between nickel (Ni) and iron (Fe) in the periodic table, hence the similar magnetic and corrosion resistance properties.

Cobalt metal was first discovered in 1935 by the Swedish chemist Georg Brandt, and established as an element in 1980 by Torbern Bergman (Fisher, 2011, Hamilton, 1994). The metal is never found in its pure form but always associated with nickel or copper ore deposits (Enghag, 2000). As a result, cobalt is often extracted as a by-product during the processing of nickel and copper minerals (Cotton and Wikinson, 1962). The Cobalt Development Institute reported in 2010 that the supply of approximately 50% of cobalt originated from nickel ores, 35% from copper ores and 15% from primary cobalt operations (Fisher, 2011). Some of the minerals known to contain cobalt include cobaltite (CoAsS),

smaltite ($CoAs_2$), erythrite ($Co_3(AsO_4)_2.8H_2O$), glucodot ($Co_{0.50}Fe_{0.50}AsS$) and many more composed of smaller amounts of the metal (Hamilton, 1994, Nicholls, 1973).

Depending on the origin and nature of the ore, various extraction methods are applicable. These methods are mainly composed of a combination of furnace, chemical and thermal reduction processes (Nicholls, 1973). One common method involves roasting of copper-cobalt ores obtained from the Democratic Republic of Congo (DRC) in a fluidized-bed furnace to convert sulphides to soluble oxides. The material is then leached with sulphuric acid, copper removed by electrolysis, and cobalt precipitated from the electrolyte as hydroxide. Finally the hydroxide is redissolved and cobalt obtained as metal through an electrolytic process (Fisher, 2011)

Cobalt-59 is the only stable naturally occurring isotope, and it is converted to cobalt-60 isomeric nuclei through thermal neutron bombardment (Enghag, 2000). The two isomers, ^{59}Co and ^{60}Co, decay through emission of β and γ-rays to a nonradioactive ^{60}Ni isotope. As a result of this, ^{60}Co has for some time been used as a source of γ-rays in radiation chemistry.

Cobalt metal is relatively unreactive under normal temperature and pressure, and only upon heating below 900 ^oC does it oxidize to the mixed oxide, Co_3O_4, which undergoes decomposition to CoO above 900 ^oC (Tang et al., 2008). During this decomposition process, it is important for cooling to be performed in a dry nitrogen atmosphere so as to avoid oxidation of CoO back to Co_3O_4 (Donaldson et al., 1986). Various other cobalt oxides are reported in literature. Some of which include CoO_2, Co_2O_3 and CoO(OH). Of these oxides, CoO and Co_3O_4 are the only ones known to be stable under atmospheric conditions and useful in industry. CoO and Co_3O_4 are reported to contain a cobalt content of about 78.7% and 73.4% respectively.

2.3 Properties and preparation of cobalt oxides

2.3.1 Physical properties of cobalt (II, III) oxide Co_3O_4

Co_3O_4 is a black solid with a molar mass of 240.80 g/mol and a melting point of 895 ^oC. The material is insoluble in water with a density of 6.11 g/cm^3. It is sometimes referred to as the mixed cobalt oxide as it possesses cobalt in both Co^{2+} and Co^{3+} valence states. This compound is also presented as $Co^{II}Co^{III}{}_2O_4$ or $CoO.Co_2O_3$ (Barceloux and Barceloux, 1999). The compound has a spinel structure in which the Co^{2+} and Co^{3+} occupy the tetrahedral and octahedral sites respectively (Cotton and Wikinson, 1962).

2.3.2 Preparation of Co_3O_4

There are various methods reported in literature for the manufacture of Co_3O_4. Cotton and Wikinson (1962) reported formation of Co_3O_4 through heating of CoO in air at 400- 500 ^oC to take place as in equation (2-1):

$$6CoO(s) + O_2(g) \rightarrow 2Co_3O_4(s) \qquad (2\text{-}1)$$

Cobalt (II,III) oxide may also be prepared through controlled oxidation of cobalt metal at ca. 900 ^oC,

$$3Co(s) + 2O_2(g) \rightarrow Co_3O_4(s) \qquad (2\text{-}2)$$

as well as through pyrolysis of cobalt (II) chloride

$$3CoCl_2(s) + O_2(g) \rightarrow Co_3O_4(s) + Cl_2(g) \qquad (2\text{-}3)$$

2.3.3 Physical properties of cobalt (II) oxide, CoO

Cobalt (II) oxide, CoO, is a grey inorganic compound with a molar mass of 74.93 g/mol and density of 6.44 g/cm^3. The compound has a cubic crystal structure and converts to Co_3O_4 on heating to 400 ^oC in air as in equation (2-1) (Nicholls, 1973).

2.3.4 Preparation of cobalt (II) oxide, CoO

Various other methods exist for the manufacture of cobalt (II) oxide which include electrolysis of a solution of cobalt chloride as shown in equation (2-4):

$$CoCl_2(s) + H_2O(g) \rightarrow CoO(s) + 2HCl(g) \quad (2\text{-}4)$$

Nicholls (1973) reported production of cobalt (II) oxide through the reaction of cobalt metal with carbon dioxide as in equation (2-5):

$$Co(s) + CO_2(g) \rightarrow CoO(s) + CO(g) \quad (2\text{-}5)$$

Donaldson et al. (1986) reported the manufacture of CoO through controlled oxidation of the metal above 900 ^oC, followed by cooling in nitrogen atmosphere. CoO may also be formed through the decomposition of Co_3O_4 at 900 ^oC in a nitrogen atmosphere.

2.4 Properties and preparation of cobalt fluorides

2.4.1 Physical properties of cobalt (II) fluoride, CoF_2

Cobalt (II) fluoride is a pink crystalline solid with a molar mass of 96.93 g/mol and a density of 4.46 g/ml. CoF_2 has a melting point and boiling point of 1200 ^oC and 1400 ^oC respectively. The compound is sparingly soluble in water, alcohol and acetone. Two forms of cobalt (II) fluoride known are known, the tetrahydrate red orthogonal crystal, $CoF_2.4H_2O$ as well as the anhydrous red tetragonal crystal, CoF_2. The tetrahydrate powder is pink with a melting poing and density of 200 ^oC and 2.19 g/ml respectively. The anhydrous compound is reported to possess a rutile structure in which the Co^{2+} ion is octahedrally coordinated.

2.4.2 Preparation of cobalt (II) fluoride, CoF_2

According to Nicholls (1973), CoF_2 can be prepared through heating of cobalt (II) oxide or cobalt (II) chloride in a stream of hydrogen fluoride as expressed in equations (2-6) and (2-7):

$$CoO(s) + 2HF(g) \rightarrow CoF_2(s) + H_2O(g) \quad (2\text{-}6)$$

$$CoCl_2(s) + 2HF(g) \rightarrow CoF_2(s) + 2HCl(g) \quad (2\text{-}7)$$

Though CoF_2 can be prepared through the reaction of $CoCl_2$ with hydrogen fluoride, this method was discarded as it was considered environmentally unfriendly and required further purification of the product (Kirk Othmer, Encyclopedia of Chemical Technology). Cotton and Wikinson (1962) reported formation of anhydrous CoF_2 through reaction of Co metal with HF at 300-400 ^oC. CoF_2 is also formed through exposure of CoF_3 to atmospheric moisture, with hydrogen fluoride released as by-product (Li et al., 2016):

$$2CoF_3(s) + H_2O(g) \rightarrow 2CoF_2(s) + 2HF(g) + 0.5O_2(g) \quad (2\text{-}8)$$

CoF_2 can be used as a catalyst to alloy metals, as well as for optical deposition where it improves optical quality. CoF_2 is also reported to be useful as an anode material for lithium ion batteries (Tan et al., 2015).

2.4.3 Physical properties of cobalt (III) fluoride, CoF_3

Cobalt (III) fluoride is a brown inorganic compound with the formula mass of 115 g/mol, melting point of 927 ^oC and a density of 3.88 g/cm^3. CoF_3 possesses a hexagonal crystal structure and readily reacts with water from the atmosphere to form CoF_2, releasing HF gas in accordance to equation (2-8). It is thus of utmost importance that the CoF_3 synthesis process be carried out in an inert dry atmosphere so as to avoid exposure of the material to atmospheric moisture. Nicholls (1973) reported heating of CoF_3 at inert temperatures above 350 ^oC to produce CoF_2 with F_2 evolved as in equation (2-9), whilst heating in air results in CoF_2 that eventually transforms to the mixed oxide (Co_3O_4) at 400-500 ^oC, equation (2-10):

$$2CoF_3(s) \rightarrow 2CoF_2(s) + F_2(g) \quad (2\text{-}9)$$

$$3CoF_2(s) + 2O_2(g) \rightarrow Co_3O_4(s) + 3F_2(g) \quad (2\text{-}10)$$

Heating in vacuum yields cobalt metal as in equation (2-11):

$$2CoF_3(s) + heat \rightarrow 2Co(s) + 3F_2(g) \quad (2\text{-}11)$$

2.4.4 Preparation of cobalt (III) fluoride, CoF_3

Cobalt fluoride can be manufactured through the reaction of cobalt (II) chloride with fluorine gas (Priest, 1950). First the cobalt chloride is dehydrated in a porcelain dish, and transferred into a hot porcelain mortar and ground to uniform powder. The powder is then transferred into a nickel reactor tray with constant flow of dry nitrogen. Fluorine is then fed into the reactor, heated to 250 ^oC and kept at this temperature for 3 hours to allow the fluorination process to complete. Completion is ascertained by the absence of chlorine from the exit gas. Fluorine is then purged from the system with dry nitrogen gas prior to product collection. The container is then placed beside the reactor, reactor cap opened, the tray is withdrawn and product transferred to the can as rapidly as possible to minimize exposure to the atmosphere. The reaction takes place according to equation (2-12):

$$2CoCl_2(s) + 3F_2(g) \rightarrow 2CoF_3(s) + 2Cl_2(g) \qquad (2\text{-}12)$$

Belmore et al.,(1947) also reported CoF_3 production through reaction of $CoCl_2$ with F_2 at 250 ^oC, as did Friedt and Adloff (1969) albeit at a slightly higher temperature of 450 ^oC.

Other methods for preparing CoF_3 involves the reaction of cobalt (II) oxide or cobalt difluoride with fluorine gas as in equations (2-13) and (2-14):

$$2CoO(s) + 3F_2(g) \rightarrow 2CoF_3(s) + O_2(g) \qquad (2\text{-}13)$$

$$2CoF_2(s) + F_2(g) \rightarrow 2CoF_3(s) \qquad (2\text{-}14)$$

Girichev et al. (1993) reported on the synthesis of CoF_3 through fluorination of the tetrahydrate difluoride, $CoF_2.4H_2O$, with F_2 gas at atmospheric pressure. This occurs through dehydration of the material (eq (2-15)) followed then by fluorination of the difluoride as in equation (2-16) to give a light brown product:

$$2CoF_2.4H_2O(g) \rightarrow 2CoF_2(s) + 4H_2O(g) \qquad (2\text{-}15)$$

$$CoF_2(s) + 0.5F_2(g) \rightarrow CoF_3(s) \quad (2\text{-}16)$$

According to Nicholls (1973), finely divided cobalt metal reacts with F_2 gas at 500 ^oC to form a mixture of CoF_2 and CoF_3:

$$3Co(s) + 4F_2(g) \rightarrow CoF_2(s) + 2CoF_3(g) \quad (2\text{-}17)$$

Nicholls (1973) further reported on the formation of CoF_3 through reaction of cobalt metal and chlorine trifluoride as in equation (2-18):

$$2Co(s) + 2ClF_3(g) \rightarrow 2CoF_3(s) + Cl_2(g) \quad (2\text{-}18)$$

2.5 Production of cobalt (III) fluoride and its applications

During "The Manhattan Project", a need arose for materials that could handle the highly reactive and corrosive uranium hexafluoride (UF_6) (Banks et al., 1994). Fluorocarbons were discovered as unreactive to UF_6 and was therefore considered the ideal material for this purpose. This prompted method development on the manufacture of these fluorine containing organic compounds (Grosse and Cady, 1947). The two stage Fowler process was then developed. In the first stage, CoF_3 is prepared through the reaction of CoF_2 with F_2 (eqn (2-19)). CoF_3 is then used in the second stage as a fluorine source to convert the hydrocarbon to a fluorocarbon, with simultaneous conversion of CoF_3 back to CoF_2 (eqn (2-20)):

$$2CoF_2(s) + F_2(g) \rightarrow 2CoF_3(s) \quad (2\text{-}19)$$

$$2CoF_3(s) + R - H(g) \rightarrow 2CoF_2(s) + R - F(g) + HF(g) \quad (2\text{-}20)$$

The CoF_2 formed during fluorination of the hydrocarbon (eq (2-20)) can be reused, and fluorinated again with F_2 gas to CoF_3 (eqn (2-19)). The second stage is less vigorous and exothermic than the direct reaction of the hydrocarbon with fluorine, mainly because the enthalpy of the reaction is divided into two parts. The enthalpy change for the direct replacement of a hydrogen atom bonded to carbon for a fluorine atom is halved when the transformation is carried out using CoF_3 rather than F_2 (Goldwhite, 1986).

Various applications of the Fowler process in which CoF_3 acts as a fluorine source to fluorinate both the aliphatic and aromatic organic compounds are described in the literature. For example, fluorination of butane to yield a complex of partially fluorinated compounds, in which the secondary C-H are preferentially fluorinated to C-F in comparison to the primary atoms (Burdon et al., 1988). The fluorination of propane (Burdon and Garnier, 1991) and butane (Burdon et al., 1988) has been reported, with CoF_3 being used in both fluorinations. Cyclopentane can also be fluorinated with cobalt fluoride at 300-525 ^{o}C to yield polyfluorocyclopentane and polyfluoropentanes (Bergomi et al., 1966). The latter arise as a result of ring opening or impurities from the 95% cyclopentane. Mizukado et al. (2006) reported on fluorination of fluoro-cyclobutene with CoF_3 whereby vicinal-difluorination proceeds preferentially. Fluorination of 1.2-dichlorobenzene through cobalt trifluoride where different kinds of chlorofluorocyclohexanes are produced has been reported (Radeck et al., 1991).

Other applications of CoF_3 are also reported, as in the battery industry where the material is seen as a potential electrode material for rechargeable batteries (Li et al., 2018).

3 Thermodynamic equilibrium calculations

3.1 Introduction

In this chapter the thermodynamic equilibrium calculations were performed with the intention to simulate product formation and provide ideal process conditions for laboratory testing. Thermodynamic equilibrium calculations makes it possible to predict reaction products without having to perform the tedious trial and error experiments in the laboratory (Roine, 2002). The equilibrium composition calculations were performed using HSC Chemistry, version 6.1 (Outotec, 2007) software program. This program offers a practical way to observe effects on product composition of process variables based on the amount of raw material, temperature and species of the system (Roine, 2002). In our case, thermodynamic equilibrium calculations were performed on the following reactions:

- Co_3O_4 with anhydrous hydrogen fluoride and fluorine gas respectively
- CoF_2 with fluorine gas, and lastly
- CoO with anhydrous hydrogen fluoride and fluorine gas respectively

Our primary focus was on the reaction of Co_3O_4 with hydrogen fluoride gas to form the lower metal fluoride, CoF_2, and the subsequent reaction of CoF_2 with F_2 gas to yield the higher metal fluoride, CoF_3 as the final product. Additional thermodynamic calculations were carried out on another oxide form, CoO, also with hydrogen fluoride and fluorine gas to form CoF_2 and CoF_3 respectively. These calculations provide valuable exploratory and feasibility studies for product formation from the respective reactants provided to the system.

The state of a system at thermodynamic equilibrium is one in which a thermodynamic potential is minimized, or for which the entropy is maximized for specific conditions (Zeleznik and Gordon, 1960). Two such potentials are the Helmholtz free energy, *A*, as well as the Gibbs free energy, *G*. For a system at constant temperature and volume,

thermodynamic equilibrium is reached when the Helmholtz free energy (*A*) is at a minimum. On the other hand, a system at constant temperature and pressure reaches a thermodynamic equilibrium when the Gibbs free energy (G) is at a minimum (Lwin, 2000). Of the two thermodynamic potentials, the Gibbs energy minimization (GEM) method is more commonly used simply because there is more interest in conditions of equilibrium when systems are at constant pressure than constant volume (Atkins, 1978, White et al., 1958, Zeleznik and Gordon, 1960). The GEM method was therefore used in our study for equilibrium composition calculations.

The program uses entropy (*S*) and enthalpy (*H*) to calculate the Gibbs energies of the individual components in the system as presented in equation.

$$\Delta G = \Delta H - T\Delta S \tag{3-1}$$

For a multi-component chemical system, the Gibbs free energy is equal to the sum of the Gibbs free energies of the individual components. The equilibrium composition is therefore determined through calculation of the Gibbs free energies of all possible combinations of chemical elements, and the total Gibbs free energy is minimized (White et al., 1958). However, it is important to note that the program is limited only to pure substances and ideal conditions in a closed system (Lwin, 2000). Additional limitations of the program include factors related to reaction kinetics, as well as mass and heat transfer issues. It is therefore crucial for experimental work to be performed for verification purposes. However, the program remains a versatile tool in the design and planning of experiments.

HSC chemistry possesses fourteen calculation models displayed as fourteen options in the HSC menu as follows:

1. Reaction Equations
2. Heat and Material Balances
3. Heat Loss Calculator
4. Equilibrium Composition
5. Electrochemical Cell Equilibrium
6. Eh - pH – Diagrams
7. H, S, C and G Diagrams
8. Phase Stability Diagrams
9. Formula Weights
10. Mineralogy Iterations
11. Water/Steam Tables
12. Conversions
13. Elements
14. Measure Units

The "Equilibrium Composition" module was employed as a method of choice for our equilibrium calculations. The equilibrium composition module has the capacity to calculate equilibrium compositions in heterogeneous systems. This is achieved through specifying a range of temperatures, pressure and quantities of raw material quantities. The program then calculates equilibrium compositions that are then plotted as a function of pressure, temperature or starting material. This information makes it possible to predict product formation from specific reactants. Also included within the program is the basic thermochemical database with enthalpy (H), entropy (S), and heat capacity (C_p) data for more than 28 000 of the most common species used in chemical industry.

The HSC program therefore makes conventional thermodynamic calculations fast and easy to perform through simple usage of personal computers. This is a valuable tool within research industries and academic institutions for the development of new chemical processes as well as improvement of old ones. Traditionally ideas were tested by writing out reaction equations and then calculating equilibrium constants and heats of reaction from standard thermochemical data available. All this can now be achieved instantly by simply typing the reaction equations in the input field and the HSC software will give the heat of reactions, equilibrium constants and amount of species at various temperatures.

Much as HSC Chemistry software is advantageous, it cannot offer solutions to all chemical problems as it does not take into consideration the kinetics of chemical reactions and non-ideality of solutions. Be that as it may, HSC chemistry software remains a versatile, fast,

and inexpensive tool to help establish ideal reaction conditions for various experimental investigations.

3.2 Equilibrium composition calculations

The thermodynamic equilibrium calculations for various reactions were performed at standard atmospheric pressure and temperatures ranging from 0 to 1000 ^{o}C. The equilibrium composition of Co_3O_4 with HF and F_2 are presented.

3.2.1 The Co_3O_4-HF system

The equilibrium composition for the reaction of Co_3O_4 with anhydrous HF calculated at temperatures of 0 to 1000 ^{o}C is presented in equation (3-2).

$$Co_3O_4(s) + 6HF(g) \rightarrow 3CoF_2(s) + 3H_2O(g) + 0.5O_2(g) \qquad (3\text{-}2)$$

Figure 3.1 shows the thermodynamic equilibrium composition calculation for the reaction of Co_3O_4 (1 kmol) with HF (6 kmol) from 0 to 1000 °C.

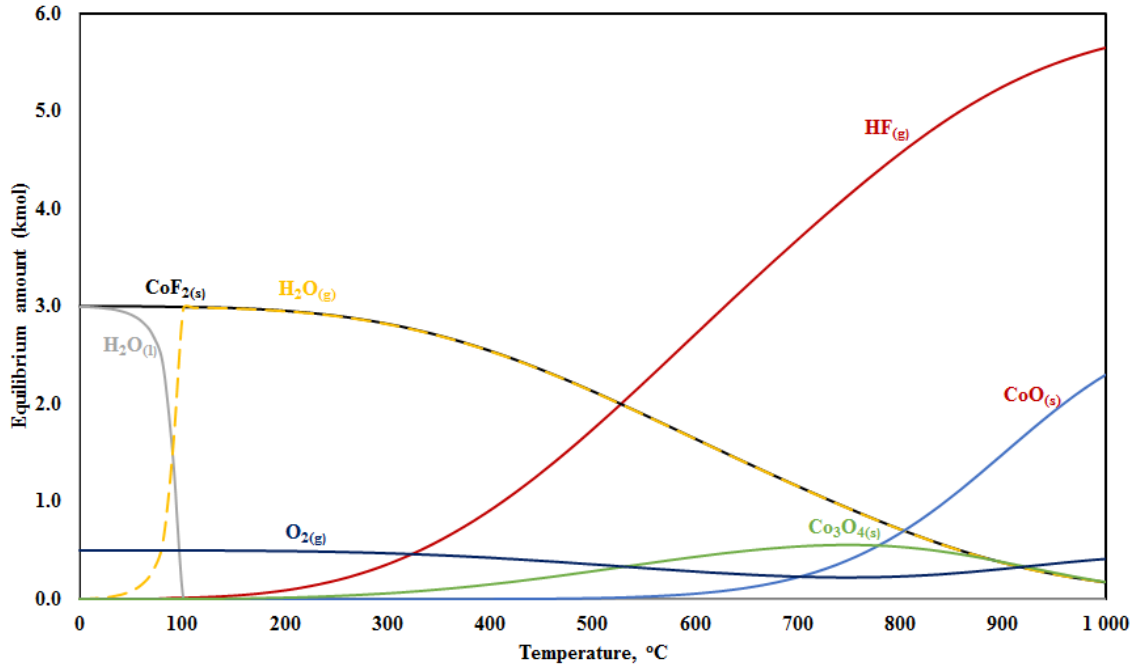

Figure 3.1. The thermodynamic equilibrium calculation for the reaction between Co_3O_4 and HF.

In Figure 3.1, CoF_2 and H_2O are predicted to form at low temperatures, whilst O_2 is predicted to form over the full temperature range studied. Most transition metal oxides were found to form oxyfluorides on reaction with hydrogen fluoride. (Pienaar et al., 2012, Vilakazi et al., 2012). Using the same analogy, fluorination of cobalt oxide with HF was anticipated to form cobalt oxyfluorides. However, no oxyfluoride formation was predicted as shown in Figure 3.1. The the fact that no cobalt oxyfluoride was predicted from our thermodynamic equilibrium calculations, does not preclude its formation. This simply shows the unavailability of the oxyfluoride specie from the HSC database. Hence, the formation of cobalt oxyfluoride could not be predicted by the software program. Also predicted from our equilibrium composition, is that H_2O starts evaporating from approximately 50 °C, with total conversion to the vapour phase at 100 °C. The CoF_2 formed is predicted to react with water vapour to form Co_3O_4 and HF from just above 150 °C. This implies that the reverse reaction of equation (3-2) is predicted to take place at temperatures above 150 °C. Based on the thermodynamic data, the forward reaction presented in

equation (3-2) is expected to reach completion at temperatures below 150 °C. However the presence of water is predicted to shift the reaction to the left just above 150 °C. Thus, constant sweeping of O_2 and H_2O is critical in order to force the reaction to the right and yield CoF_2 as preferred product. Also predicted is the initial formation of CoO at temperatures above 600 °C, from the decomposition of Co_3O_4.

3.2.2 The Co_3O_4-F_2 system

$$Co_3O_4(s) + 4.5F_2(g) \rightarrow 3CoF_3(s) + 2O_2(g) \qquad (3\text{-}3)$$

Figure 3.2 shows the equilibrium composition calculation for the reaction of Co_3O_4 (1 kmol) with F_2 (4.5 kmol) from 0 to 1000 °C.

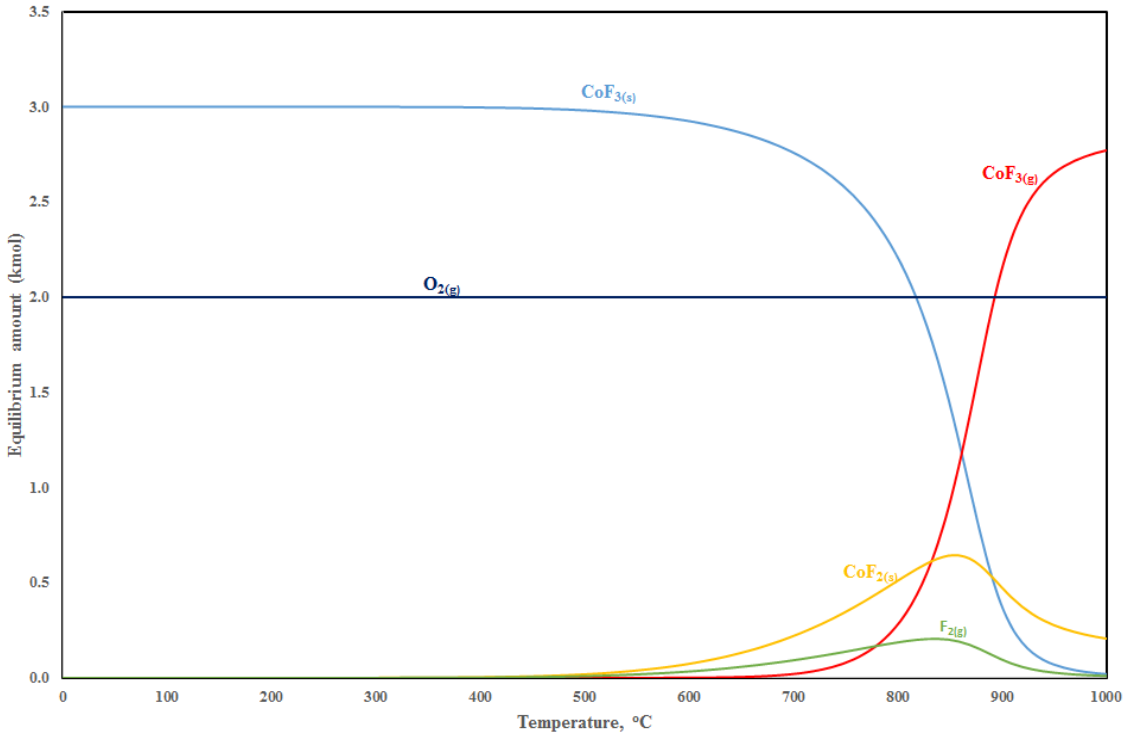

Figure 3.2: The thermodynamic equilibrium calculation for the reaction between Co_3O_4 with F_2.

The diagram predicts CoF_3 formation between 0 to about 500 ^oC. Fluorine is known to be the stronger fluorinating agent when compared to hydrogen fluoride (Muetterties and Castle, 1961). Hence the reaction with F_2 is expected to form the highest known cobalt metal fluoride, CoF_3. The CoF_3 formed decomposes to CoF_2 and F_2 at temperatures above 500 ^oC, whilst some of the CoF_3 starts evaporating just above 650 ^oC. O_2 is predicted to form over the full temperature range studied. From the thermodynamic data, the CoF_3 formed decomposes and sublimates just above 500 ^oC. Literature reports various decomposition temperatures based on experimental conditions (Li et al., 2018, Popovic et al., 2001). Balducci et al. (1997) reports decomposition and sublimation of CoF_3 on a torsion effusion method to take place at 427- 557 ^oC (Balducci et al., 1997). These findings correspond well with our thermodynamic predictions where both sublimation and decomposition are predicted to occur just above 500 ^oC. It is therefore vital for the reaction temperature not to exceed 500 ^oC to improve on the product yield.

3.3 The reaction of CoO with HF and F_2

3.3.1 The CoO-HF system

$$CoO(s) + 2HF(g) \rightarrow CoF_2(s) + H_2O(g) \quad (3\text{-}4)$$

The thermodynamic equilibrium composition calculation for the reaction of CoO (1 kmol) with HF (2 kmol) from 0 to 1000 ^{o}C is shown in Figure 3.3.

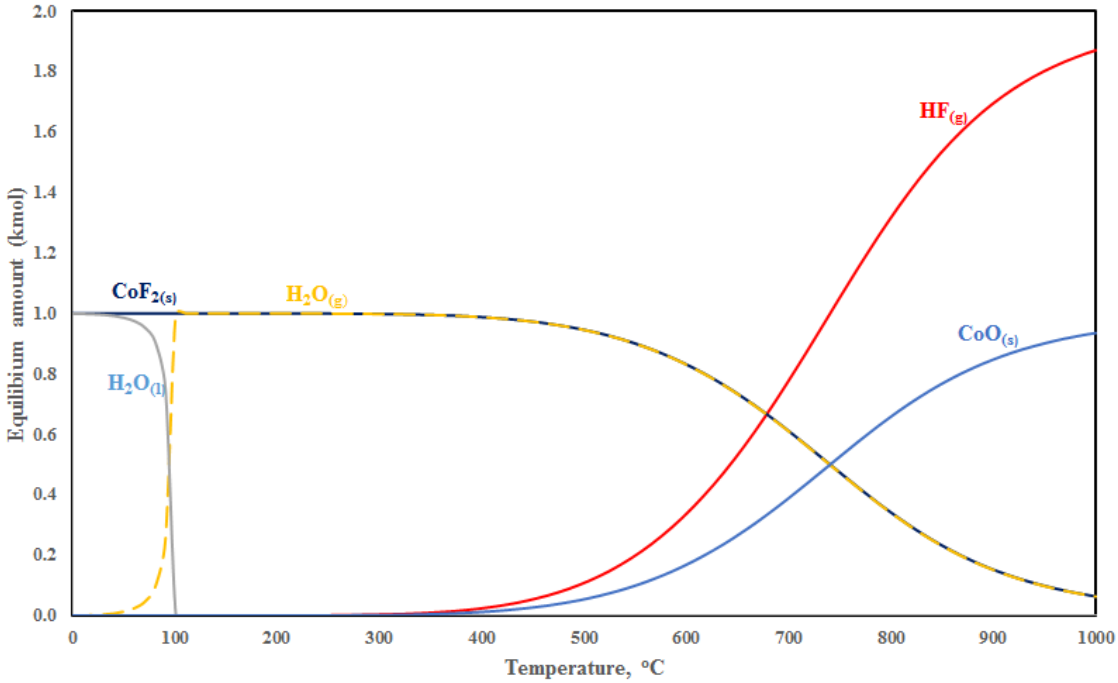

Figure 3.3: The thermodynamic equilibrium calculation for the reaction between CoO with HF.

The thermodynamic equilibrium composition for the reaction of CoO (1 kmol) with HF (2 kmol) predicts formation of CoF_2 and H_2O between 0 and 300 ^{o}C temperature range Figure 3.3. The H_2O is predicted to evaporate from 50 ^{o}C, with complete evaporation at 100 ^{o}C. Above 350 ^{o}C, CoF_2 is predicted to react with the gaseous water to form CoO and HF. This suggests shifting of the equilibrium reaction, as presented in equation (3-4), to the left. From the thermodynamic data, we can predict formation of CoF_2 to reach completion below 300 ^{o}C. At temperatures exceeding 300 ^{o}C, the equilibrium shifts to the left due to the reaction of CoF_2 with gaseous water. Water removal is therefore vital to force the reaction to the right and obtain the desired product (CoF_2).

3.3.2 The CoO-F system

$$CoO + 3F_2(g) \rightarrow 2CoF_3(s) + O_2(g) \quad (3\text{-}5)$$

The thermodynamic equilibrium composition for the reaction of CoO (2 kmol) with F_2 (3 kmol) from 0 to 1000 ^oC is shown in Figure 3.4.

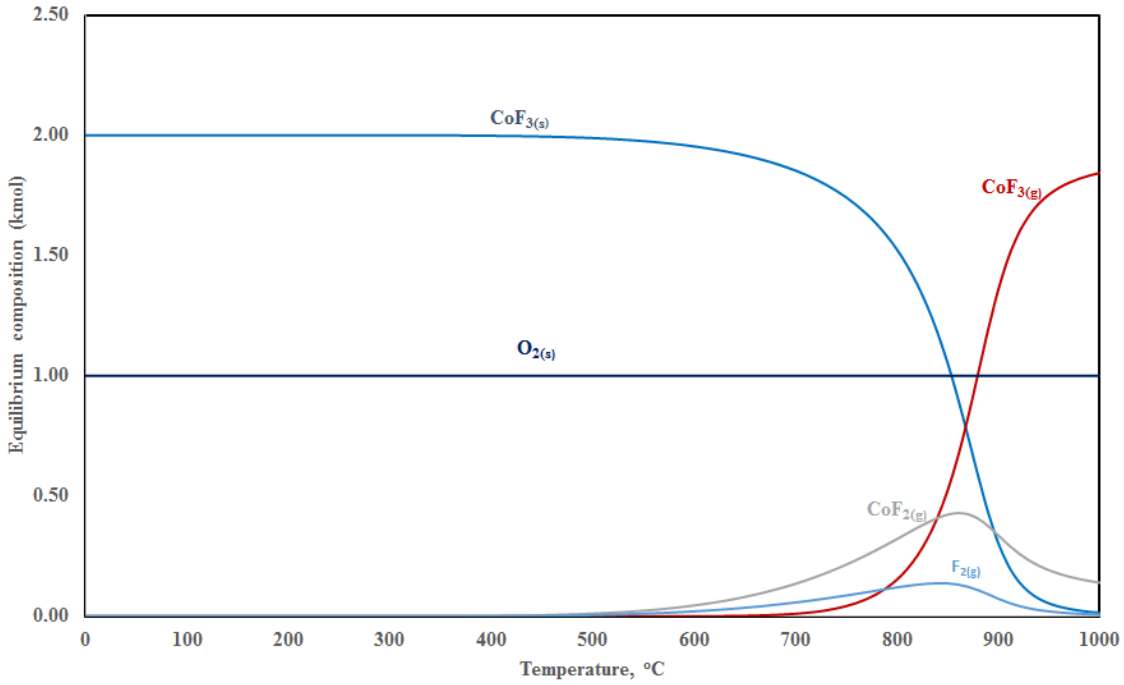

Figure 3.4: The thermodynamic equilibrium calculation for the reaction between CoO with F_2.

CoF_3 is predicted to form from very low from 0 to about 500 ^oC, whilst O_2 prevails stable from 0 to 1000 ^oC temperature range. Just as in the thermodynamic data obtained for the calculation Co_3O_4 with F_2, the CoF_3 formed is predicted to decompose into CoF_2 and F_2 just above 500 ^oC, with some (CoF_3) transforming into the gaseous form. The thermodynamic data predicts formation of CoF_3 from ambient temperature in accordance to equation (3-5). Whilst at temperatures above 500 ^oC, the decomposition and sublimation of CoF_3 is predicted.

3.4 The reaction of CoF_2 with F_2

3.4.1 The CoF_2-F system

$$2CoF_2(s) + F_2(g) \rightarrow 2CoF_3(s) \quad (3\text{-}6)$$

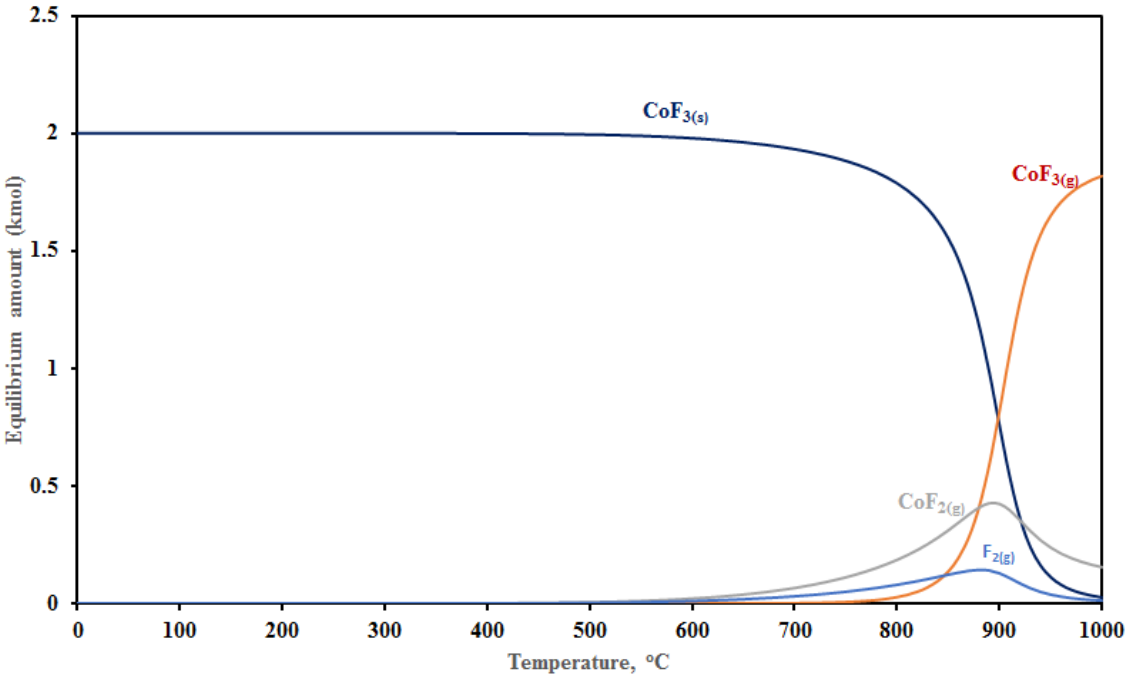

Figure 3.5: The thermodynamic equilibrium calculation for the reaction between CoF_2 with F_2.

The thermodynamic equilibrium composition for the reaction of CoF_2 (2 kmol) and F_2 (1 kmol) is depicted in Figure 3.5. Again, fluorine being the strongest fluorinating agent, forms the highest known cobalt fluoride, CoF_3. CoF_3 is predicted to form at over a temperature range of 0 to about 600 ^oC. At temperatures exceeding 600 ^oC, the decomposition of CoF_3 to CoF_2 and F_2, as well as transformation of some of the CoF_3 to the gaseous form is shown. Once again, it is important to keep the reaction temperature below 600 ^oC as the product transforms to the gaseous form at temperatures above this.

3.5 Conclusions

The HSC chemistry software has been successfully employed to predict products for reactions of Co_3O_4 with HF and F_2, CoO with HF and F_2 as well as CoF_2 with F_2 in a closed system. The equilibrium calculation for both Co_3O_4 and CoO oxides with HF predicts formation of CoF_2 at low temperatures. Also predicted, is that the CoF_2 formed reacts with H_2O at temperatures above 150 ^oC to form Co_3O_4 and HF. The presence of water plays a negative role in our quest to form CoF_2, and it is recommended that the water be removed to force the reaction to the right and form the desired product, CoF_2.

On the other hand, reactions of the cobalt oxides with F_2 are predicted to form CoF_3 at temperatures up to 500 ^oC. For temperatures exceeding 500 ^oC, both decomposition and sublimation of CoF_3 is predicted. The thermodynamic equilibrium calculation for the reaction of CoF_2 with F_2 predicts formation of CoF_3 from 0 to 600 ^oC. Again, the CoF_3 formed is predicted to decompose and sublimate at temperatures above 600 ^oC. It is therefore recommended that experiments be conducted at temperatures not higher than 500 ^oC, in order to avoid decomposition and sublimation of the product.

Much as thermodynamic equilibrium calculations are important in the planning and design of our experiments, it important to note that the program assumes a closed system. On the other hand, our TGA experimental setup operates in an open system where gaseous products formed are allowed to escape. As a result, some of the gaseous products predicted to form, e.g. H_2O and O_2, will escape. Deviations in the experimentally obtained results are therefore expected due to this limitation.

4 Thermal and spectroscopic characterization of commercial cobalt oxides and cobalt fluorides.

4.1 Introduction

The chemical reactivity of a material is related to its physical and chemical properties. This chapter is therefore devoted to a study on the thermal analysis and spectroscopic characterisation of commercial Co_3O_4, CoO and CoF_2 compounds used as starting materials in fluorination reactions. Also included is the thermal and spectroscopic characterization of commercial CoF_3, which is the desired product we intend synthesising in this study.

A thermogravimetric analyser (TGA) was used to follow the thermal behaviour of the oxides in oxidising (air) and inert (N_2) atmospheres. A comprehensive spectroscopic analysis of commercial compounds of the starting materials, as well as products obtained from decomposition experiments were done in order to assist with identification of these during fluorination reactions. Techniques used include X-ray powder diffraction (XRD), Attenuated Total Reflectance-Fourier Transform Infrared spectroscopy (ATR-FTIR) and Raman spectroscopy.

4.2 Experimental

4.2.1 Materials

Co_3O_4 (99.99% pure, CAS-1308-06-1), $CoF_2.4H_2O$ (99.99% pure, CAS-13817-37-3) and CoF_3 (99% pure, CAS-10026-18-3) were supplied by Sigma Aldrich Chemical Co. CoO (95% pure, CAS-1307-96-6) and anhydrous CoF_2 (98% pure, CAS-10026-17-2) were obtained from Alfa Aesar Chemical Co. Nitrogen gas (99.999% pure) and the synthetic air mixture (21% oxygen in nitrogen gas) were supplied by Air Liquide.

4.2.2 Characterization techniques employed

4.2.2.1 Thermogravimetric analyses (TGA)

Commercial samples of Co_3O_4, CoO and CoF_2 were characterized prior to treatment with HF and F_2 gases. The thermal behaviour of cobalt oxides and cobalt fluorides was studied using a TA Instruments SDT Q600 instrument. About 15 mg of sample was placed on an alumina pan and heated from ambient to various final temperatures at a heating rate of 10 ^oC/min under constant N_2 or air flow. Since analyses on the TA SDT Q600 instrument involves periodic exposure of samples to atmospheric moisture, a Perkin Elmer TGS-2 system was also employed, especially for samples sensitive to atmospheric moisture. The Perkin Elmer instrument is housed within a dry glovebox that precludes exposure of the sample to atmospheric moisture, and was more suitable for analysis of the moisture sensitive CoF_3 compound.

4.2.2.2 X-ray diffraction (XRD)

XRD analyses were collected on a Bruker D8 Advance diffractometer and interpreted in conjunction with International Centre for Diffraction Data (ICDD) Powder Diffraction Files (PDF-2) Release 2007 database for chemical phase identification. The measurement parameters were set as follows: target tube Cu; diffraction pattern range 22-100^o; step size 0.02^o; counting time 2.0 seconds. No sample preparation took place and the samples were analysed as received. The samples were loaded on an airtight specimen holder ring with dome-like X-ray transparent cap for environmentally sensitive materials. The sample reception has a 25 mm diameter and 1 mm depth.

4.2.2.3 Attenuated Total Reflectance Infrared spectroscopy (ATR-FTIR) analysis

The infrared reflectance spectra were acquired with Bruker's Tensor 70 FTIR spectrometer fitted with a Harrick MVP-Pro Diamond ATR cell. The force applied was 70N. The reflectance spectra were recorded over 400-4000 cm^{-1} range and averaged over 64 scans, using the total internal reflectance configuration with a diamond crystal. A resolution of 4 cm^{-1} was maintained throughout the analysis.

4.2.2.4 Raman spectroscopy

The Raman spectra were acquired with a Renishaw Invia spectrometer fitted with a 50x magnification lens. The spectra were recorded over 50-4000 cm^{-1} range using a 514.5 nm laser. A laser power of 10 mW was maintained throughout the analysis.

4.3 Results and Discussion

4.3.1 Thermal treatment of Co_3O_4 in N_2 and air

Thermogravimetric (TG) profiles of Co_3O_4 heated from ambient to 1200 ^oC in N_2 (black) and air (blue) are shown in Figure 4.1.

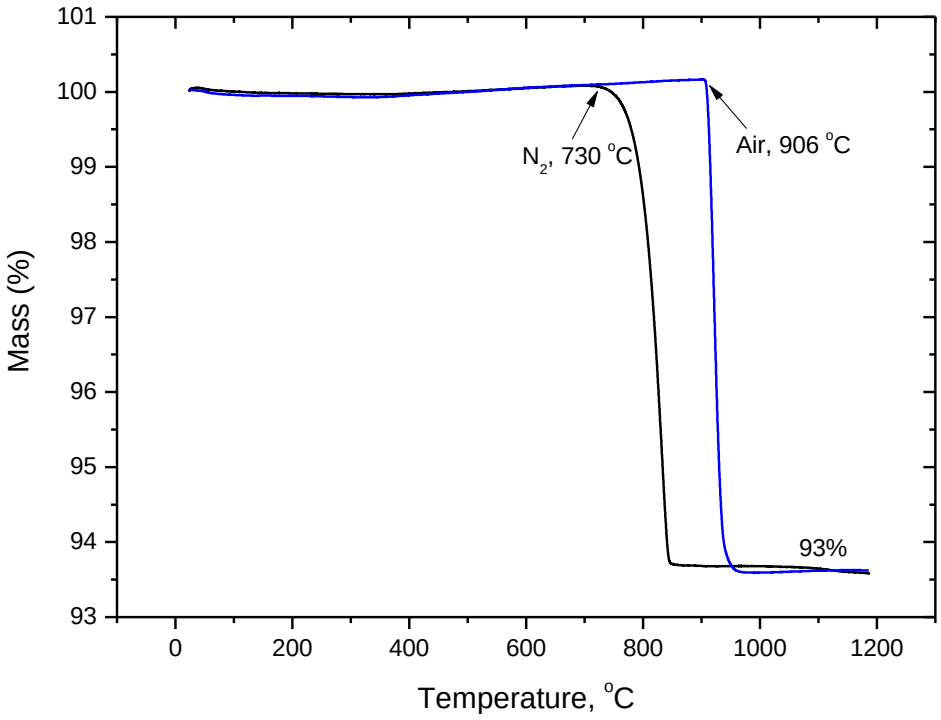

Figure 4.1: Thermogravimetric curves of Co_3O_4 heated from 30 to 1200 °C in N_2 (black) and air (blue).

In Figure 4.1 it is shown that Co_3O_4 decomposes at 730 °C and 906 °C in N_2 and air respectively. Both environments yield a single mass loss profile according to equation (4-1):

$$2Co_3O_4(s) \rightarrow 6CoO(s) + O_2(g) \qquad (4\text{-}1)$$

The 7% mass loss (Figure 4.1) agrees well with the theoretical value (6.6%) calculated for the decomposition of Co_3O_4 to CoO (equation (4-1)) and is consistent with that reported by Tang et al. (2008). On the other hand, Sakamoto et al. (1997) reported an endothermic peak from the decomposition of Co_3O_4 to CoO at 915° to 998 °C from differential thermal analysis (DTA). Risbud et al. (2005) also confirmed a structural change to take place on heating of Co_3O_4 beyond the endothermic peak. Based on the results reported in Figure 4.1, and supporting data

obtained from literature, Co_3O_4 was heated beyond 900 ^oC to ensure full decomposition and structural conversion to CoO.

Additional experiments were performed where the mass change was recorded on cooling the samples after heat treatment to 1000 ^oC was recorded. This was to determine the effect of cooling in either N_2 or air environment. The TG curve for the heat-cool cycle (Figure 4.2), shows that the mass loss (7%) observed on heating, is followed by mass gain of 1% and 7% on cooling in N_2 and air respectively. Cooling in air shows mass gain to reach a mass almost similar to the initial mass prior to decomposition of Co_3O_4. This indicates reoxidation of CoO to Co_3O_4 on cooling in air in accordance to reverse reaction of equation (4-2):

$$Co_3O_4(s) \rightleftharpoons 3CoO + 0.5O_2 \qquad (4\text{-}2)$$

The phenomenon of reoxidation of CoO to Co_3O_4 was also observed by Oku and Sato (1992) and Wang et al. (2014). The sample obtained from cooling in air was submitted for XRD analysis where the Co_3O_4 diffraction pattern was confirmed. This indicates the need for cooling to be performed in a N_2 atmosphere if CoO is the desired product. The solid residue obtained from decomposition performed in N_2 was confirmed through XRD as constituted of CoO, as in Figure 4.6 (to be discussed later).

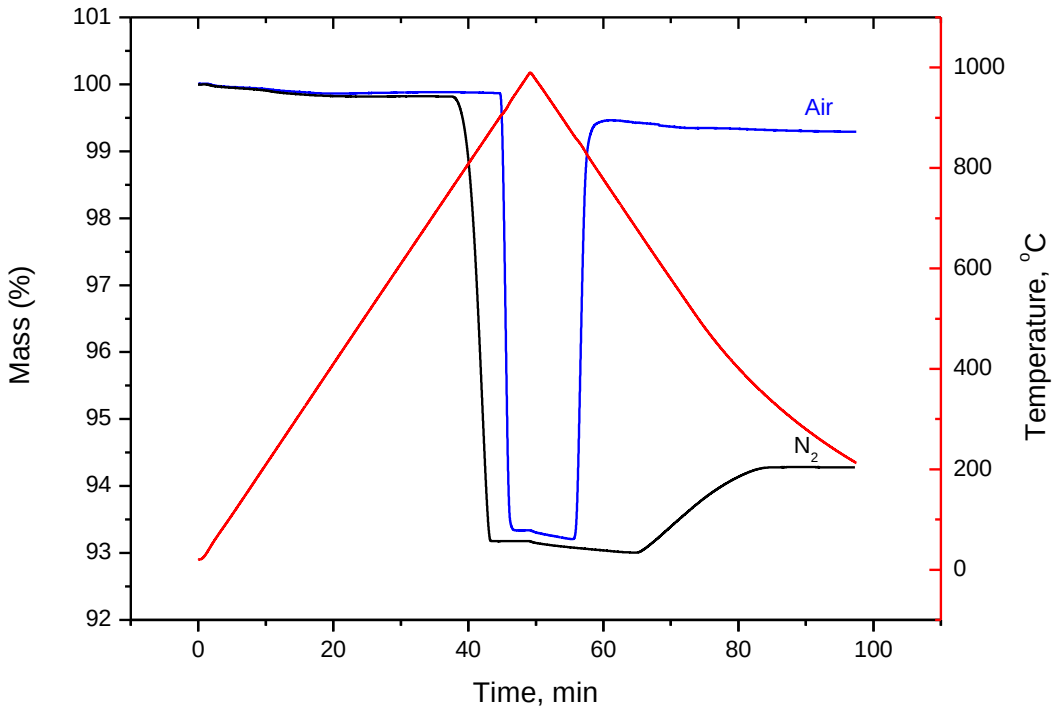

Figure 4.2: Thermogravimetric curves for the heat-cool cycle of Co_3O_4 in nitrogen (black) and air (blue).

4.3.2 Thermal treatment of CoO in N_2 and air

Similar set of experiments of heating in N_2 and air were performed on another oxide form, CoO. The TG curve for CoO heated in N_2 (black) and in air (blue) is shown in Figure 4.3.

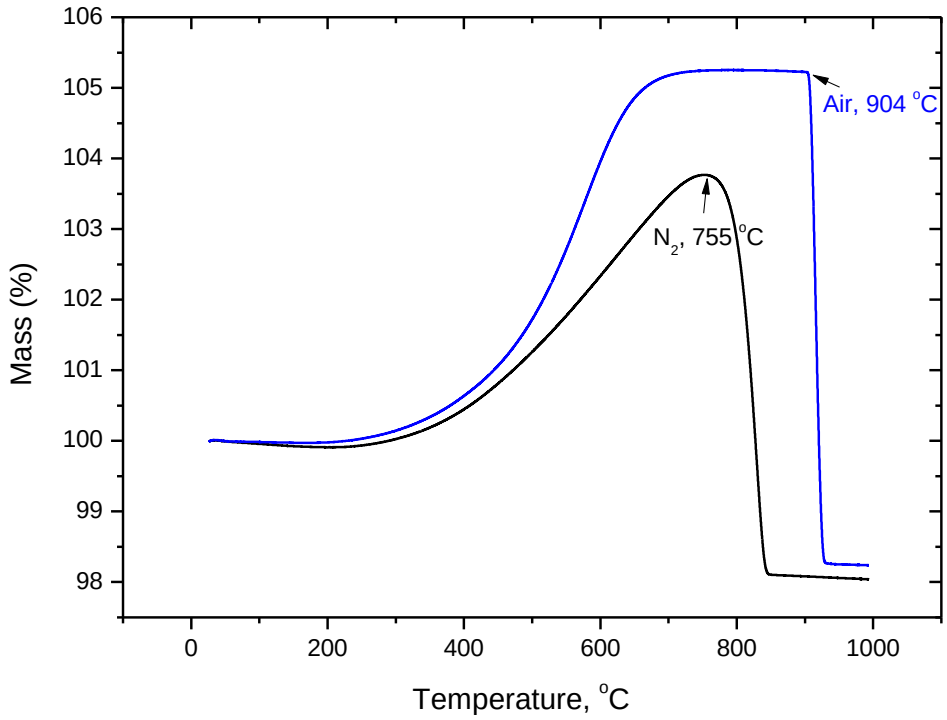

Figure 4.3: Thermogravimetric curves for CoO heated from 30 to 1000 °C in N_2 (black) and in air (blue).

A mass gain (+ 5%) was recorded from 280 °C, followed then by a mass loss (- 7%) at approximately 904 °C in air atmosphere. The initial mass gain suggests oxidation of CoO to Co_3O_4 via the reverse reaction in equation 4.2, with subsequent decomposition of Co_3O_4 to CoO at 904 °C via the forward reaction. Interestingly, the decomposition takes place at approximately the same temperature as previously recorded for the commercial Co_3O_4 compound (906 °C, Figure 4.1). This further supports reoxidation of CoO to Co_3O_4. The TG curve of CoO heated in nitrogen (Figure 4.3) also shows a mass gain (+ 4%) prior to decomposition at approximately 755 °C. The mass gain in N_2 cannot be explained at this stage, and further investigation will be performed at a later stage of the project.

4.3.3 Thermal treatment of CoF_3 in N_2

In Figure 4.4, the TG curve of CoF_3 heated from 30 to 800 ^oC at a heating rate of 10 ^oC/min under a constant flow of nitrogen gas is shown.

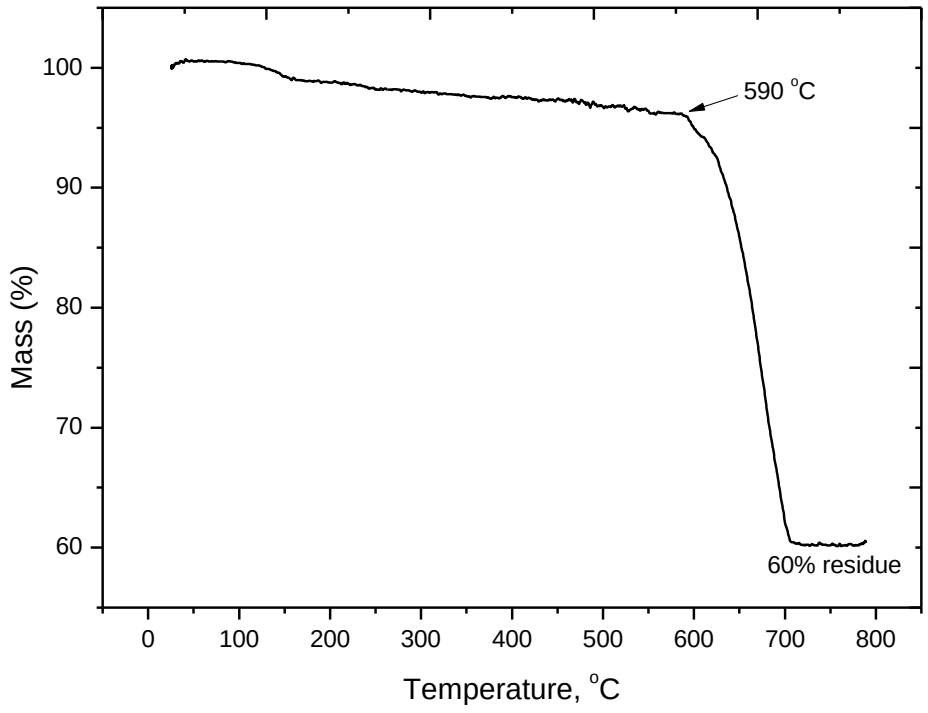

Figure 4.4: Thermogravimetric curve of CoF_3 heated from 30 to 800 ^oC in N_2.

The TG curve first shows a small mass loss around 150 ^oC attributed to loss of surface adsorbed water. This is followed by 40% mass loss from approximately 590 ^oC, ascribed to the decomposition of CoF_3 according to equation (4-3). Theoretically, the decomposition of CoF_3 to CoF_2 should be accompanied by a 16.4% mass loss. The higher mass loss recorded suggests that decomposition occurs simultaneously with sublimation of $CoF_3(s)$ to $CoF_3(g)$ as in equation (4-3):

$$2CoF_3(s) \rightarrow 2CoF_2(s) + F_2(g) \qquad (4\text{-}3)$$

$$CoF_3\ (s) \rightarrow CoF_3(g) \qquad (4\text{-}4)$$

The simultaneous decomposition and sublimation discovered was in agreement with what is reported in the literature. Leskiv et al. (2008) performed decomposition studies on CoF_3, and found that the decomposition of CoF_3(s) to CoF_2(s) is accompanied by sublimation of CoF_3(s). Balducci et al. (1997) performed a vapour pressure study on CoF_3 between 427-557 ^oC, and from the amount of residue CoF_2 obtained it was concluded that sublimation occur simultaneously with decomposition. The conclusion was made owing to the amount of residue material collected after heat treatment experiments. In our work in which the TGA is used, this is clearly shown from the higher mass loss (40%) recorded on the TG curve in Figure 4.4.

Rau et al. (1999) heated CoF_3 in a Knudsen cell and reported the presence of CoF_3 below 627 ^oC whilst CoF_2 was detected only at temperatures exceeding 627 ^oC. Louvain et al. (2014), on the other hand reported decomposition of CoF_3 in the presence of moisture to take place according to equation (4-5):

$$2CoF_3(s) + H_2O(g) \rightarrow 2CoF_2(s) + 2HF(g) + ½O_2(g) \qquad (4\text{-}5)$$

This shows that the presence of moisture promotes decomposition of CoF_3 to take place according to equation (4-5), and confirms the importance of having to maintain moisture free conditions in order to avoid decomposition of CoF_3 with subsequent formation of HF. It is advisable that fluorination reactions in which CoF_3 is the desired product be performed at temperatures below 600 ^oC. Fluorinations performed above 600 ^oC will result in reduced product yields as sublimation is predicted to take place at this temperature as it was shown in Figure 4.4.

4.3.4 Thermal treatment of $CoF_2.4H_2O$ in N_2

$CoF_2.4H_2O$ was heated from 30 to 600 °C at a heating rate of 10 °C/min under a constant flow of nitrogen purge gas as shown in Figure 4.5.

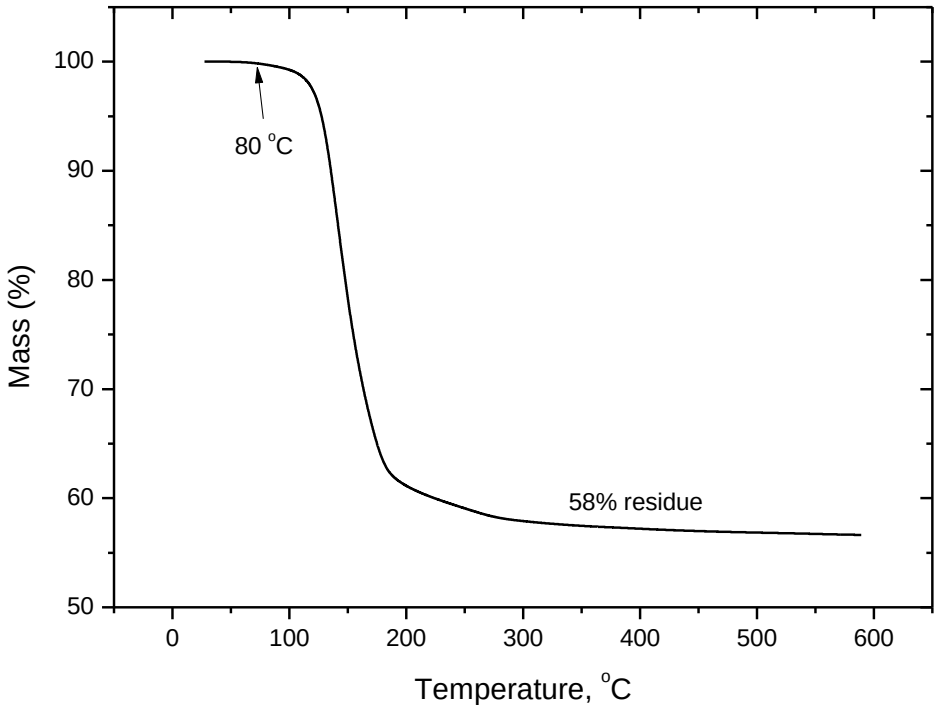

Figure 4.5: Thermogravimetric curve of $CoF_2.4H_2O$ heated from 30 to 600 °C in N_2.

A 42% mass loss was recorded within the 80 to 300 °C range, characteristic of the loss of four molecules of water to yield the anhydrous CoF_2 compound in accordance with equation (4-6).

$$CoF_2.4H_2O(s) \rightarrow CoF_2(s) + 4H_2O(g) \qquad (4\text{-}6)$$

This is consistent with the theoretical mass loss (42%) for the dehydration of $CoF_2.4H_2O$ to give anhydrous CoF_2. The TG curve indicates the temperature at which dehydration is

achieved. This provides valuable information as the intention was to carry out fluorination reactions on the anhydrous compound.

4.3.5 XRD results

The XRD pattern of the commercial CoF_3 (magenta), CoF_2 (cyan), CoO (blue), Co_3O_4 (red) and the product obtained from the decomposition of Co_3O_4 (black) are presented in Figure 4.6.

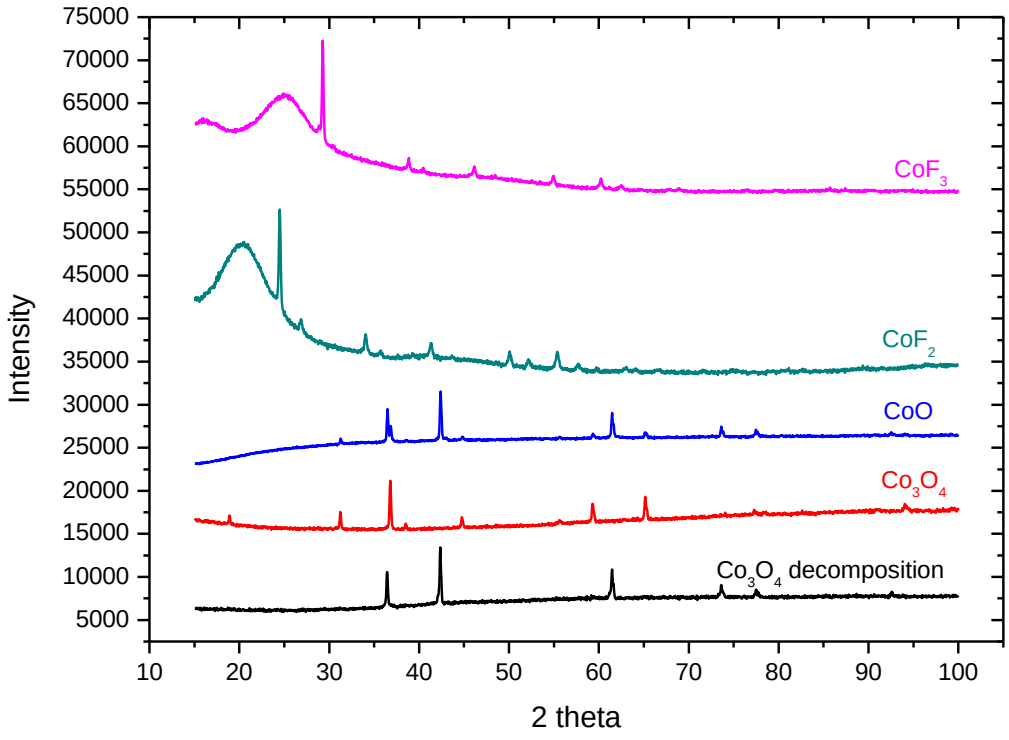

Figure 4.6: XRD patterns of commercial CoF_3 (purple), CoF_2 (cyan), CoO (blue), Co_3O_4 (red) and the product obtained from decomposition of Co_3O_4 (black).

The chemical composition was carried out using the ICDD PDF-2 Release 2007 database. The commercial CoF_3 presented an XRD pattern matching that of CoF_3 with a primitive rhombohedral structure and *R-3c*(167) space group. This is consistent with literature, where Hepworth et al. (1957) reported CoF_3 to have a *R-3c* space group. The XRD pattern for pure

CoF_2 (cyan) shows peaks with very low intensity, and a tetragonal structure with a *P42/mnm* (136) space group, quite consistent with Li et al. (2018). The humps are due to the amorphous content present in the two compounds. The tetrahydrate compound, $CoF_2.4H_2O$, was amorphous and its XRD data was therefore not included herein.

The diffraction pattern of commercial CoO (blue) matches that of CoO from the database, with some traces of a pattern matching Co_3O_4. The commercial Co_3O_4 sample (red) gave a pattern matching that of Co_3O_4 with a face centred cubic (fcc) structure and *Fd-3m* (227) space group. The product obtained from the decomposition and cooling of Co_3O_4 in N_2 showed patterns matching CoO with a face centred cubic structure and *Fm-3m* (225) space group. Risbud et al. (2005) reported CoO to crystallize in one of two stable phases, rock salt CoO (space group Fm3m) with octahedral Co^{2+}, whilst the spinel Co_3O_4 (Fd-3m) crystallizes with Co^{2+} and Co^{3+} tetrahedrally and octahedrally coordinated respectively.

Our experimental XRD data complements the TG results in Figure 4.2, where heating and cooling of Co_3O_4 in N_2 was shown to have decomposed to CoO. The XRD result showed commercial CoO to possess minor peaks that correspond to Co_3O_4. These peaks were not present from the product obtained from decomposition of Co_3O_4, suggesting that the product (CoO) obtained from decomposition of Co_3O_4, was purer than the commercial compound.

4.3.6 ATR-FTIR spectroscopy results

The ATR-FTIR spectra for commercial CoF_3 (purple), CoF_2 (cyan), CoO (blue), Co_3O_4 (red), and the product obtained from the decomposition of Co_3O_4 (black) are presented in Figure 4.7.

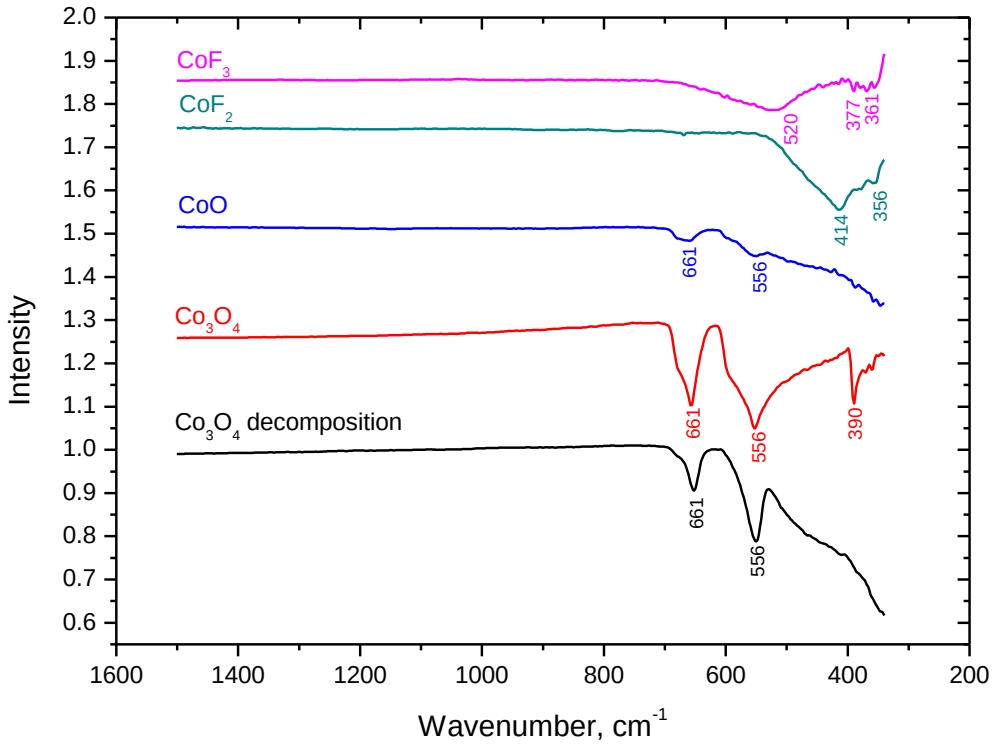

Figure 4.7: ATR-FTIR spectra of commercial CoF_3 (purple), CoF_2 (cyan), CoO (blue), Co_3O_4 (red) and the product obtained from decomposition of Co_3O_4 (black).

Only the range from 250 to 1500 cm^{-1} is displayed as there were no data peaks recorded beyond the 1500 cm^{-1} range. Three modes were recorded for the commercial CoF_3 compound at 361, 377 and 520 cm^{-1}. The commercial CoF_2 resulted in two modes at 356 and 414 cm^{-1}. Rau et al. (1999) detected modes for gaseous CoF_2 (v_3 and v_2) at 722.5 and 150.8 cm^{-1} respectively, through heat treatment of CoF_3 in an effusion cell. This author suggested the molecule to be linear, owing to the absence of the stretching mode (v_1) at 587cm^{-1} that was found to be present in the Raman spectra. He further reported FTIR spectra with bands at 161.2 and 736.9 cm^{-1} corresponding to gaseous CoF_3 below 627 ^oC, whilst only CoF_2 was detected above 627 ^oC.

Our experimental data differs from data reported in the literature, however our analyses were on the solid compounds while literature reports only on gaseous CoF_2 and CoF_3 compounds.

The commercial Co_3O_4 sample possessed three distinctive bands at 390, 556 and 661 cm^{-1}, whilst only two bands at 556 and 661 cm^{-1} were recorded for commercial CoO and the product obtained from decomposition of Co_3O_4. Christoskova et al. (1999) reported two distinctive bands for Co_3O_4, namely, the band associated with Co-O bond stretching (ν_1) at 571 cm^{-1} (associated with BOB_3 in the spinel lattice) and the ν_2 band at 664 cm^{-1} (associated with ABO_3 where A denotes the metal in tetrahedral position). The same author reported a single band at 586 cm^{-1} for commercial CoO, assumed to be due to the stretching of the Co-O bond.

4.3.7 Raman spectroscopy results

Raman spectra for commercial CoF_3 (purple), CoF_2 (cyan), CoO (blue), Co_3O_4 (red) and the product of Co_3O_4 decomposition in N_2 (black) are shown in Figure 4.8. Four Raman bands were recorded for commercial CoF_3 at 166, 459, 792 and 912 cm^{-1}. Two bands with very weak intensity were recorded at 559 and 1101 cm^{-1} for commercial CoF_2. The commercial CoO had four bands at 459, 559, 681, 792 and 1096 cm^{-1}, whilst five were recorded for commercial Co_3O_4 at 187, 459, 559, 681 and 1096 cm^{-1}. According to our Raman experimental data, CoO and Co_3O_4 have spectra that are almost similar, and this is consistent with the XRD data, where it was established that CoO was not pure and possessed peaks ascribed to Co_3O_4 (Figure 4.6). Tang et al. (2008) reported Raman bands at 469, 512, 607 and 674 cm^{-1} for Co_3O_4, and low intensity bands at 468 and 672 cm^{-1} for CoO oxides. Hadjiev et al. (1988) found Co_3O_4 to have five Raman active modes at 194, 482, 522, 618 and 691 cm^{-1}. The product from decomposition of Co_3O_4 in N_2 produced three bands at 454, 556 and 1096 cm^{-1}. CoO obtained from decomposition of Co_3O_4 seems pure in comparison to the commercial compound. This shows the difficulty in avoiding exposure of CoO to atmospheric moisture, especially during large scale production. As a result, results reported from the literature are not exactly identical owing to possible oxidation of CoO during its production process.

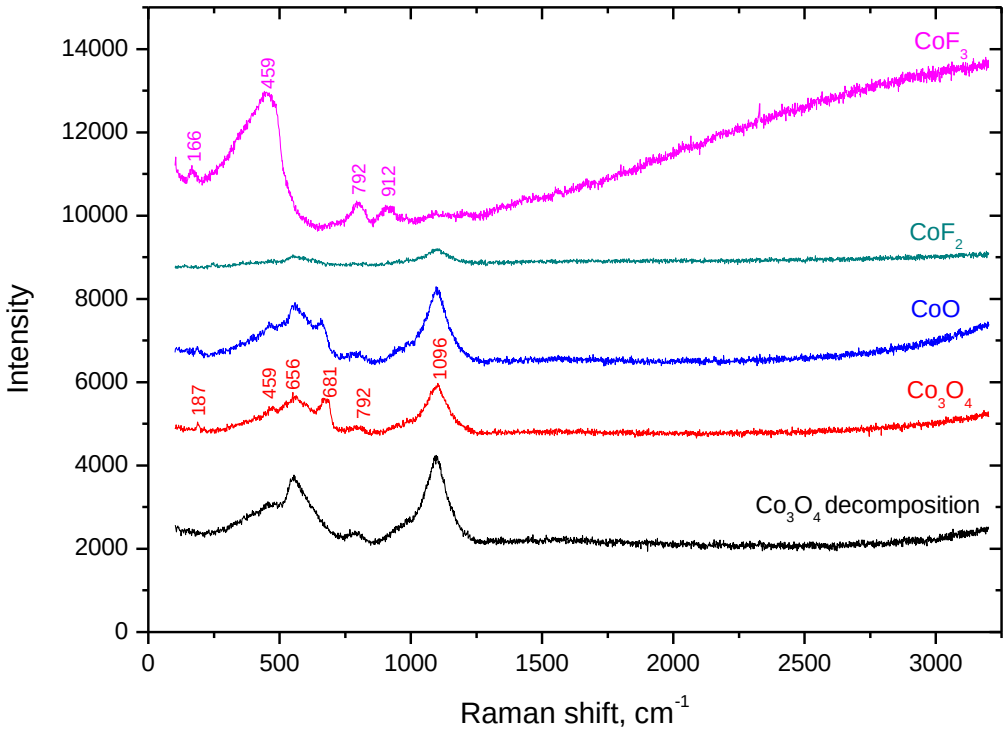

Figure 4.8: Raman spectra of commercial CoF_3 (purple), CoF_2 (cyan), CoO (blue) Co_3O_4 (red) and product obtained from decomposition of Co_3O_4 (black).

A summary of the XRD crystal structure, ATR-FTIR and Raman spectroscopy results is presented in Table 4.1.

Table 4.1: Summary of XRD, FTIR and Raman results for commercial samples and the product of Co_3O_4 decomposition.

Samples	XRD structure[a]	Space group[a]	ATR-FTIR, cm^{-1}	Raman shift, cm^{-1}
CoF_3	Primitive rhombo hedral	*R3c* (167)	361, 377, 520	166, 459, 792, 912
CoF_2	Tetragonal	*P42/mnm* (136)	356, 414	559, 1096
CoO	Fcc	*Fm-3m* (225) *Fd-3m* (227)	556, 661	187, 459, 559, 681, 792, 1096
Co_3O_4	Fcc	*Fd-3m* (227)	390, 556, 661	187, 459, 559, 681, 792, 1096
Co_3O_4 decomposition	Fcc	*Fm-3m* (225)	556, 661	459, 559, 792, 1096

[a] Based on ICDD PDF-2 Release 2007 database.

According to Table 4.1, two space groups are indicated, the *Fd-3m* and *Fm-3m*. The commercial Co_3O_4 has the *Fd-3m* space group, whilst the product (CoO) of the decomposition of Co_3O_4 possesses the *Fm-3m* space group. The commercial CoO possesses both the *Fm-3m* and the *Fd-3m* space groups. This supports the XRD finding where the commercial CoO was found to possess Co_3O_4 pattern in addition to patterns for CoO. The ATR-FTIR data shows the 556 and 661 cm^{-1} to appear consistently on all cobalt oxide forms. The Raman bands were a challenge to interpret as some of the bands (459, 559, 1096 cm^{-1}) appear for both oxides and fluorides.

4.4 Conclusions

Our TG results show that decomposition of Co_3O_4 to CoO taking place at 900 ^oC in agreement with literature. From the TG curves we observe the importance of cooling in N_2 to avoid reoxidation of CoO back to Co_3O_4. The XRD results confirmed formation of CoO from the decomposition of Co_3O_4, and this product was found to be of high purity when compared to the commercial compound as displayed by the XRD and Raman data. The TG results show the commercial CoF_3 to decompose with sublimation taking place simultaneously. Furthermore, the presence of moisture will promote decomposition of CoF_3 with subsequent formation of HF. These results should be used as guidelines for fluorination reactions to be carried out under dry conditions and at temperatures below 600 ^oC in order to form the desired product CoF_3. Temperatures beyond 600 ^oC should be avoided as it is predicted that decomposition and sublimation of CoF_3 will occur, leading to lower product yields. From our experimental TG data, separating decomposition from sublimation seems to be a challenge.

5 Reactions of Co_3O_4 with HF and F_2 gas

5.1 Introduction

Hydrogen fluoride (HF) and fluorine (F_2) are known to be useful fluorinating agents for the preparation of high oxidation state metal fluorides (Tumarov, 1993). Gas solid reactions are effective for the fluorination of oxides (Kim et al., 2002). This chapter therefore reports on the gas solid reactions carried out for Co_3O_4 with hydrogen fluoride (HF) and with fluorine gas (F_2) to form CoF_2 and CoF_3 respectively. Four fluorination reactions were performed: (i) reaction of Co_3O_4 with HF gas, (ii) reaction of Co_3O_4 with F_2 gas, (iii) reaction of CoF_2 with F_2, and the results obtained from these three reactions were used as guidance for reaction (iv), where Co_3O_4 was treated sequentially with HF and then F_2 in a single experimental run.

All fluorination reactions were performed with the corrosive resistant thermogravimetric analyser (TGA) as a primary fluorination tool. The basic principle of a TGA instrument involves the measurement of mass change of a substance as a function of temperature or time in a controlled atmosphere (Brown, 1998). Most common commercial TGA instruments are not suitable for corrosive gases like HF and F_2, and modifications were performed to make the instrument resistant to corrosive gases. A schematic diagram of the TGA is shown in Figure 5.1 under the Experimental section. This TGA provides a unique advantage and makes it possible to follow the degree of fluorination from the respective mass uptakes recorded.

Reaction responses were measured for both isothermal as well as non-isothermal conditions, and residue samples were characterized using powder XRD, ATR-FTIR and Raman spectroscopy. There is not much data available in literature on the characterization of CoF_3, probably owing to the instability of the compound when exposed to atmospheric moisture and the lack of technical ability to undertake reactions and analyse products thereof under dry inert conditions. The unique capability of the instrumental setup employed in this study was therefore exploited not only to study the synthesis of CoF_3 but also to provide valuable characterization data of the compound without the complicating moisture induced hydrolysis effects.

5.2 Experimental

Commercial samples of Co_3O_4, CoO and anhydrous CoF_2 purchased from Sigma Aldrich and Alfa Aesar were used as received. The results obtained from thermal and spectroscopic characterization of these compounds were discussed in the previous chapter. The anhydrous hydrogen fluoride, AHF, (>99.99% pure) and fluorine, F_2 (>99.4% pure) were supplied by Pelchem SOC Ltd, a chemical manufacturing division of Necsa. AHF is manufactured through the reaction of sulphuric acid (H_2SO_4) with fluorspar (CaF_2), whilst F_2 is manufactured through electrolysis of AHF (Crouse, 2015). The two gases, HF and F_2, are highly reactive thereby requiring special apparatus for its handling. F_2 is the most reactive element capable of reacting will all elements bar noble gases like helium and neon. Due to the dangers posed by these gases, dilute mixtures of 10% (v/v) reactive gas in nitrogen were prepared and used throughout this study.

Fluorination reactions were performed on a Perkin Elmer TGS-2 instrument housed within a dry glove box with continuous nitrogen purge gas. Besides a safety measure, the dry glove box also serves to protect samples from exposure to atmospheric moisture. A schematic of the modified TGA instrument is given in Figure 5.1.

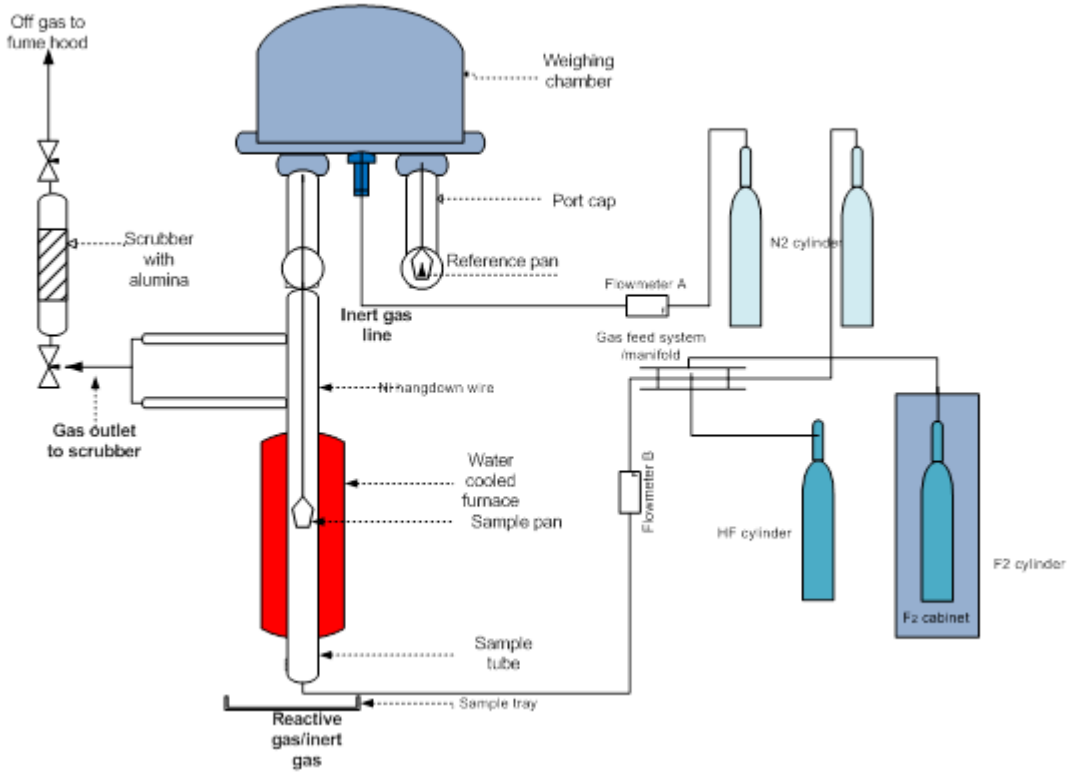

Figure 5.1: Schematic diagram of modified TGA instrument

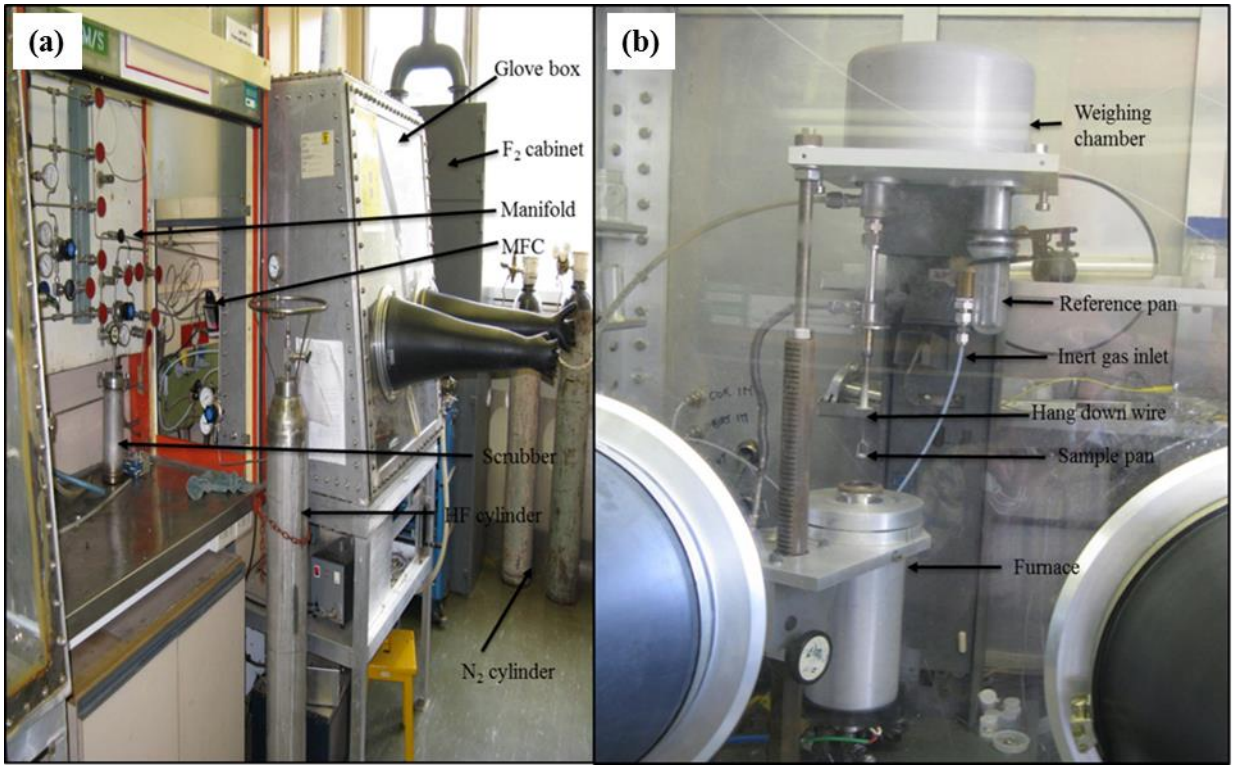

Figure 5.2: (a) Image of the experimental setup outside the glove box, (b) TGA instrument within the glove box.

Figure 5.2a shows an image of the experimental setup and the manifold outside of the glove box, while the TGA instrument located within the dry glovebox is shown in Figure 5.2b. The TGA instrument is made up of the weighing chamber in which the weighing unit is situated, the sample and reference pans suspended on a hang down wire through a stirrup, the inert gas line for purging of the weighing unit, as well as the furnace. The sample pan and the stirrup are made of nickel (Ni) as the material are resistant to HF and F_2 gases. Bukhmarina et al. (1992) also reported on the preparation of CoF_3 through fluorination of CoF_2 with F_2 on a reactor with nickel as the construction material. The sample pan has a type K thermocouple located directly beneath the pan for accurate temperature measurements. This thermocouple is composed of chromel-alumel and is considered more suitable within the nuclear industry where corrosive and high temperature (up to 1350 ^oC) conditions prevail.

The furnace is composed of a corrosive/inert gas inlet at the bottom, with an outlet port at the top leading through to the scrubber which then leads to the fume hood. The scrubber is composed of limestone packing for the abatement of the off gas prior to being directed to the fume hood. This serve to ensure that no gases are released to the atmosphere. Our system ensures constant purging of the weighing chamber with nitrogen gas so as to protect the sensitive electronic components from being damaged by the corrosive gases. A higher flow of 72 ml/min is maintained on the inert gas line with 54 ml/min flow for the reactive gas. The electronic weighing components section is separated from sample reaction zone by an orifice through which the vertically oriented hang-down wire protrudes. The axial velocity of inert nitrogen purge gas through an orifice serves to prevent diffusion of the reactive gases into the vulnerable electronics chamber. The HF and F_2 feed gases are stored within 20 L stainless steel cylinders. As an additional safety measure, the 20 L fluorine cylinder is enclosed within a fluorine cabinet. Both the corrosive and inert gas feeds are operated via a mass flow controller through simple opening and closing of the required valves on the manifold.

5.3 TGA reactions of Co_3O_4 with HF/F_2 (reactive) gas

5.3.1 Dynamic reactions

The dynamic experimental runs were performed as follows:

- About 20 mg of a sample was loaded on a nickel (Ni) crucible under a flow of nitrogen purge gas.
- The nitrogen feed gas line was closed, the reactive gas feed line opened, and the sample allowed to equilibrate at ambient temperature.
- Whilst under HF feed, the sample was heated to a predetermined temperature at a rate of 10 °C/min while the mass change as a function of temperature was monitored.
- The TG curve was recorded as the reaction progressed until the set temperature was reached.
- The reactive gas was then closed and the sample flushed with nitrogen gas for a while to remove excess reactive gas prior to sample recovery.
- The residue sample was then collected and kept within the dry inert glove box for further characterization purposes.

5.3.2 Isothermal reactions

From the results obtained from the dynamic runs, valuable information was extracted and used as guideline to predict temperatures at which the isothermal runs were performed. The procedure for executing isothermal runs was slightly different from the dynamic experiments:

- Approximately 20 mg sample was loaded on a Ni crucible that was positioned on the sample platform with constant nitrogen purge gas.
- The furnace was closed, the temperature raised to a predetermined isothermal temperature at a rate of 10 ^oC/min and allowed to equilibrate at this temperature whilst still under nitrogen purge gas.
- The reactive gas, (HF or F_2), was then introduced through closing of the nitrogen feed gas line for the reactive gas line.
- The reaction progress was monitored and data recorded until set run completed.

- On completion of the reaction, the reactive gas was closed and the nitrogen purge gas opened to flush excess reactive gas prior to collection of the residue sample.
- The residue was then collected for further characterization.
  The product was kept within the glove box under constant flow of nitrogen purge gas to avoid exposure to atmospheric moisture until further use or analysis.

The aim of performing the non-isothermal and isothermal reactions in the TGA was to provide guidelines on the conditions at which the reactions of Co_3O_4 with HF and Co_3O_4 with F_2 should be performed. These were then used for the sequential reaction of Co_3O_4 with HF (g) and then F_2 (g) in a single experiment.

5.4 Characterization of the reaction products

Products obtained from Co_3O_4 treated with HF, Co_3O_4 treated with F_2, CoF_2 treated with F_2 and finally Co_3O_4 treated sequentially with HF and with F_2 were characterized using XRD, ATR-FTIR and Raman spectroscopy. These instruments were found to be suitable as they possess special sample holders that allows loading of the sample in the glove box without having to expose the sample to atmospheric moisture.

5.5 Results and discussion

5.5.1 Reactions of Co_3O_4 with HF

The TG profile for the reaction of Co_3O_4 with HF, heated from ambient to 700 ^oC, is presented in Figure 5.3. A mass gain was recorded from 300 ^oC, to give a total mass gain of 10%. This was followed by a mass loss starting at 595 ^oC. The mass gain is ascribed to formation of CoF_2 and CoOF, while the mass loss is attributed to possible volatilization of the oxyfluoride in accordance to equation (5-1):

$$Co_3O_4(s) + 4HF(g) \rightarrow CoF_2(s) + 2CoOF(s,g) + 2H_2O(g) \qquad (5\text{-}1)$$

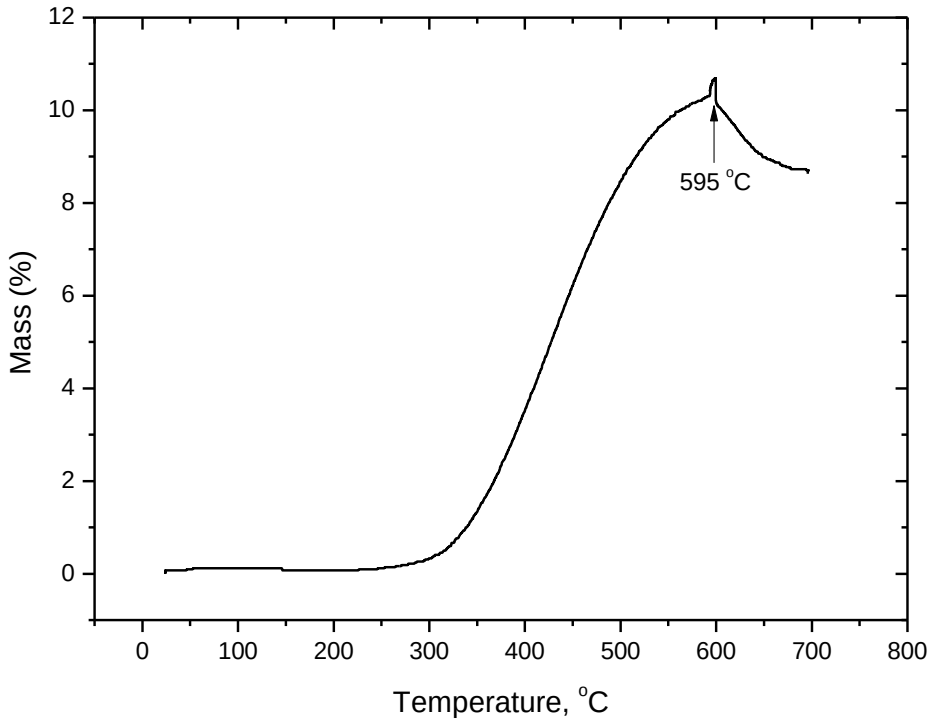

Figure 5.3: Thermogravimetric curve for reaction of Co_3O_4 with HF from ambient to 700 →°C.

The theoretical mass gain for the conversion of the Co_3O_4 to CoF_2 and CoOF (18.7%) was not attained, with only 10% mass gain recorded as shown in Figure 5.3. Additional experiments were performed at isotherms of 500, 550 and 600 °C. The TG curves for the respective isotherms are shown in Figure 5.4, and a summary of the mass uptake recorded at various isotherms is presented in Table 5.1.

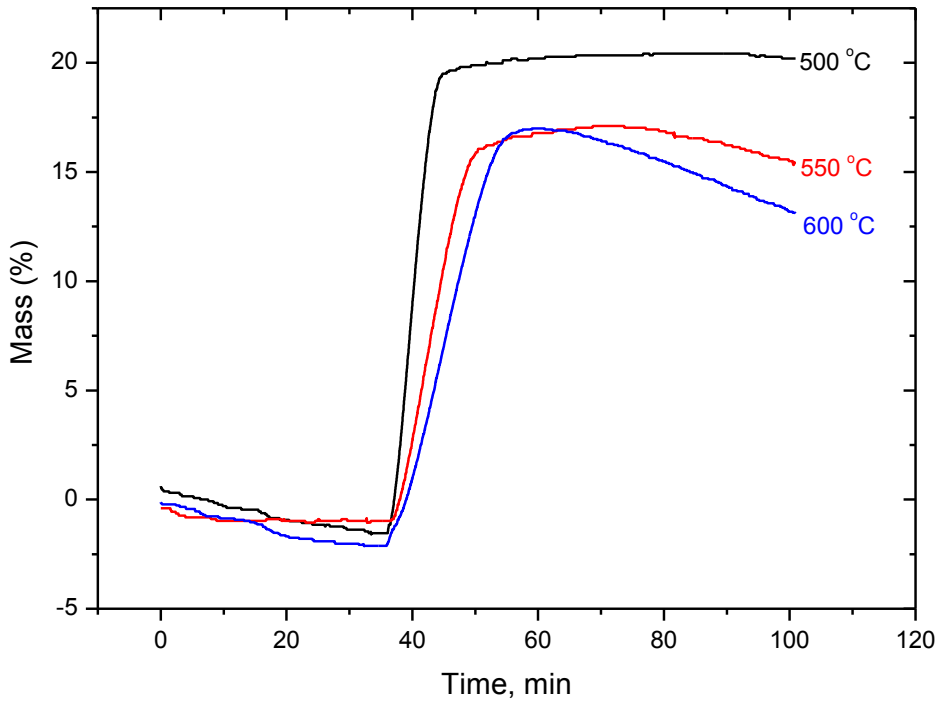

Figure 5.4: Thermogravimetric curves for reactions of Co_3O_4 with HF at isotherms of 500, 550 and 600 °C.

Table 5.1. Summary of the mass gain data recorded for the reaction of Co_3O_4 with HF at various isotherms.

Isothermal temperature, °C	Mass gain, %	Remarks
500	20	The highest mass uptake is recorded at this temperature
550	17	The lower uptake recorded suggests possible sublimation of the product taking place
600	17	

Contrary to the low mass gain (10%) obtained for the dynamic experiment (Figure 5.3), a 20% mass gain was recorded for the experiment performed at an isotherm of 500 °C (Figure 5.4), whilst 17% was recorded for reactions performed isothermally at 550 and 600 °C. The lower mass gain at the two isotherms suggests sublimation of the product already taking place. From

the isothermal results, it was discovered that 500 ^{o}C was the ideal temperature condition for the reaction of Co_3O_4 with HF as the mass gain recorded at this isotherm (20%) was closest to the theoretical mass gain (18.7%). It was at this temperature where the mass gain had reached a plateau with no mass loss characteristic of sublimation of the product observed.

The solid product obtained from the isothermal reaction at 500 ^{o}C was collected and characterized. The XRD results in Figure 5.5 indicates a diffraction pattern matching CoF_2, with additional patterns matching those of the unreacted Co_3O_4 and CoO Figure 5.5. The oxyfluoride could not be identified because it is not available within the ICDD PDF-2 database.

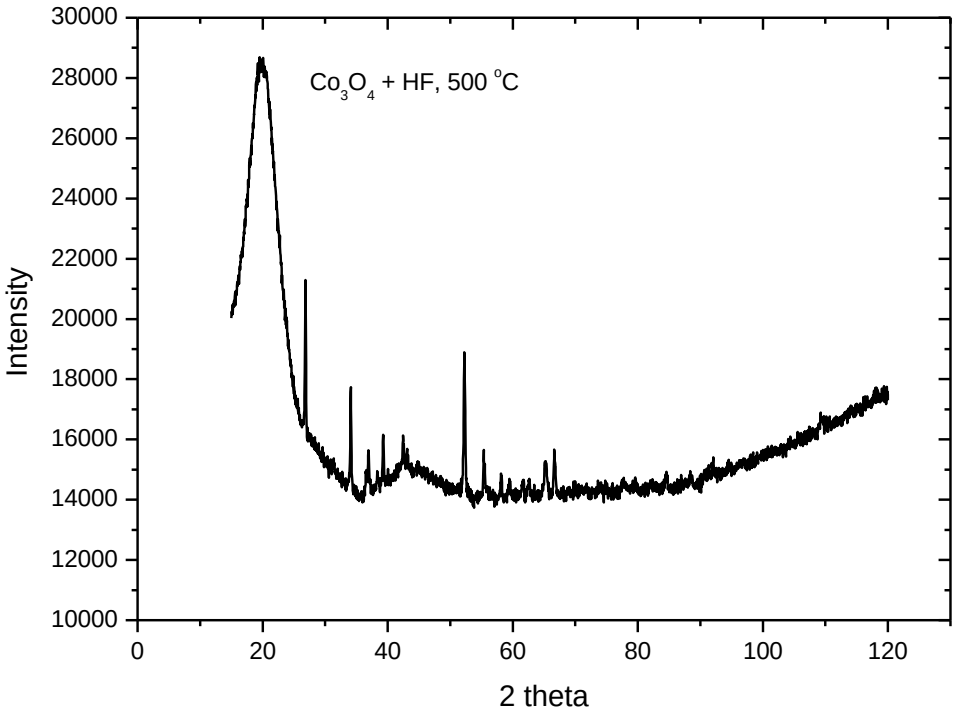

Figure 5.5: XRD pattern of Co_3O_4 treated with HF at 500 ^{o}C showing CoF_2 pattern with traces of Co_3O_4 and CoO phases.

The ATR-FTIR analysis of the product of Co_3O_4 treated with HF showed spectra composed of four bands; two strong bands at 354 and 408 cm^{-1} and two weak bands at 568 and 661 cm^{-1} (Figure 5.6). Tang et al. (2008) reported M-O stretching vibrations, the v_1 at 570 cm^{-1} for Co^{3+} in the octahedral position and v_2 at 661 cm^{-1} attributed to Co^{2+} metal ions in the tetrahedral

position. Based on this, the two bands, at 568 and 661 cm^{-1} are assigned to the Co-O stretching vibrations for Co^{3+} and Co^{2+} respectively. The other two bands at 354 and 408 cm^{-1} are then assigned to Co-F vibrations. This shows conversion of Co_3O_4 to CoF_2 product.

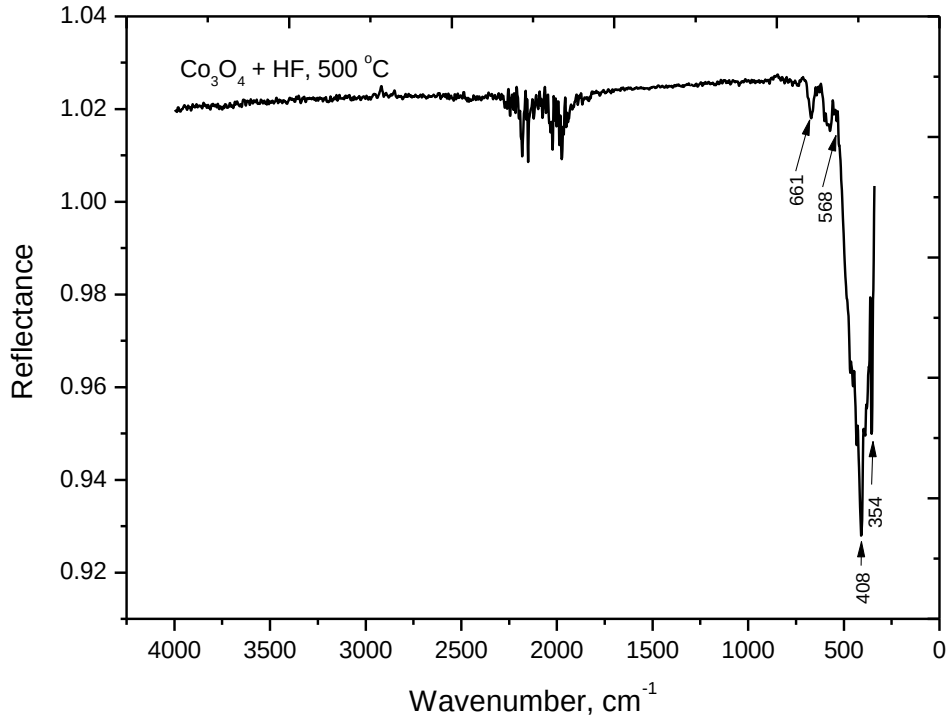

Figure 5.6: ATR-FTIR spectra of Co_3O_4 treated with HF at 500 ^oC.

As illustrated in Figure 5.6, the two bands at 568 and 661 cm^{-1} has not completely diminished, suggesting incomplete conversion of Co_3O_4 to CoF_2. These bands are absent on the commercial CoF_2 compound.

Raman analysis for the product of Co_3O_4 treated with HF at 500 ^oC was performed. The spectrum shows very weak bands at 477, 813 and 913 cm^{-1}, Figure 5.7.

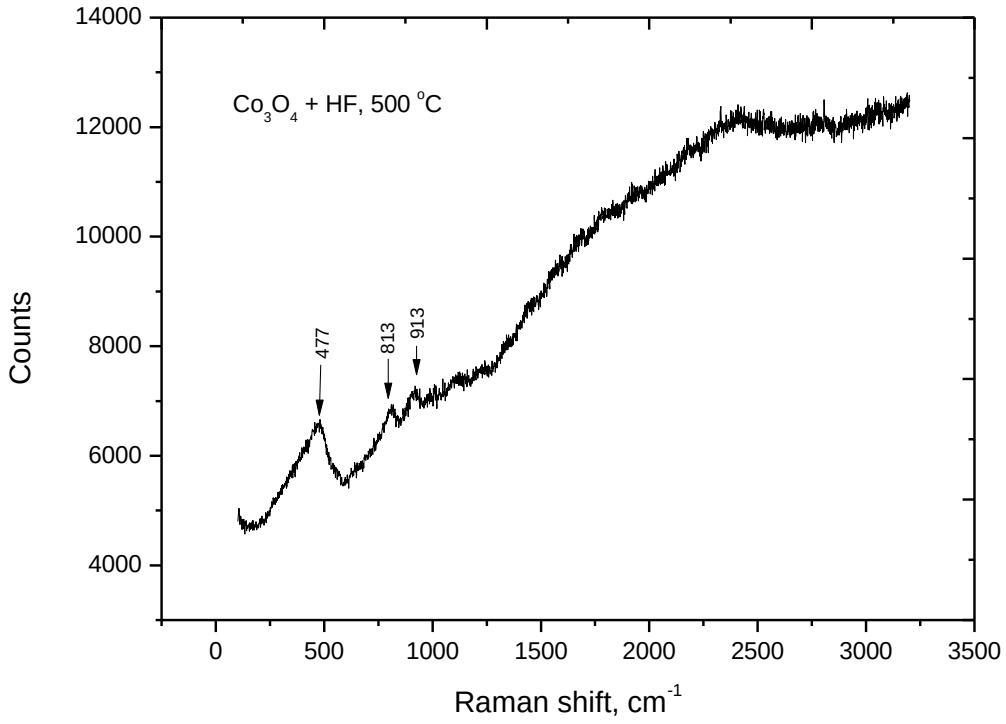

Figure 5.7: Raman curve of product of Co_3O_4 treated with HF at 500 ^oC.

A summary of the characterization data for the commercial Co_3O_4, commercial CoF_2 and product of Co_3O_4 treated with HF is presented in Table 5.2.

Table 5.2: Summary of characterization data obtained from commercial Co_3O_4, commercial CoF_2 and product of Co_3O_4 treated with HF at 500 ^oC.

Sample	XRD phases	ATR-FTIR wavenumbers, cm^{-1}	Raman shift, cm^{-1}
Co_3O_4 + HF, 500 ^oC	CoF_2, Co_3O_4, CoO	354, 408, 568, 664	477, 813, 913
Commercial CoF_2	CoF_2	356, 414	459, 559, 656, 1101
Commercial Co_3O_4	Co_3O_4, CoO	390, 566, 661	476, 555, 799, 1097

The 356 and 408 cm^{-1}ATR-FTIR bands recorded for the product from the reaction of Co_3O_4 with HF corresponds to the two bands (356, 414 cm^{-1}) recorded for the commercial CoF_2. These bands assigned to Co-F vibrations indicate formation of CoF_2. Raman results obtained were not conclusive and further work is recommended when the instrument is back operational.

5.5.2 Reaction of Co_3O_4 with F_2

Fluorine is known to be a stronger fluorinating agent than hydrogen fluoride, and it is expected to form higher oxidation state metal fluorides, as in this case CoF_3 (Muetterties and Castle, 1961). The reaction between Co_3O_4 and F_2 is presented in equation (5-2).

$$Co_3O_4(s) + 4.5F_2(g) \rightarrow 3CoF_3(s) + 2O_2(g) \qquad (5\text{-}2)$$

Figure 5.8 shows the TG profile for the dynamic reaction of Co_3O_4 with F_2 gas.

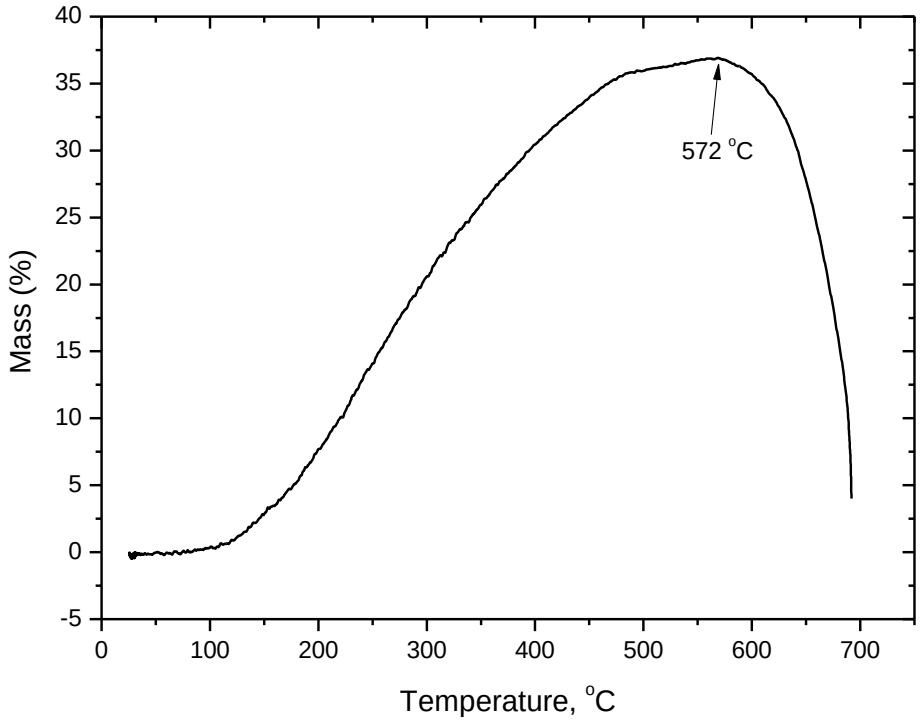

Figure 5.8: Thermogravimetric curve for the reaction of Co_3O_4 with F_2 heated from ambient to 700 °C.

A mass gain starts from 100 °C to yield a total uptake of about 35 %, followed then by mass loss from 572 °C (Figure 5.9). According to equation 5.2, the formation of CoF_3 through reaction of stoichiometric amounts of Co_3O_4 with F_2 ought to be accompanied by a 44.4% mass gain.

As the theoretical mass gain was not attained, isothermal reactions were performed to find the ideal temperature condition that would result in the theoretical mass uptake for the conversion of Co_3O_4 to CoF_3. Isothermal reactions were performed at 200, 300, 400, 500 and 550 °C and the corresponding TG profiles are shown in Figure 5.9.

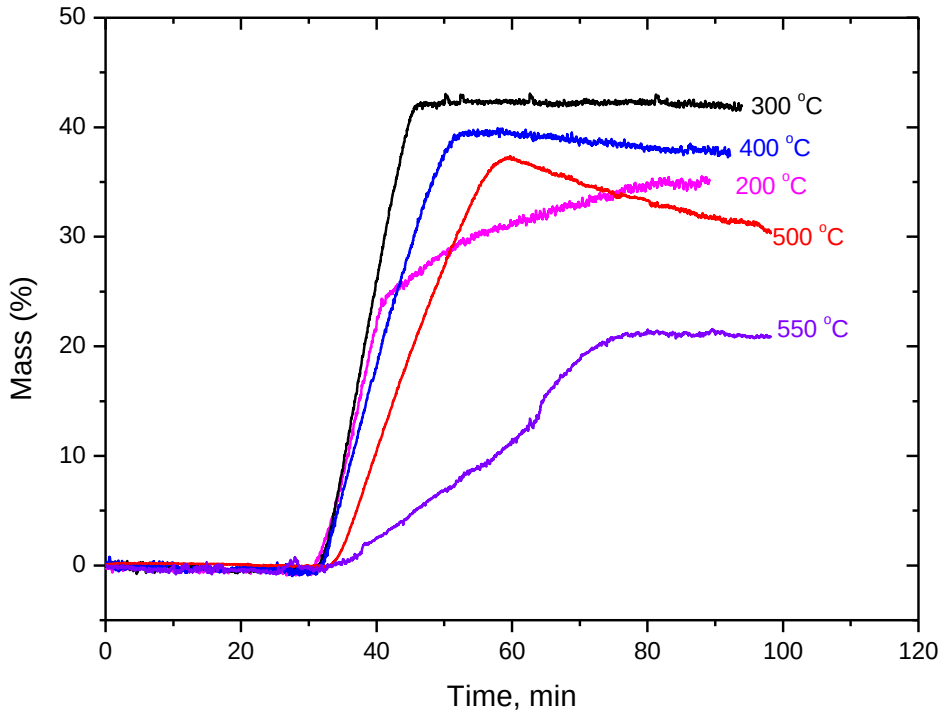

Figure 5.9: TGA curves for the reaction of Co_3O_4 with F_2 at isotherms of 200, 300, 400, 500, 550 and 600 °C.

The respective mass uptakes obtained were 34% at 200 °C, 43% at 300 °C, 39% at 400 °C, 37% at 500 °C and finally 20% at 550 °C, as summarized in Table 5.3.

Table 5.3. Summary of the respective mass gains recorded at various isotherms of Co_3O_4 with F_2.

Isothermal temperature, ^oC	Mass gain, %	Remarks
200	34	Increase in mass uptake with increase in isotherms at 200 and 300 ^oC, with maximum uptake recorded at 300 ^oC
300	43	
400	39	The lower mass uptake recorded in comparison to that obtained at 300 ^oC shows signs of volatilization taking place. This phenomena is more dominant at 550 ^oC where an even lower mass gain (20%) is recorded
500	37	
550	20	

The experiment performed isothermally at 300 ^oC yielded a mass gain (ca 43%) closest to the theoretical mass gain (44.4%) anticipated for the conversion Co_3O_4 to CoF_3. XRD, ATR-FTIR and Raman analysis were therefore performed on the product obtained at 300 ^oC.

Results obtained for the XRD analysis of the product obtained from the isothermal reaction between Co_3O_4 and F_2 at 300 ^oC is shown in Figure 5.10.

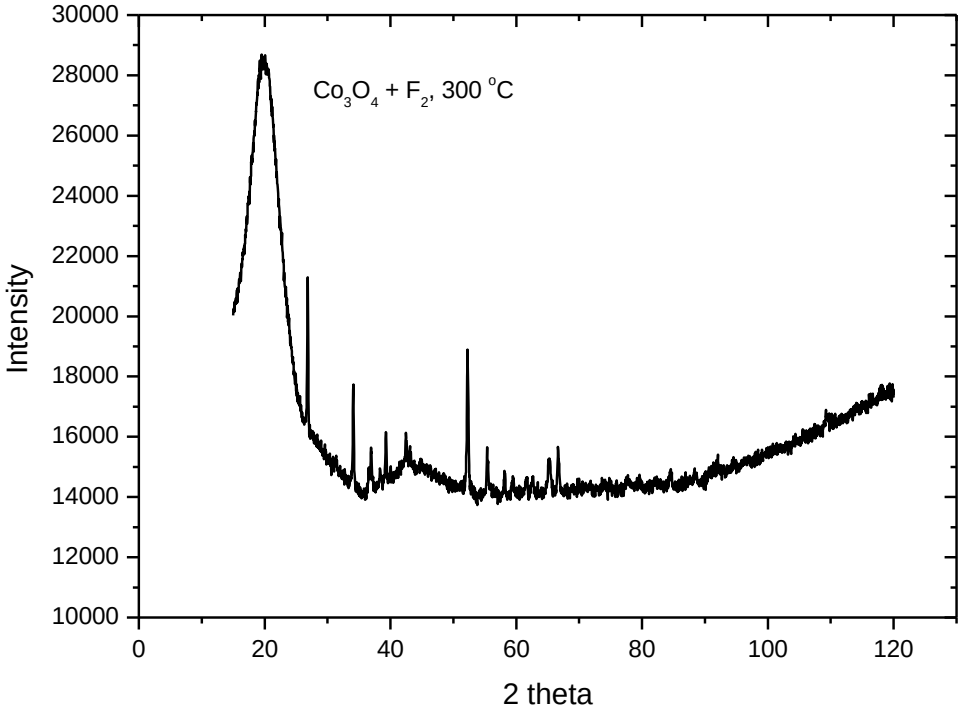

Figure 5.10: XRD pattern of the product obtained from the isothermal reaction of Co_3O_4 with F_2 at 300 ^oC.

The XRD pattern for product of Co_3O_4 treated with F_2 at 300 ^oC (Figure 5.10) matched CoF_3 from the ICDD PDF-2 database. There were secondary peaks that could not be assigned.

The corresponding ATR-FTIR spectra is presented in Figure 5.11. The two bands at 378 and 526 cm^{-1} are assumed to be due to Co-F vibrations of CoF_3. This assumption is made based on the ATR-FTIR experimental data of the commercial CoF_3, where three bands at 361, 377 and 520 cm^{-1} were recorded (Figure 4.7). Comparison to the experimental data of the commercial CoF_3 was done as there was no literature data available for CoF_3 for confirmation purposes.

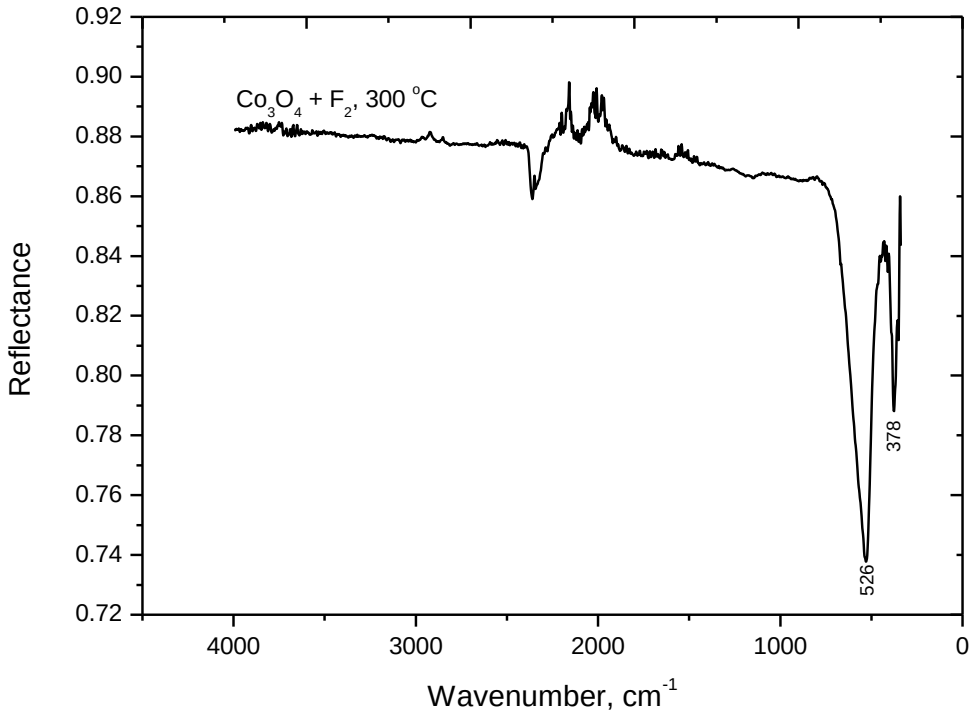

Figure 5.11: ATR-FTIR spectrum of product obtained from the isothermal reaction of Co_3O_4 treated with F_2 at 300 ^oC.

The results obtained for Raman analysis of the product obtained from the isothermal reaction Co_3O_4 treated with F_2 at 300 ^oC is shown in Figure 5.12.

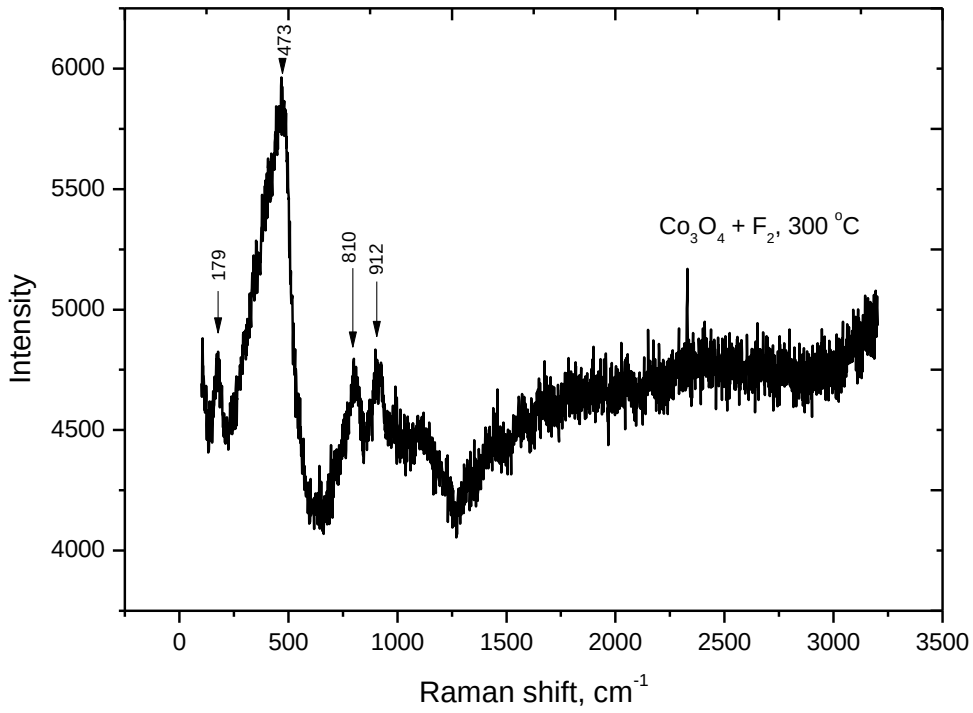

Figure 5.12: Raman data for product obtained from the isothermal reaction Co_3O_4 treated with F_2 at 300 ^oC.

The Raman spectrum shows one prominent band at 473 cm^{-1} in addition to three weak bands at 179, 810 and 912 cm^{-1}. The weak band at 912 cm^{-1}, which was also present for the commercial CoF_3 compound was assigned to the Co-F vibration and indicates formation of CoF_3.

5.5.3 Reaction of CoF_2 with F_2

A reaction was performed to establish the temperature condition at which the commercial CoF_2 converts to CoF_3. This was performed through reaction of CoF_2 with F_2 to form CoF_3 as in equation (5-3):

$$CoF_2(s) + 0.5F_2(g) \rightarrow CoF_3(g) \qquad (5\text{-}3)$$

This reaction should be accompanied by 19.5% theoretical mass gain. The dynamic TG curve for the anhydrous CoF_2 treated with F_2 from 30 to 550 ^oC is shown in Figure 5.13.

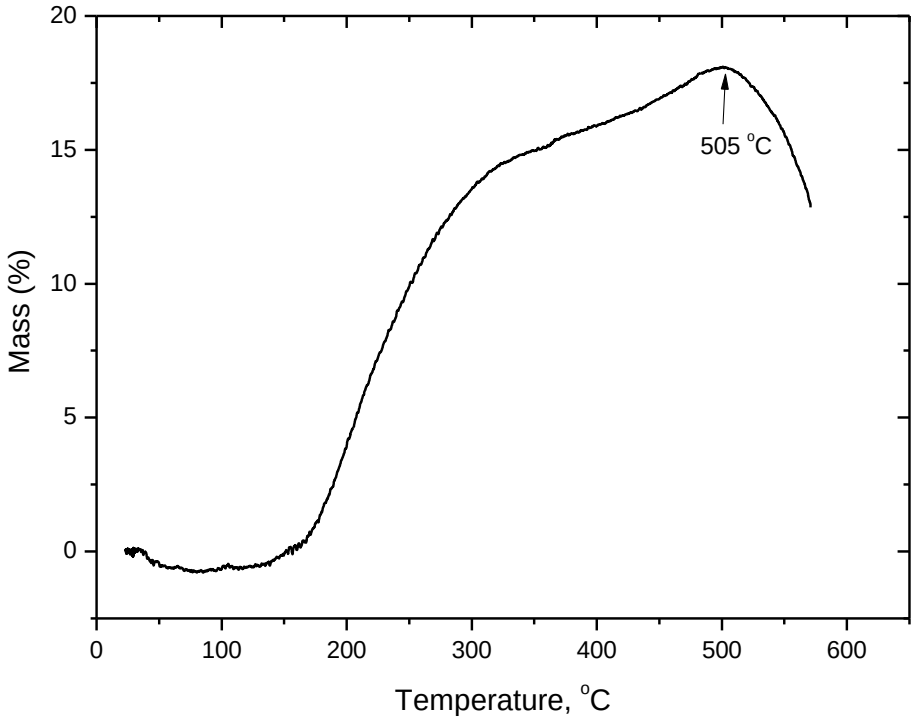

Figure 5.13: TG curve for the reaction of CoF_2 with F_2 heated from 30 to 550 ^oC.

An 18% mass uptake was recorded from 150 ^oC, followed by mass loss from 505 ^oC. The mass gain is attributed to the conversion of CoF_2 to CoF_3, whilst the mass loss suggests sublimation of the CoF_3 compound.

In our quest to seek the optimal temperature condition to result in the theoretical mass uptake, isotherms were then performed at 200, 300, 400 and 500 ^oC (Figure 5.14). The respective mass uptakes recorded were 15% at 200 ^oC, 16% at 300 ^oC, 17% at 400 ^oC and 13% at 500 ^oC, as summarized in Table 5.4. A maximum uptake of 17 % was recorded at 400 ^oC, and the residue obtained at this particular isotherm was further characterized.

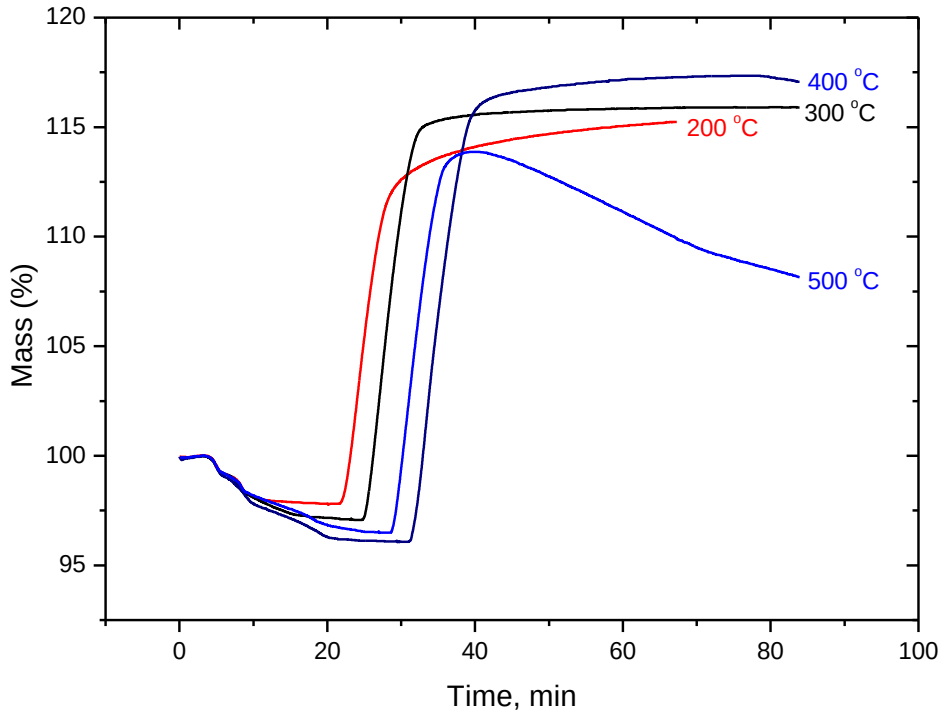

Figure 5.14: Thermogravimetric curves for the reaction of CoF_2 with F_2 at isotherms of 200 (red), 300 (black), 400 (purple) and 500 °C (blue).

Table 5.4: Summary of the respective mass gains recorded at various isotherms of CoF_2 with F_2

Isothermal temperature, °C	Mass gain, %	Remarks
200	15	Higher mass uptakes are recorded with an increase in the isothermal temperature between 200 and 400 °C.
300	16	
400	17	
500	13	The lower mass gain suggests sublimation already taking place as the product is formed

The XRD analysis showed a similar pattern as the one obtained for the product of Co_3O_4 with F_2, which matched CoF_3. As a result, reference is given to Figure 5.10 for the XRD pattern in this case.

The corresponding ATR-FTIR spectra for the product of CoF_2 treated with F_2 is presented in Figure 5.15, where two bands at 374 and 518 cm^{-1} were obtained. The two bands are almost similar to those obtained for the product of the reaction between Co_3O_4 and F_2 (378 and 526 cm^{-1},Figure 5.11) and were assigned to Co-F vibrations of CoF_3. This supports formation of CoF_3 through the reaction of CoF_2 with F_2 at 300 ^oC.

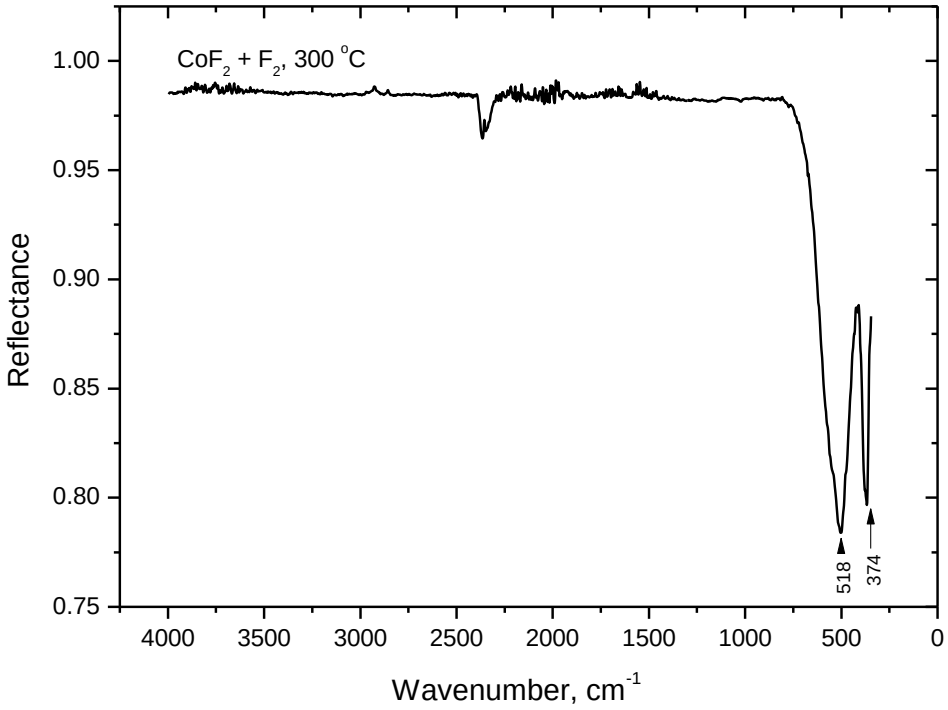

Figure 5.15: ATR-FTIR for residue of CoF_2 treated with F_2 at 400 ^oC.

The results obtained for Raman analysis of the product obtained from the isothermal reaction of CoF_2 treated with F_2 at 400 ^oC is shown in Figure 5.16.

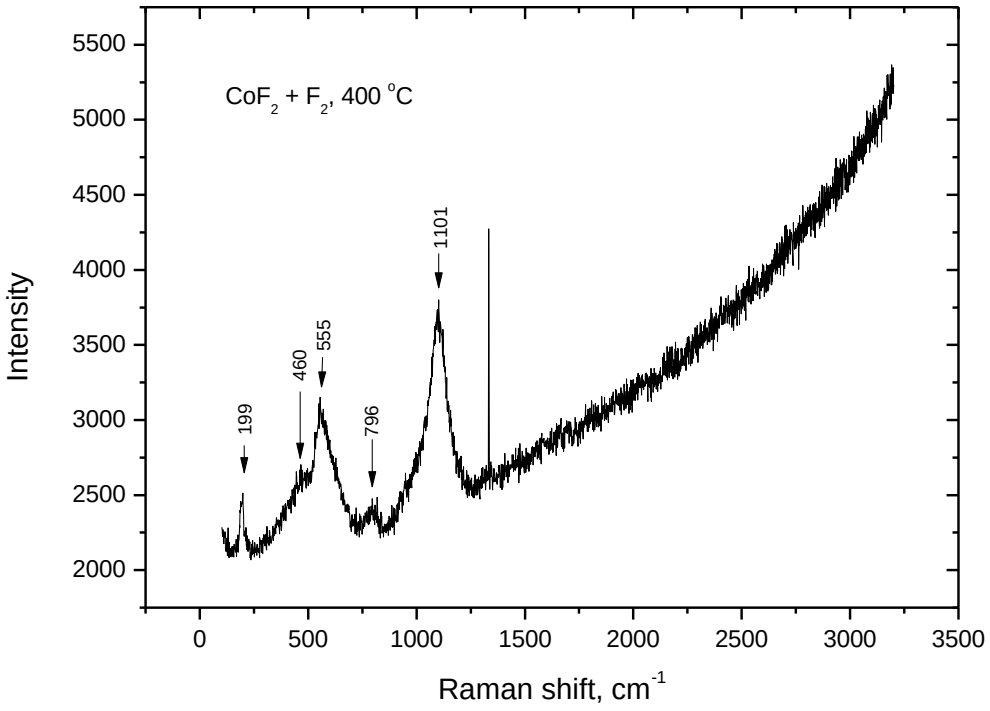

Figure 5.16: Raman curve for product of CoF_2 reacted with F_2 at 400 °C.

The Raman bands obtained for the product of CoF_2 treated with F_2 are 199, 460, 555, 796 and 1101 cm^{-1}. The band at 460 cm^{-1} is assigned to Co-F vibrations. Other bands are difficult to assign as they are present in both the oxide and the fluoride.

5.5.4 Sequential reaction of Co_3O_4 with HF and F_2

Experimental data indicate that synthesis of CoF_3 could be achieved through fluorination with F_2 used as the sole fluorinating agent. However it is known that F_2 is costly, and a process in which F_2 is used as a sole fluorination agent will result in high operational costs (Banks et al., 1994). The most viable option was to undertake a sequential reaction in which Co_3O_4 is first fluorinated with HF to form CoF_2, which is then converted to CoF_3 with F_2. This process will result in less amount of fluorine used, thereby leading to less operational costs incurred.

Based on the TG results obtained for the reaction of Co_3O_4 with HF (Figure 5.4), Co_3O_4 with F_2 (Figure 5.9) and CoF_2 with F_2 (Figure 5.14), the ideal temperature conditions were found to

be 500 ºC, 300 ºC and 400 ºC, respectively. A single experiment was then performed where Co_3O_4 was sequentially treated with HF gas at 500 ºC, followed by treatment with F_2 gas at 300 ºC (Figure 5.18). The 300 ºC isotherm was chosen as is known that low temperature reactions are significantly cheaper to carry out. The reaction was carried out as follows:

- Co_3O_4 sample was heated to 500 ºC and allowed to equilibrate at this temperature whilst under nitrogen purge gas.
- HF was introduced through gas switching and the reaction monitored until a plateau was reached.
- Gas switching from HF to N_2 was performed to remove excess HF within the line.
- The temperature was then decreased to 300 ºC.
- Finally F_2 was introduced until yet another plateau was reached.
- The sample was then flushed with nitrogen to remove excess F_2 gas prior to collection of the residue sample for characterization.

An image of the product obtained from sequential treatment of Co_3O_4 with HF and F_2 is shown in Figure 5.17. A light brown colour characteristic of CoF_3 is obtained in comparison to the original black of Co_3O_4. This shows fluorination to have been accompanied by a colour change from black to light brown corresponding to formation of CoF_3.

Figure 5.17: Image for Co_3O_4 (black) and Co_3O_4 fluorinated with HF and F_2 (brown).

The thermogravimetric curve (black) and temperature profile (red) for the sequential reaction of Co_3O_4 with HF (500 ºC) and then F_2 (300 ºC) is shown in Figure 5.18.

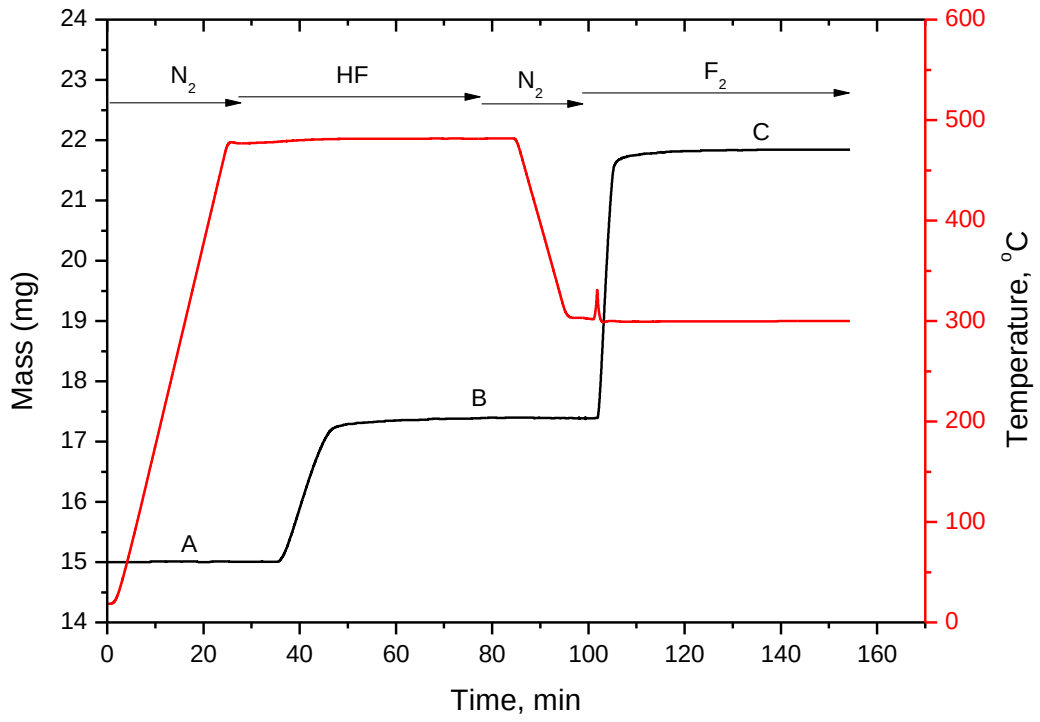

Figure 5.18: Temperature profile (red) and TG curve (black) for the sequential reaction of Co_3O_4 with HF (500 °C) and then F_2 (300 °C).

The theoretical mass gain for the conversion of Co_3O_4 to CoF_2 and CoOF through fluorination with HF is 18.7% (equation (5-1)), Co_3O_4 to CoF_3 via fluorination with F_2 is 44.4% (equation (5-2)), and that of CoF_2 to CoF_3 via fluorination with F_2 is 19.6% (equation (5-3)). This was used to perform a sequential reaction with HF (500 °C) and with F_2 (300 °C) in one single experiment. The sequential reaction of Co_3O_4 with HF and F_2 show two distinct mass uptakes; a 17% mass gain for the reaction with HF and a further 25% mass gain on switching to F_2 gas, to give a total mass uptake of 42% (Figure 5.18). The first mass gain is assumed to be due to Co_3O_4 (A) conversion to CoF_2 & CoOF (B), whilst the second mass uptake is ascribed to formation of CoF_3 (C).

The residual product for the sequential reaction with HF and F_2 was analysed with XRD and a pattern matching CoF_3 was obtained as shown in Figure 5.19. The diffraction pattern obtained indicates conversion of Co_3O_4 to CoF_3.

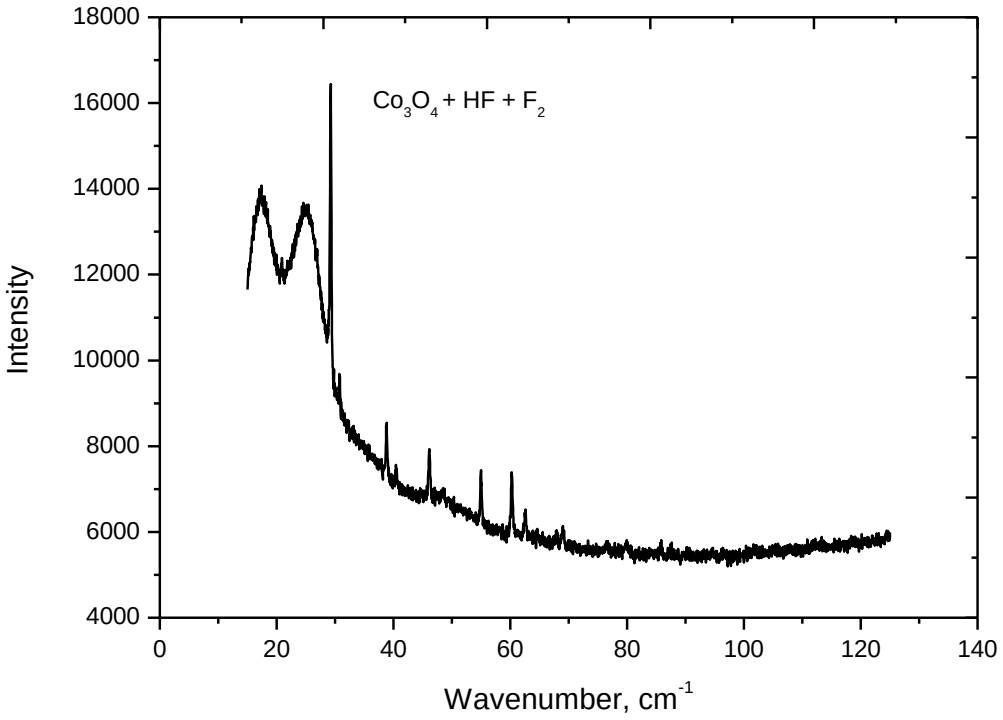

Figure 5.19: XRD pattern of the product obtained from the sequential reaction of Co_3O_4 with HF and F_2.

The results obtained from ATR-FTIR analysis of the product of Co_3O_4 sequentially treated with HF and F_2 is shown in Figure 5.20. The ATR-FTIR analysis showed two bands at 378 and 532 cm^{-1}, assigned to Co-F vibrations. This suggests formation of CoF_3.

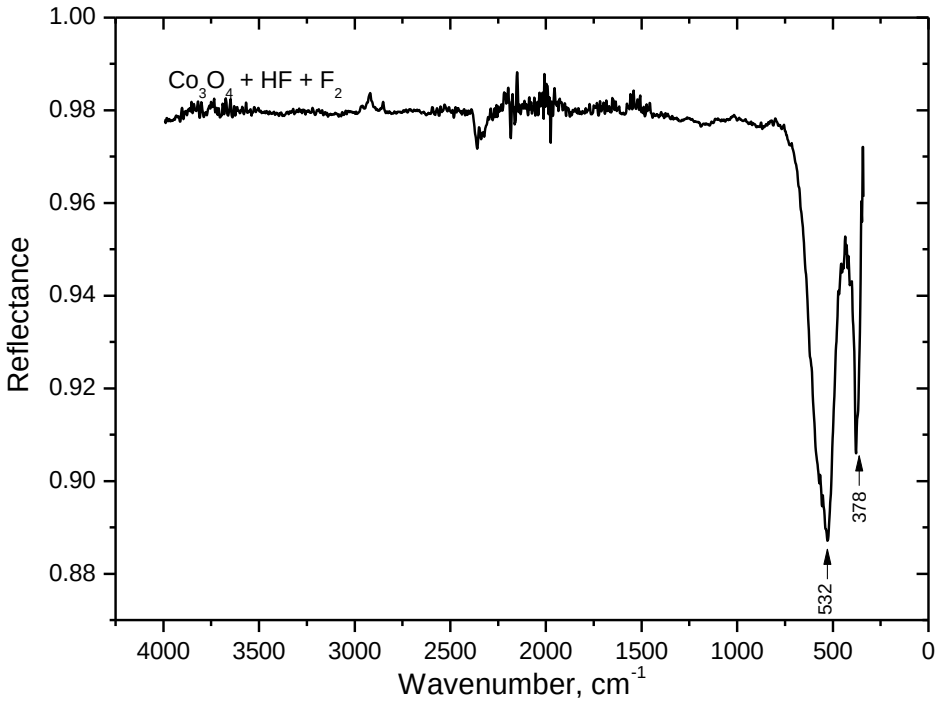

Figure 5.20: ATR-FTIR of product of Co_3O_4 with HF (500 ^oC) and then F_2 (300 ^oC).

The Raman spectrum for the product obtained from the sequential reaction of Co_3O_4 with HF and F_2 is presented in Figure 5.21. The Raman results gave two strong bands at 569 and 1097 cm^{-1}, in addition to the weak bands at 460, 797 and 1533 cm^{-1}. The Raman bands were not consistent and indicates that the Raman instrument was not a good instrument for our characterization efforts.

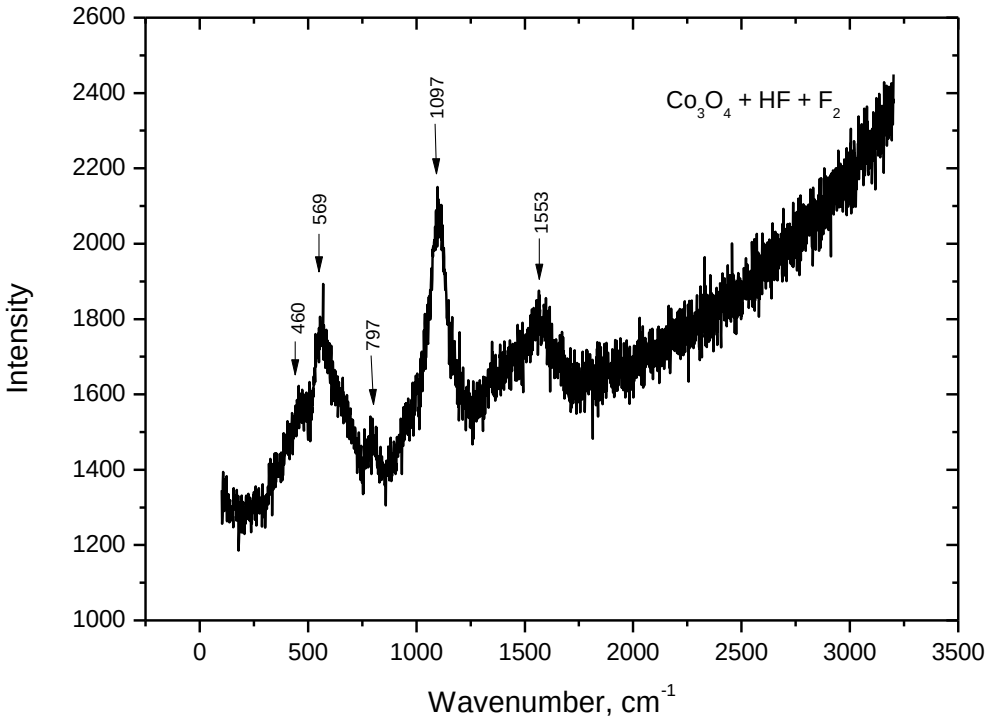

Figure 5.21: Raman spectra of the product of Co_3O_4 sequentially treated with HF and then F_2 gas.

The next section combines and summarizes the characterization data obtained from all the three analytical instruments utilized.

5.5.5 Summary of characterization data of commercial Co_3O_4, CoF_2, CoF_3 and products obtained from the reaction of Co_3O_4 with HF and product of Co_3O_4 with HF and F_2.

An overlay of the XRD patterns for commercial Co_3O_4 (black) , CoF_2 (red), CoF_3 (blue), and the product of Co_3O_4 treated with HF (cyan), and product of Co_3O_4 treated with HF and F_2 (purple) is presented in Figure 5.22.

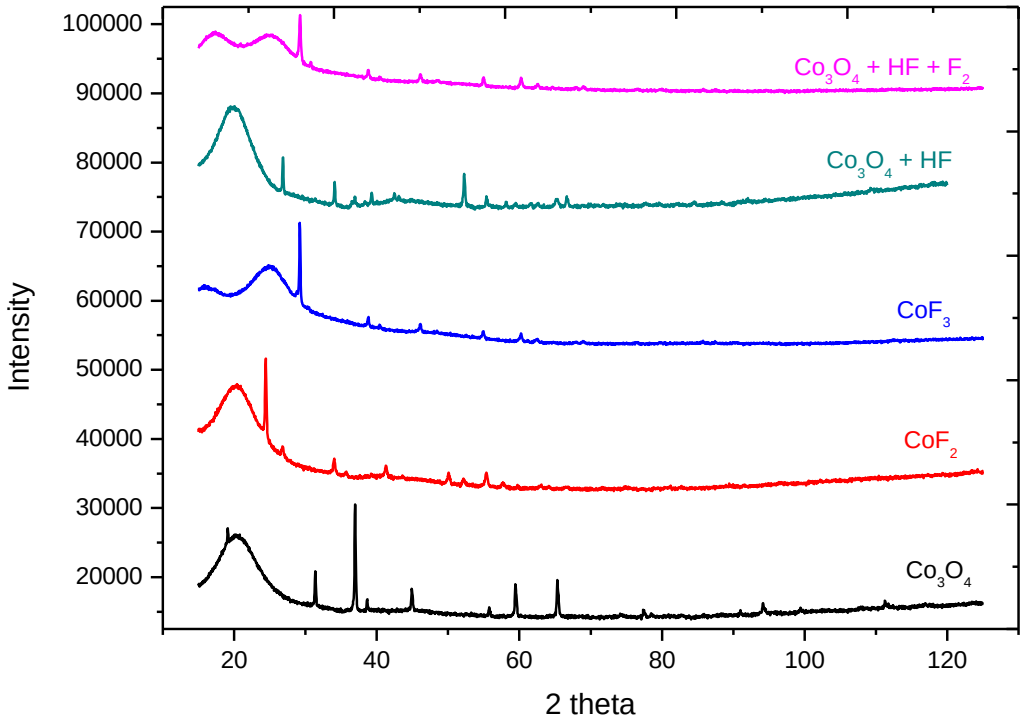

Figure 5.22: XRD pattern of commercial Co_3O_4 (black), CoF_2 (red), Co_3O_4 (blue) and the product of Co_3O_4 with HF (cyan) and Co_3O_4 with HF and F_2 (purple).

The XRD patterns for product of CoF_2 with F_2 and Co_3O_4 with F_2 are not included as they result in a pattern similar to that obtained for fluorination of Co_3O_4 with HF and F_2, indicating CoF_3 formation. These two patterns matched the CoF_2 from the ICDD PDF 2007 database. This shows successful conversion of Co_3O_4 to CoF_2. The XRD pattern for the product obtained from the sequential reaction of Co_3O_4 with HF and F_2 matched the CoF_3 from the database, also showing successful formation of CoF_3.

Figure 5.23 shows the ATR-FTIR spectra of the commercial Co_3O_4 (black), the commercial CoF_3 (red), product of Co_3O_4 treated with F_2 (blue), product of Co_3O_4 with HF (cyan) and the product of Co_3O_4 sequentially treated with HF and then F_2 (ruby red).

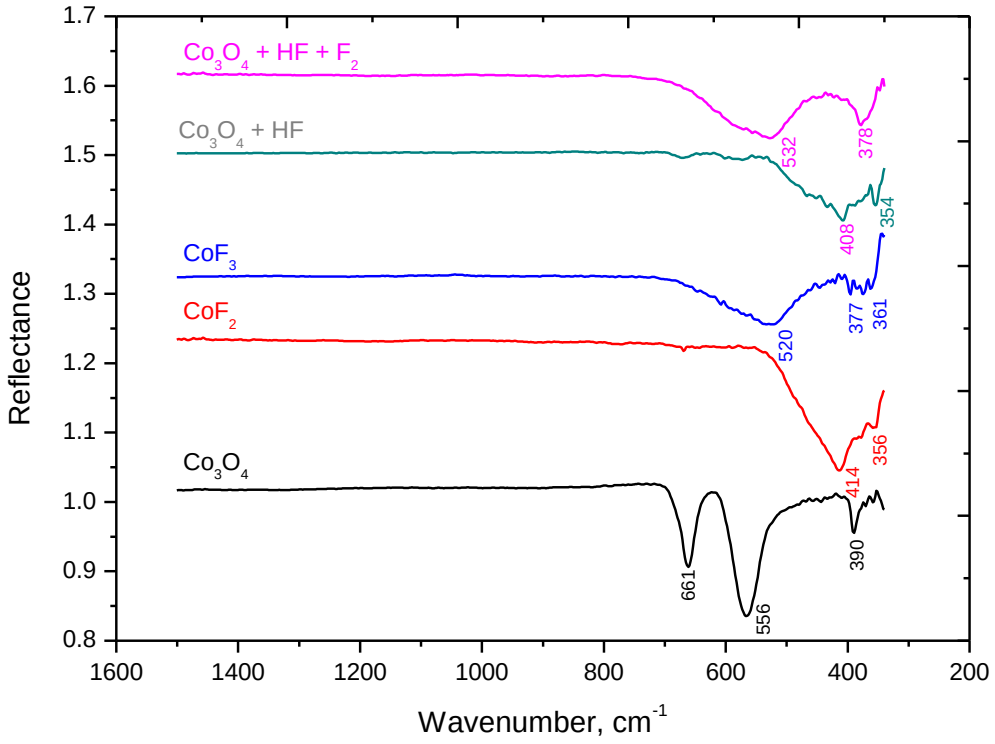

Figure 5.23: ATR-FTIR spectra of commercial Co_3O_4 (black), CoF_2 (red), CoF_3 (blue), product of Co_3O_4 treated with HF (cyan) and product of Co_3O_4 sequentially treated with HF and with F_2 (ruby red).

The product of Co_3O_4 treated with HF showed spectra that were almost similar to that of commercial CoF_2. There were two bands at 354 and 408 cm^{-1} assigned to Co-F vibrations. The two bands were obtained for the commercial CoF_2 compound. The spectra obtained from the sequential reaction of Co_3O_4 with HF and F_2 recorded two bands at 378 and 532 cm^{-1}. These were assigned to Co-F vibrations as they were present for the commercial CoF_3 (361, 377, 520 cm^{-1}). The scarcity of characterization data makes it difficult to confirm compounds formed via comparison to literature. Bukhmarina et al. (1992), (Grosse and Cady, 1947) also alluded to the limited availability of spectroscopic data for transition metal fluorides, and though this statement was made some years ago, there has not been much progress made as there is still not much characterization data available.

The Raman spectra of the commercial Co_3O_4 (purple), the commercial CoF_3 (cyan), product of Co_3O_4 treated with F_2 (blue), product of CoF_2 with F_2 (red) and the product of Co_3O_4 sequentially treated with HF and then F_2 (black) is presented in Figure 5.24.

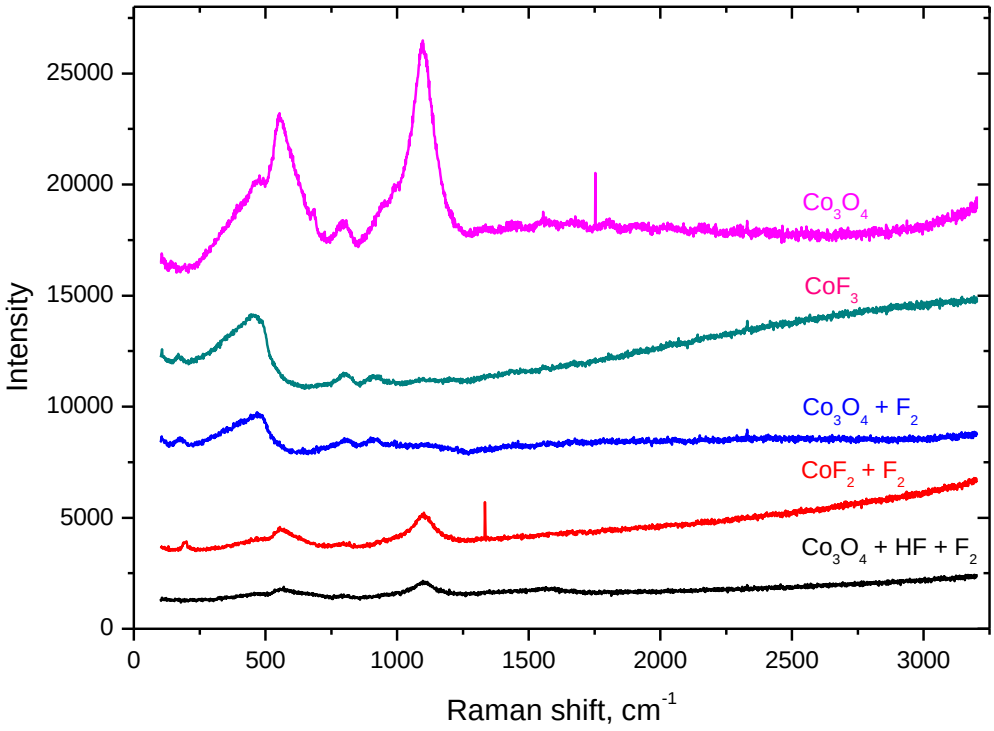

Figure 5.24: Raman spectra of product of Co_3O_4 sequentially treated with HF and F_2 (black), CoF_2 treated with F_2 (red), Co_3O_4 treated with F_2 (blue), commercial CoF_3 (cyan) and commercial Co_3O_4 (purple).

A summary of the XRD, ATR-FTIR and Raman characterization data is presented in

Table 5.5.

Table 5.5: Summary of characterization data obtained for commercial samples and fluorination processes studied.

Sample	XRD phases	ATR-FTIR wavenumbers, cm^{-1}	Raman cm^{-1}
Co_3O_4 + HF at 500 ^oC	CoF_2,Co_3O_4, CoO	354, 408, 568, 664	477, 813, 913
Commercial CoF_2	CoF_2	356, 414	559, 1101
Co_3O_4 + F_2 at 300 ^oC	CoF_3	378, 526	179, 473, 810, 912
CoF_2 + F_2 at 400 ^oC	CoF_3	374, 518	199, 460, 555, 796, 1101
Co_3O_4 + HF + F_2	CoF_3	378, 532	460, 569, 797, 1097, 1553
Commercial CoF_3	CoF_3	361, 377, 520	166, 459, 792, 912, 1101
Commercial Co_3O_4	Co_3O_4, CoO	390, 566, 661	187, 459, 559, 681, 792, 1096
Commercial CoO	Co_3O_4, CoO	360, 556, 661	459, 559, 681, 792, 1096

The XRD data confirmed successful formation of CoF_2 and CoF_3 from the reaction of Co_3O_4 with HF and F_2 reactive gases.

5.6 Conclusions

The TGA was successfully used as a fluorination tool for the synthesis of CoF_3. This was performed through sequential treatment of Co_3O_4 with HF and then F_2 to form CoF_3. Using TGA, this process was developed by a systematic study of the conditions required to complete the separate reactions within the sequential fluorination process proposed. The degree of fluorination of these reactions was followed via the respective mass uptakes recorded at various isotherms. The ideal temperature condition for the synthesis of CoF_2 (and CoOF) through reaction of Co_3O_4 with HF was found to be 500 ^oC, whilst the ideal temperature for the synthesis of CoF_3 through reaction of Co_3O_4 with F_2 and CoF_2 with F_2 was found to be 300 ^oC and 400 ^oC respectively. XRD and ATR-FTIR analyses were instrumental in the characterization of the reaction products obtained.

Through XRD analysis, patterns of CoF_2 and CoF_3 were obtained thereby confirming formation of the compounds, based on the XRD ICDD PDF-2 database. The ATR-FTIR and Raman spectroscopy analysis presented spectra which was assigned to CoF_2 and CoF_3 compounds. Confirmation was made through analysis and comparison with data obtained for commercial compounds, as not much literature data was available in for CoF_3. This was achieved through an overlay of spectra of commercial Co_3O_4, commercial CoF_2 and the product of Co_3O_4 fluorination with HF. Similar comparisons were made for commercial Co_3O_4, commercial CoF_3 and the products obtained for the treatment of Co_3O_4 with F_2, CoF_2 with F_2, and sequential treatment of Co_3O_4 with HF and F_2.

6 Reactions of CoO with HF and F_2

6.1 Introduction

In this Chapter we report on the gas solid reactions of CoO with HF and F_2 to CoF_2 and CoF_3 respectively. Though our primary focus was on the synthesis of CoF_3 through fluorination of the mixed oxide, Co_3O_4, synthesis through fluorination of CoO was performed for comparative and academic purposes.

6.2 Experimental

As in Chapter 5, both the dynamic and isothermal fluorinations were performed on a corrosive resistant TGA, and reaction products characterized using ATR-FTIR spectroscopy. The amounts of product formed in the TGA from the respective isotherms were not sufficient for XRD and Raman analysis to be carried out. The procedures followed for the fluorination experiments and product characterisation were described in detail in the previous chapter.

6.3 Results and Discussion

6.3.1 Reaction of CoO with HF

The reaction between CoO and HF is presented by

$$CoO(s) + 2HF(g) \rightarrow CoF_2(s) + H_2O(g) \qquad (6\text{-}1)$$

with a corresponding theoretical mass gain of 29.5%. The dynamic TG profile for the reaction of CoO with HF, heated from ambient to 600°C indicated a mass gain of about 4% as shown

in Figure 6.1. The mass gain obtained for this fluorination experiment was significantly lower than the mass gain expected for full conversion of CoO to CoF_2. This could indicate that CoO is less reactive to hydrogen fluoride at the experimental conditions at which the run was carried out. It could furthermore suggest that the mass gain observed might be from reactivity of the Co_3O_4 component available from the CoO sample. The commercial CoO were found to have traces of Co_3O_4 sample present (Figure 4.6). This warrants further investigation at a later stage.

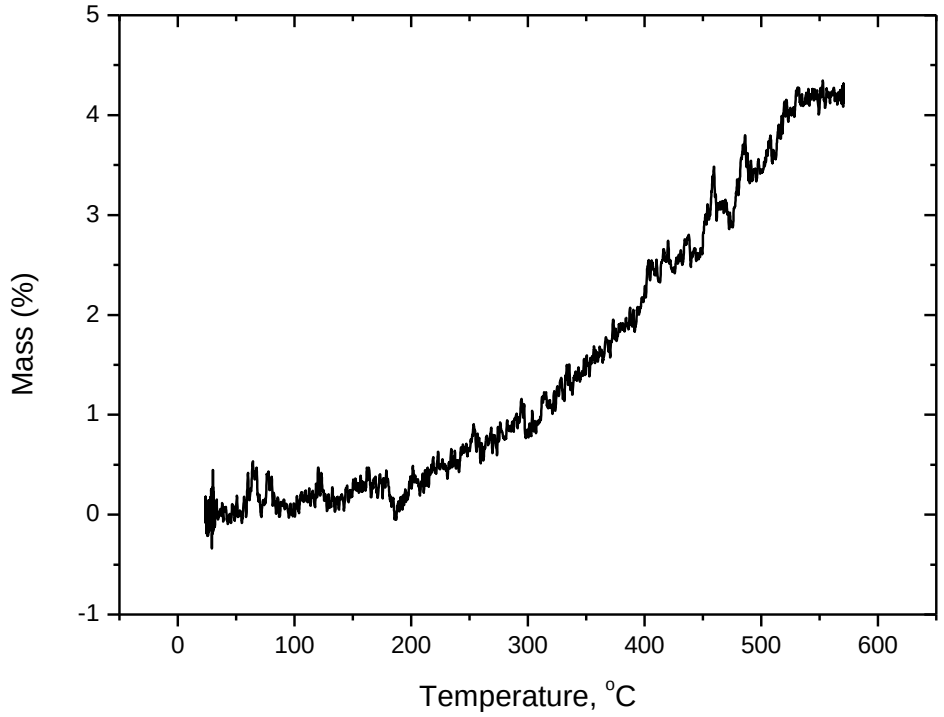

Figure 6.1: Thermogravimetric curve for the reaction of CoO with HF from ambient to 600 °C.

The TGA instrument was rendered unoperational at a critical stage of the project. Thus only two isothermal reactions, 400 and 500 °C, were performed (Figure 6.2). A mass gain of 6% was obtained for the fluorination experiment performed isothermally at 400 °C, while a 10% mass gain was recorded when performing the fluorination experiment at 500 °C.

The conversion of CoO to CoF_2 should be accompanied by a 29% mass gain, however only 10% mass gain could be attained under the conditions studied. The experimental mass gain obtained for fluorination of Co_3O_4 (20%, Chapter 5) agreed very well with the theoretical value

(19%) and XRD and FTIR characterisation data indicated good conversion of Co_3O_4 to CoF_2. Results obtained for the fluorination of CoO with HF on the other hand, shows a low extent of conversion of CoO to CoF_2 when comparing the experimental mass gain (10%) to the theoretical value (29%).

Further work will have to be performed, possibly performing fluorination reactions of CoO at higher isothermal temperatures to check whether it will be possible to increase the mass gain.

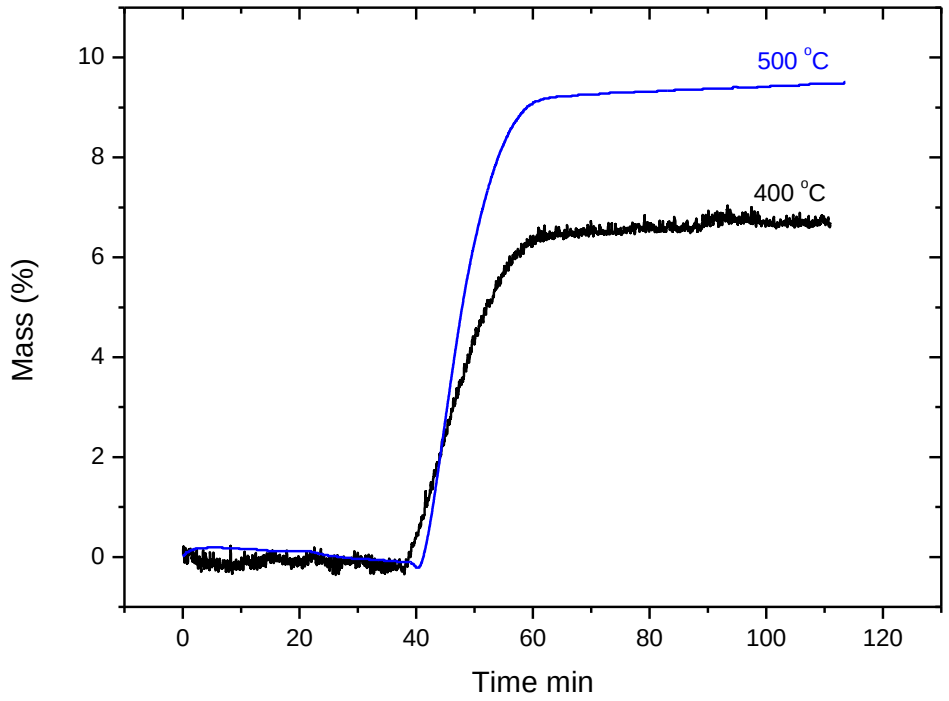

Figure 6.2: Thermogravimetric curves for the reaction of CoO with HF at isotherms of 400 (black) and 500 °C (blue).

The product obtained from the isotherm at 500 °C was submitted for ATR-FTIR analysis where two prominent bands at 414 and 661 cm^{-1} were recorded. The band at 414 cm^{-1} was assigned to Co-F vibrations, while the 661 cm^{-1} band was assigned to Co-O vibration of CoO (Tang et al., 2008). The presence of 661 cm^{-1} band associated with Co-O vibrations suggests incomplete fluorination of the CoO material.

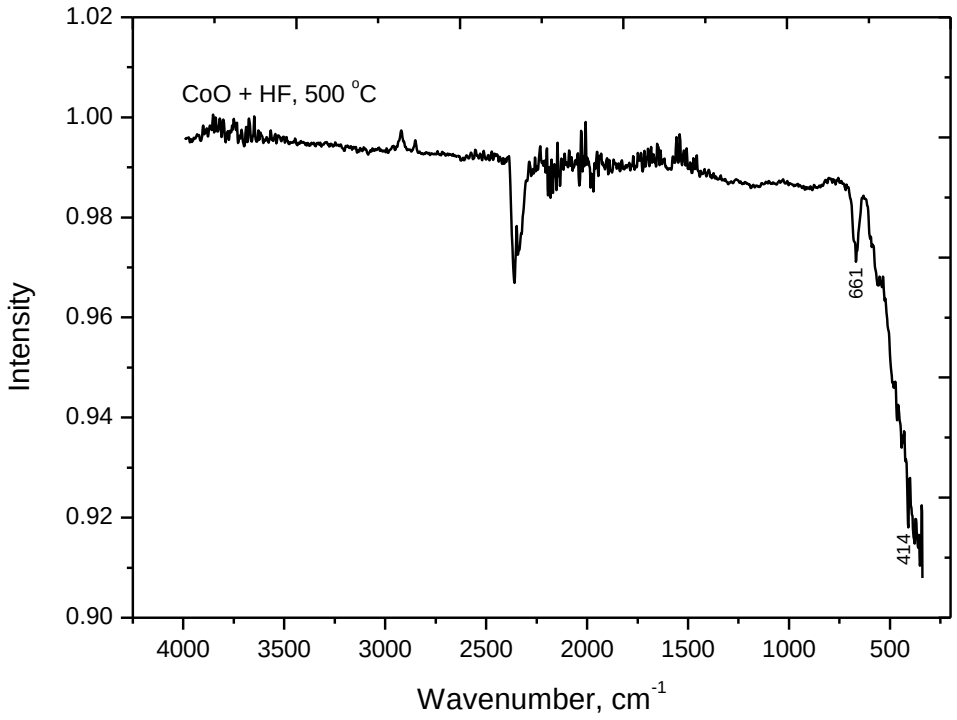

Figure 6.3: ATR-FTIR spectrum of CoO with HF at 500 °C.

6.3.2 Reaction of CoO with F_2

The reaction between CoO and F_2 is presented by

$$CoO(s) + 1.5F_2(g) \rightarrow CoF_3(s) + 0.5O_2(g) \quad (6\text{-}2)$$

The theoretical mass gain for the conversion of CoO to CoF_3 is 54.7%. The TG profile for the reaction of CoO with F_2 gas from 30 to 600 °C at a heating rate of 10 °C/min is shown in Figure 6.4.

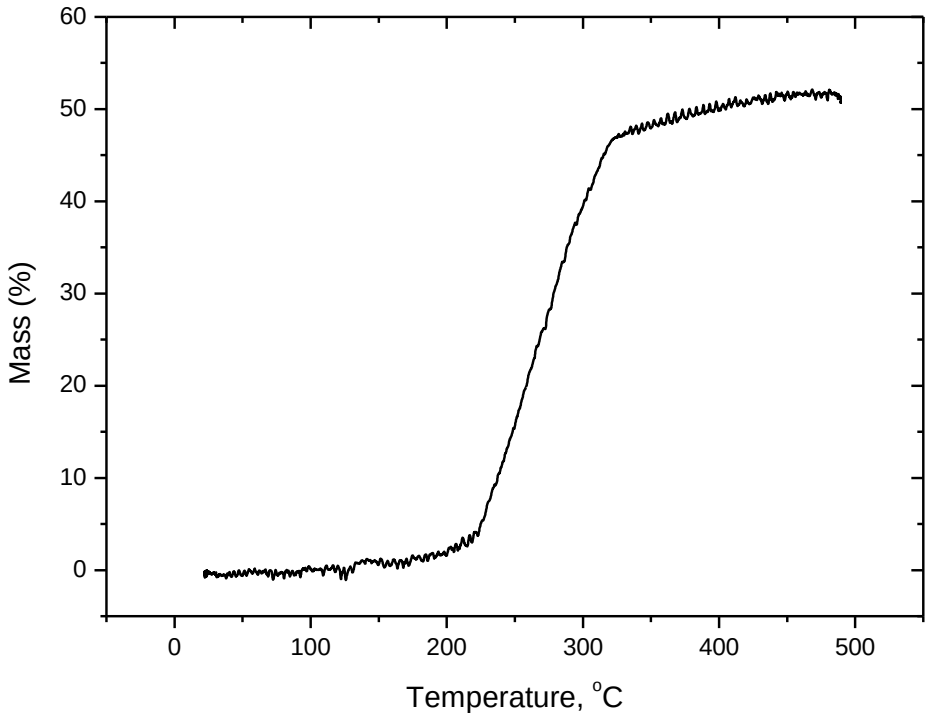

Figure 6.4: Thermogravimetric curve of CoO treated with F_2 from 30 to 500 °C at a heating rate of 10 °C/min.

The TG profile shows a mass gain from just above 150 °C to reach a maximum of 51% at 500 °C. Isothermal reactions were subsequently performed with the intent to achieve the theoretical mass gain. These fluorination reactions were performed at isotherms of 200, 300, 400 and 500 °C as shown in Figure 6.5.

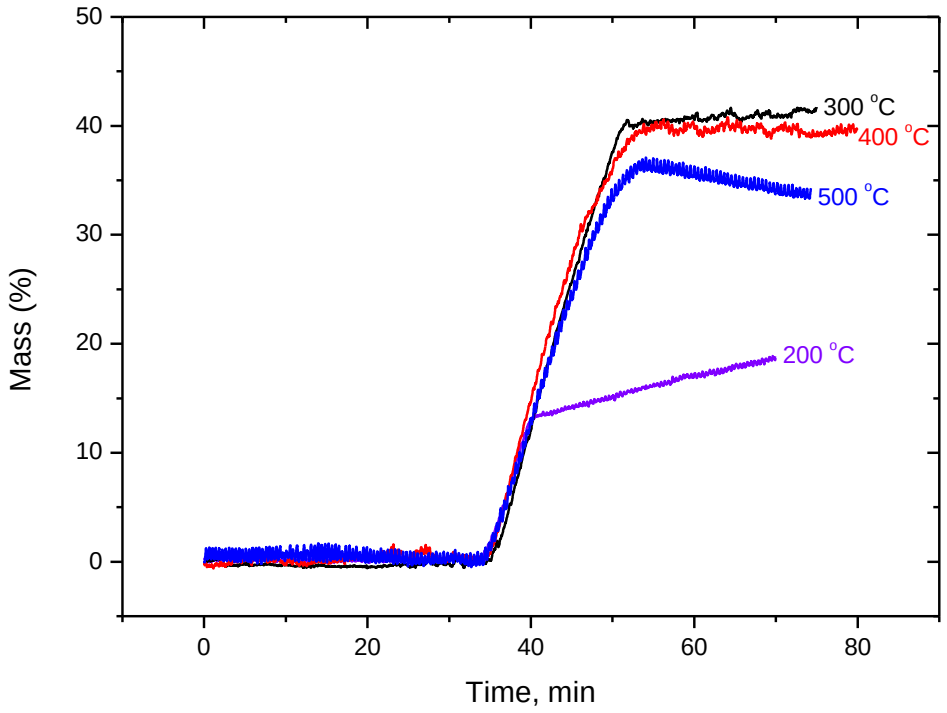

Figure 6.5: Thermogravimetric curve for the reaction of CoO treated with F_2 at isotherms of 200 (purple), 300 (black), 400 (red) and 500 °C (blue).

About 18% mass gain was recorded for the experiment performed at 200 °C, where the reaction was stopped prior to completion as the rate was very slow and not ideal. Isothermal fluorination at 300 °C resulted in a maximum uptake of 42%, whilst mass gain of 39 and 36% were recorded at 400 and 500 °C respectively. The isotherms at 400 and 500 °C already shown mass loss taking place. The mass loss at 400 and 500 °C is ascribed to sublimation of the CoF_3 product formed. The commercial CoF_3 was found to sublimate at 590 °C (Figure 4.4).

Nicholls (1973) reported the reaction of CoO with F_2 to take place at 500 °C, giving a mixture of CoF_2 and CoF_3. According to our TG results, the ideal temperature condition for the reaction of CoO with F_2 was found to be 300 °C, and therefore the product obtained at this isotherm was submitted for ATR-FTIR characterization. In Figure 6.6 is the spectrum for the product obtained from the reaction of CoO with F_2 at isotherm of 300 °C.

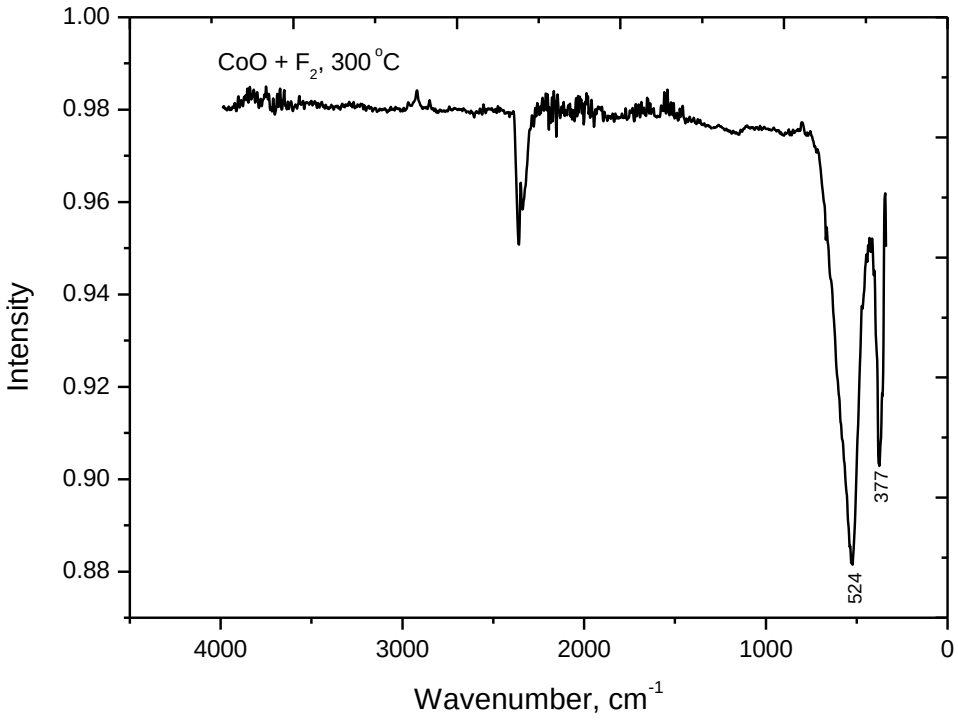

Figure 6.6: ATR-FTIR of the product of CoO with F_2 at 300 ^oC.

The spectrum of the product of CoO with F_2 shows too intense peaks at 377 and 524 cm^{-1}. The two bands are assigned to Co-F vibrations as they were shown to appear for the commercial CoF_3 compound. This shows good conversion of CoO to CoF_3 on using F_2 as the fluorinating agent.

6.3.3 Summary of the ATR-FTIR data obtained from the products of reactions of CoO with HF and with CoO with F_2.

A summary of the ATR-FTIR data for commercial CoO (black), CoF_2 (red), CoF_3 (blue) and products obtained from the reaction of CoO with HF (cyan) and CoO with F_2 (purple) are presented in Figure 6.7.

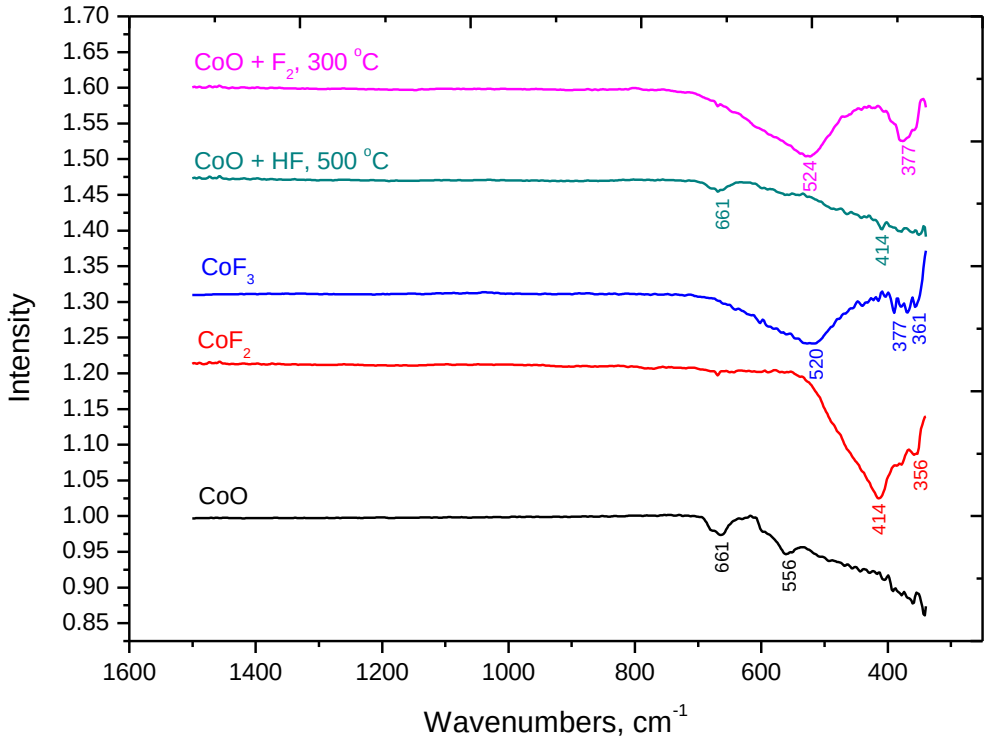

Figure 6.7: ATR-FTIR spectra of commercial CoO (black), CoF_2 (red), CoF_3 (blue), the product of CoO treated with HF (cyan) and CoO treated with F_2 (purple).

The product of CoO with HF has a very weak band at 414 cm^{-1}. This shows CoO to be less reactive with HF in comparison to Co_3O_4. Alternatively this finding might indicate reaction of Co_3O_4 that was found to be present within the commercial CoO. It was discovered that commercial CoO contains traces of Co_3O_4, and the low reactivity observed could be due from the traces of Co_3O_4 found within the commercial CoO. This inference could be proven through fluorination of the CoO material that is free of Co_3O_4 material.

A summary of the experimental data obtained for the reaction of CoO with HF and with F_2 gas is presented in Table 6.1.

Table 6.1: Summary of ATR-FTIR data obtained for the reaction of CoO with HF and with F_2 gas.

Sample	ATR-FTIR, cm^{-1}
Commercial CoO	556, 661
Commercial CoF_2	356, 414
Commercial CoF_3	361, 377, 520
CoO + HF, 500 ^oC	414, 661
CoO + F_2, 300 ^oC	377, 524

The spectrum of the product of CoO with HF shows very weak bands at 356 and 414 cm^{-1}. Of the two bands, the weak band at 414 cm^{-1} is assigned to Co-F vibrations, whilst the band at 661 cm^{-1} is ascribed to Co-O vibrations. The spectrum of the product of CoO with F_2 is different from that of the commercial CoO. This product gave strong bands at 377 and 520 cm^{-1} assigned to Co-F vibrations. This indicates formation of CoF_3, however more analysis should be carried out to support this.

6.4 Conclusions

Fluorination reactions of CoO with HF performed in the TGA show very small mass gains at the temperatures studied, indicating a low degree of fluorination. ATR-FTIR analysis of the obtained product suggested partial formation of CoF_2 due to a small peak appearing at 414 cm^{-1}, while presence of the reactant (CoO) was substantial. On the other hand, the reaction of CoO with F_2 resulted in formation of CoF_3. A fluorination temperature of 300 °C was recommended due to sublimation of CoF_3 at higher temperatures and slow reaction rates at lower temperatures. Our findings from Chapter 5 show that Co_3O_4 is more reactive towards fluorination with HF than CoO probably due its different oxidation states. On the other hand, complete conversion of these oxides to CoF_3 could be achieved via fluorination with F_2 gas.

7 Conclusions and recommendations

The aim of this study was to synthesize CoF_3 through the reaction of Co_3O_4 with HF and F_2 gas. The results indicate synthesis of CoF_3 through reaction of Co_3O_4 with HF to form an intermediate product (CoF_2), followed by reaction with F_2 to yield CoF_3. Using the thermodynamic equilibrium calculations, we were able to predict formation of CoF_2 and CoF_3 through reactions of Co_3O_4 with HF and F_2 respectively. This information was used as a guideline to carry out the actual experimental reactions of Co_3O_4 with HF and with F_2. Four reactions were performed, (i) Co_3O_4 with HF, (ii) Co_3O_4 with F_2 and (iii) CoF_2 with F_2. It was established that CoF_3 could be formed through direct fluorination of Co_3O_4 with F_2. However, due to high costs of F_2, (iv) a sequential reaction of Co_3O_4 with HF and then F_2 was undertaken for the synthesis of CoF_3.

Prior to the fluorination reactions, a study on the thermal analysis and spectroscopic characterisation of commercial Co_3O_4, CoO and CoF_2 compounds used as starting materials, as well as CoF_3 which was the desired product was performed. TGA results indicated simultaneous decomposition and sublimation of CoF_3 at temperatures exceeding 600 ^oC. Additionally, the presence of moisture promotes formation of HF from CoF_3. Fluorination reactions should therefore be carried out under dry conditions and at temperatures below 600 ^oC to form the desired product CoF_3.

The TGA was successfully used as a fluorination tool for the synthesis of CoF_3. The degree of fluorination of the respective reactions was followed via the mass uptakes recorded at various isotherms. The ideal temperature condition for the synthesis of CoF_2 through reaction of Co_3O_4 with HF was found to be 500 ^oC, whilst the ideal temperature for the synthesis of CoF_3 through reaction of Co_3O_4 with F_2 and CoF_2 with F_2 was found to be 300 ^oC and 400 ^oC respectively. These results were used to synthesise CoF_3 successfully through a sequential reaction of Co_3O_4 with HF and F_2 gas. Co_3O_4 was found to be more reactive towards fluorination with HF than CoO, while complete conversion of these oxides to CoF_3 could be achieved via fluorination with F_2. XRD and ATR-FTIR analyses were instrumental in the characterization of the reaction products obtained. Raman spectroscopy data was not so conclusive.

Suggestions for future work include the following:

- Completion of fluorination reactions of commercial CoO and HF/F_2 at higher isothermal temperatures, and characterization of the products formed, to establish the optimum temperature for these fluorination reactions and confirm the products that form.
- Carry out additional fluorination reactions with Co_3O_4 as well as with the purified CoO material.
- Based on the overall results obtained in this study, design and construct a small laboratory scale reactor to perform fluorination reactions. This will result in sufficient CoF_3 formed for further characterization required.
- Carry out phonon calculations using the computer software program (e.g. Materials Design MedeA software) to aid with spectroscopic characterization of the structure of CoF_3 and intermediate products.
- Attempt to confirm that CoOF is formed as an intermediate in some reaction schemes.
- Due to the mass transfer limitation of the TGA, this tool is not ideal to determine the intrinsic kinetics of gas-solid reactions. It should be considered to perform a kinetics study using a more suitable tool like the Carberry spinning basket reactor.
- Use a lab scale reactor to produce sufficient CoF_3 product for the next phase of the project, the fluorination of hydrocarbons to fluorocarbons. Several grams of product would be needed for these further studies.

8 References

Atkins, P. 1978. *Physical chemistry Oxford: Oxford University Press*.

Balducci, G., Brunetti, B. & Piacente, V. 1997. On the vapourization thermodynamics of cobalt trifluoride. *Journal of Alloys and Compounds,* 260**,** 56-58.

Banks, R. E., Smart, B. E. & Tatlow, J. C. 1994. *Organofluorine chemistry : principles and commercial applications,* New York :, Plenum.

Barceloux, D. G. & Barceloux, D. 1999. Cobalt. *Journal of Toxicology: Clinical Toxicology,* 37**,** 201-216.

Bergomi, A., Burdon, J., Hodgins, T. M., Stephens, R. & Tatlow, J. C. 1966. Fluorocyclopentanes—IV:The fluorination of cyclopentane with cobalt trifluoride. *Tetrahedron,* 22**,** 43-51.

Brown, M. E. 1998. *Introduction to Thermal Analysis: Techniques and Applications,* New York, Chapman and Hall

Bukhmarina, V. N., Gerasimov, A. Y. & Predtechenskii, Y. B. 1992. Vibrational spectra of matrix isolated VF_3 and CoF_3. *Vibrational Spectroscopy,* 4**,** 91-94.

Burdon, J., Ezmirly, S. T. & Huckerby, T. N. 1988. The fluorination of butane over cobalt trifluoride. *Journal of Fluorine Chemistry,* 40**,** 283-318.

Burdon, J. & Garnier, L. 1991. The fluorination of propane over cobalt trifluoride. *Journal of Fluorine Chemistry,* 54**,** 50-50.

Chambers, D. R. 2004. *Fluorine in Organic Chemistry,* CRC Press, Blackwell Publishing.

Christoskova, S. G., Stoyanova, M., Georgieva, M. & Mehandjiev, D. 1999. Preparation and characterization of a higher cobalt oxide. *Materials Chemistry and Physics,* 60**,** 39-43.

Cotton, F. A. & Wikinson, G. 1962. *Avanced Inorganic Chemistry,* New York.

Crouse, P. L. 2015. Fluorine: A key enabling element in the nuclear fuel cycle. *Journal of the Southern African Institute of Mining and Metallurgy,* 115**,** 931-935.

Donaldson, J., Clark, S. J. & Grimes, S. 1986. *Cobalt in Chemicals: The Monograph Series*, Cobalt Development Institute.

Enghag, P. 2000. Encyclopedia of the Elements. Wiley-VCH: Stockholm.

Fisher, K. Cobalt processing developments. 6th Southern African Base Metals Conference, SAIMM, 2011.

Friedt, J. M. & Adloff, J. P. 1969. Mössbauer spectrum of ^{57}Co: CoF_3. *Inorganic and Nuclear Chemistry Letters,* 5**,** 163-167.

Girichev, G. V., Giricheva, N. I., Krasnova, O. G., Krasnov, A. V., Shlykov, S. A., Rakov, E. G. & Khaustov, S. V. 1993. Electron-diffraction investigation of the molecular structure of CoF_3. *Journal of Structural Chemistry,* 33**,** 838-843.

Goldwhite, H. 1986. The Manhattan Project. *Journal of Fluorine Chemistry.*

Grosse, A. & Cady, G. 1947. Properties of Fluorocarbons. *Industrial & Engineering Chemistry,* 39**,** 367-374.

Groult, H., Neveu, S., Leclerc, S., Porras-Gutierrez, A. G., Julien, C. M., Tressaud, A., Durand, E., Penin, N. & Labrugere, C. 2017. Nano-CoF_3 prepared by direct fluorination with F_2 gas: Application as electrode material in Li-ion battery. *Journal of Fluorine Chemistry,* 196**,** 117-127.

Hadjiev, V. G., Iliev, M. N. & Vergilov, I. V. 1988. The Raman spectra of Co_3O_4. *Journal of Physics C: Solid State Physics,* 21**,** L199.

Hamilton, E. I. 1994. The geobiochemistry of cobalt. *Science of the Total Environment,* 150**,** 7-39.

Haszeldine, R. N. & Smith, F. 1950. 715. Organic fluorides. Part V. Fluorination of hydrocarbons with cobalt trifluoride. *Journal of the Chemical Society (Resumed)***,** 3617.

Hepworth, M. A., Jack, K. H., Peacock, R. D. & Westland, G. J. 1957. The crystal structures of the trifluorides of iron, cobalt, ruthenium, rhodium, palladium and iridium. *Acta Crystallographica,* 10**,** 63-69.

Kim, E. H., Kwon, S. W., Hwang, D. S., Cheong, W. M., Park, J. H. & Yoo, J. H. 2002. *Journal of Industrial and Engineering Chemistry,* 8.

Kurosawa, S., Arimura, T. & Sekiya, A. 1997. Monofluorination of fluorinated ethers with high-valency metal fluorides. *Journal of Fluorine Chemistry,* 85**,** 111-114.

Lemal, D. M. 2004. Perspective on fluorocarbon chemistry. *The Journal of organic chemistry,* 69**,** 1-11.

Leskiv, M. S., Chilingarov, N. S., Rau, J. V., Ferro, D., Abramov, S. V., Spiridonov, F. M. & Sidorov, L. N. 2008. Atomic fluorine in cobalt trifluoride thermolysis. *Journal of Fluorine Chemistry,* 129**,** 529-534.

Lewandowski, G., Meissner, E. & Milchert, E. 2006. Special applications of fluorinated organic compounds. *Journal of Hazardous Materials,* 136**,** 385-391.

Li, W., Groult, H., Borkiewicz, O. J. & Dambournet, D. 2018. Decomposition of CoF_3 during battery electrode processing. *Journal of Fluorine Chemistry,* 205**,** 43-48.

Li, Y., Qiu, W., Qin, F., Fang, H., Hadjiev, V. G., Litvinov, D. & Bao, J. 2016. Identification of Cobalt Oxides with Raman Scattering and Fourier Transform Infrared Spectroscopy. *The Journal of Physical Chemistry C,* 120**,** 4511-4516.

Louvain, N., Peyroux, J., Dubois, M., Simond, W. & Leroux, F. 2014. Efficient fluorinating agent through Topochemical Fluorination of Co–Fe Layered Double Hydroxides. *Inorganic Chemistry,* 53**,** 852-860.

Lwin, Y. 2000. Chemical equilibrium by Gibbs energy minimization on spreadsheets. *International Journal of Engineering Education,* 16**,** 335-339.

Mizukado, J., Matsukawa, Y., Quan, H.-D., Tamura, M. & Sekiya, A. 2006. Fluorination of fluoro-cyclobutene with high-valency metal fluoride. *Journal of Fluorine Chemistry,* 127**,** 79-84.

Muetterties, E. L. & Castle, J. E. 1961. Reactors of hydrogen fluoride with metals and metalloids. *Journal of Inorganic and Nuclear Chemistry,* 18**,** 148-153.

Nicholls, D. 1973. Comprehensive inorganic chemistry. *by JC Bailar, HJ Emeleus, Sir Ronald Nyholm, and AF Trotman-Dickenson, Pergamon Press, Oxford.*

O'hagan, D. 2008. Understanding organofluorine chemistry. An introduction to the C-F bond. *Chemical Society reviews,* 37**,** 308-19.

Oku, M. & Sato, Y. 1992. In-situ X-ray photoelectron spectroscopic study of the reversible phase transition between CoO and Co_3O_4 in oxygen of 10^{-3} Pa. *Applied Surface Science,* 55**,** 37-41.

Pienaar, A. D., Wagener, J. B. & Crouse, P. L. 2012. Niobium and tantalum separation by gas-phase fluorination. *International Journal of Mineral Processing,* 114-117**,** 7-10.

Popovic, A., Lesar, A., Rau, J. V. & Bencze, L. 2001. Sublimation properties of CoF_3: mass spectrometric and quantum chemical studies. *Rapid Commun Mass Spectrom,* 15**,** 749-57.

Priest, H. F. 1950. Anhydrous Metal Fluorides. *Inorganic Syntheses.* New York: McGraw-Hill.

Radeck, W., Lehmann, A. & Peplinski, T. 1991. On the fluorination of 1,2-dichlorobenzene over cobalt trifluoride. *Journal of Fluorine Chemistry,* 54**,** 266-266.

Rau, J. V., Nunziante Cesaro, S., Chilingarov, N. S. & Balducci, G. 1999. Identification of gaseous cobalt tetrafluoride: MS and FTIR spectroscopic studies. *Inorganic Chemistry,* 38**,** 5695-5697.

Risbud, A. S., Snedeker, L. P., Elcombe, M. M., Cheetham, A. K. & Seshadri, R. 2005. Wurtzite CoO. *Chemistry of Materials,* 17**,** 834-838.

Roine, A. 2002. Outokumpu HSC chemistry for windows: chemical reaction and equilibrium software with extensive thermochemical database. *Pori: Outokumpu research OY*.

Sakamoto, S., Yoshinaka, M., Hirota, K. & Yamaguchi, O. 1997. *Journal of the American Ceramic Society*
80**,** 267-268.

Sandford, G. 2003. Perfluoroalkanes. *Tetrahedron,* 59**,** 437-454.

Sen, K. D., Jørgensen, C. K. L. & Alonso, J. A. 1987. *Electronegativity,* Berlin ;, Springer-Verlag.

Tan, J., Liu, L., Guo, S., Hu, H., Yan, Z., Zhou, Q., Huang, Z., Shu, H., Yang, X. & Wang, X. 2015. The electrochemical performance and mechanism of cobalt (II) fluoride as anode material for lithium and sodium ion batteries. *Electrochimica Acta,* 168**,** 225-233.

Tang, C.-W., Wang, C.-B. & Chien, S.-H. 2008. Characterization of cobalt oxides studied by FT-IR, Raman, TPR and TG-MS. *Thermochimica Acta,* 473**,** 68-73.

Tumarov, Y. N. 1993. Feasible technological routes for processing zircon. Necsa.

Vilakazi, B. M., Monnahela, O. S., Wagener, J. B., Carstens, P. A. & Ntsoane, T. 2012. A thermogravimetric study of the fluorination of zirconium and hafnium oxides with anhydrous hydrogen fluoride gas. *Journal of Fluorine Chemistry,* 141**,** 64-68.

Wang, J., Sanchez-Rosello, M., Acena, J. L., Del Pozo, C., Sorochinsky, A. E., Fustero, S., Soloshonok, V. A. & Liu, H. 2014. Fluorine in pharmaceutical industry: fluorine-containing drugs introduced to the market in the last decade (2001-2011). *Chem Rev,* 114**,** 2432-506.

White, W. B., Johnson, S. M. & Dantzig, G. B. 1958. Chemical Equilibrium in Complex Mixtures. *The Journal of Chemical Physics,* 28**,** 751-755.

Zeleznik, F. J. & Gordon, S. 1960. An analytical investigation of three general methods of calculating chemical-equilibrium compositions.